2015 / Volume 53 / Number 1
ISSN 1641-4640

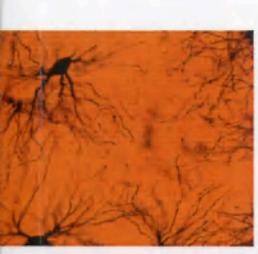

Folia NEUROPATHOLOGICA

www.folianeuro.termedia.pl

Official Journal of Mossakowski Medical Research Centre Polish Academy of Sciences and
Polish Association of Neuropathologists

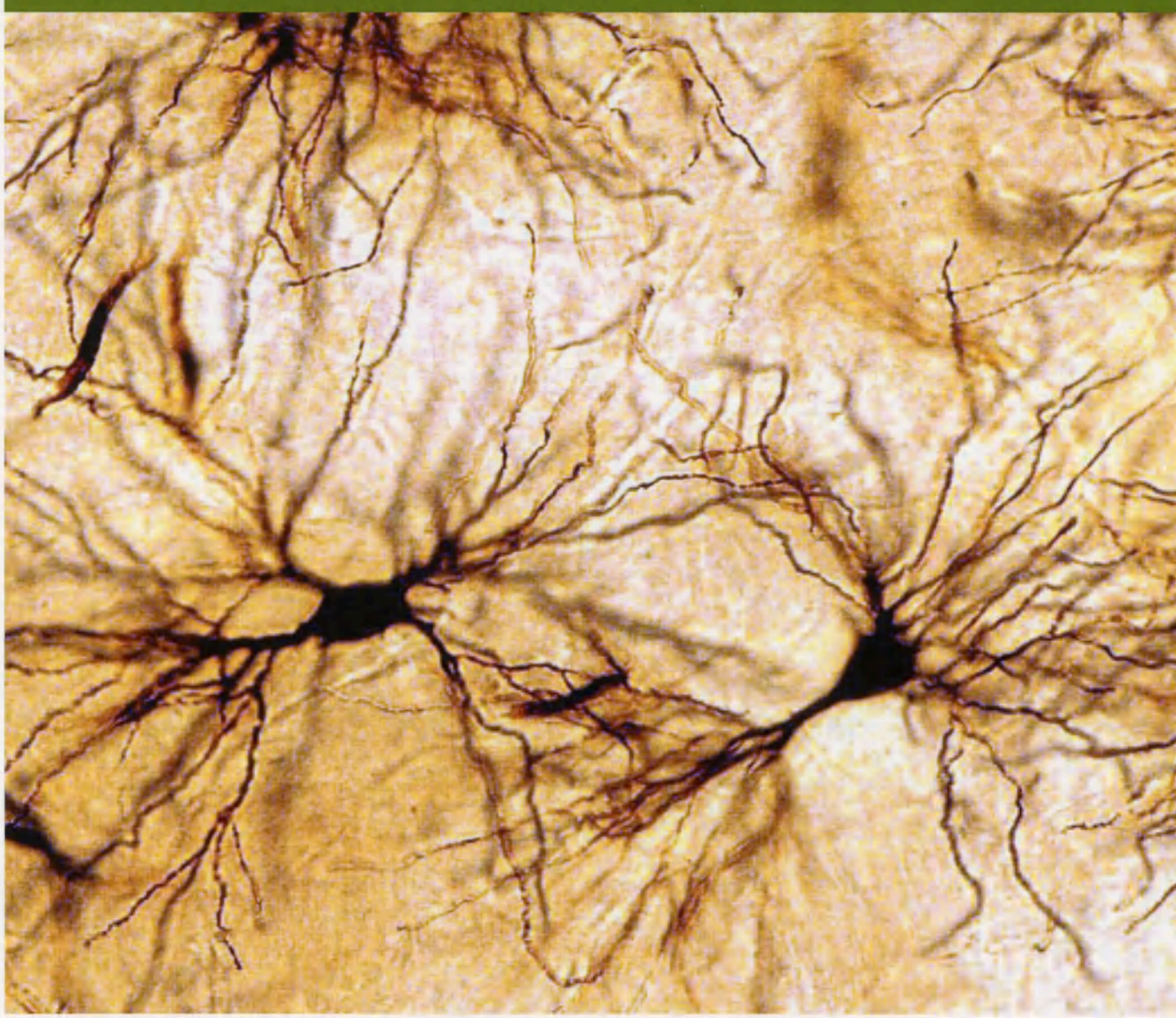

ISSN 1641-4640

Folia Neuropathologica

TERMEDIA Publishing House

Folia
Neuropathologica
former *Neuropatologia Polska*

Official Journal of Mossakowski Medical Research Centre Polish Academy of Sciences and Polish Association of Neuropathologists

The journal is partly financially supported by the Ministry of Science and Higher Education

termedia

Termedia Publishing House
Kleeberga 2, 61-615 Poznan, Poland
phone/fax: +48 61 822 77 81
e-mail: termedia@termedia.pl
www.termedia.pl
www.folianeuro.termedia.pl

Warsaw office
phone/fax: +48 22 827 75 14
e-mail: biuro.warszawa@termedia.pl

president of the management board
editor-in-chief of the Publishing House, director
Janusz Michalak
e-mail: j.michalak@termedia.pl

director of the Publishing House
Andrzej Kordas
e-mail: a.kordas@termedia.pl

Marketing and Advertising Department
Renata Dolata
phone: +48 61 822 77 81 ext. 508
e-mail: r.dolata@termedia.pl

Distribution Subscription Department
Jolanta Jankowiak
phone: +48 61 656 22 00
e-mail: prenumerata@termedia.pl

Impact Factor for Folia Neuropathologica equals 1.667
MNiSW score for Folia Neuropathologica equals 15.00
Index Copernicus score (2011) for Folia Neuropathologica equals 18.13
Position in Index Copernicus ranking systems available at http://www.indexcopernicus.pl

Abstracted and indexed in Index Medicus/MEDLINE, Neuroscience Citation Index, SciSearch, Research Alert, Chemical Abstracts, EMBASE/Excerpta Medica, Polish Medical Bibiography, Index Copernicus

The journal is financially supported by the Ministry of Sciences and Higher Education.

Print run: 450 copies

Folia
Neuropathologica
2015; 53/1: 1-88

Contents

Review paper

Folia Neuropathologica

The role of genetic factors in the pathogenesis of neonatal intraventricular hemorrhage

Dawid Szpecht[1], Marta Szymankiewicz[1], Agnieszka Seremak-Mrozikiewicz[2], Janusz Gadzinowski[1]

[1]Department of Neonatology, Poznan University of Medical Sciences, [2]Department of Perinatology and Women's Diseases, Poznan University of Medical Sciences, Poznan, Poland

Folia Neuropathol 2015; 53 (1): 1-7 DOI: 10.5114/fn.2015.49968

Abstract

Intraventricular hemorrhage (IVH) affects 15-20% of babies born before 32 weeks of pregnancy. Besides gestational age (below 32 weeks) there are a number of IVH risk factors. Increasing attention is being paid to genetic factors in the development of IVH. The authors discuss genetic factors (mutations of coagulation factors, gene polymorphisms in pro-inflammatory cytokines, mutation of type IV collagen gene, polymorphisms of genes responsible for the regulation of systemic blood pressure and cerebral blood flows) whose involvement in IVH pathogenesis has been confirmed in the highest number of reports and for which being a carrier plays an important role in their pathophysiology. The role of genetic factors in IVH remains unclear. Further analysis of the role of genetic factors in the pathophysiology of IVH will make it possible to determine the group of newborns who are specifically at risk of developing IVH in the perinatal period.

Key words: *neonatal intraventricular hemorrhage, genetic factors, pathophysiology.*

Intraventricular hemorrhage (IVH) is a condition which mainly affects prematurely born infants. It affects 15-20% of babies born before 32 weeks of pregnancy. The condition rarely occurs in full-time infants. About 90% of cases of intraventricular hemorrhage occur within the first 3 days of the newborn's life. In 20-40% of cases the spread of the initial bleeding becomes more extended, which is most often observed at the end of the first week of life. In the majority of cases involving mild bleeding (classified as grades 1 and 2) no clinical effects are observed. Grade 3 or 4 hemorrhage may manifest itself in a sudden deterioration in the clinical condition, seizures, consciousness disorders and neurological symptoms, such as eye movement disorders, decreased spontaneous movement, and muscle tone disturbances. Grade 1 and 2 hemorrhages usually resolve themselves and cause no long-term problems. About 40-80% of newborns with grade 3 or 4 hemorrhages develop symptoms of cerebral palsy [25].

Besides gestational age (below 32 weeks) and body weight at birth (less than 1500 g) there are also other IVH risk factors identified in the literature, including: absence of prenatal steroid therapy in women at risk of premature delivery, early clamping of the umbilical cord (up to 30 seconds after birth), symptoms of intrauterine infection in the mother and the newborn, and labor and delivery complicated by bleeding or perinatal hypoxia. The group of infants with elevated IVH risk also includes

Communicating author:
Dawid Szpecht, Department of Neonatology, Poznan University of Medical Sciences, 33 Polna St., 60-535 Poznań, Poland,
e-mail: dawid.szpecht@poczta.fm

newborns with intrauterine growth retardation, and those who in the first days of their life were treated with crystalloids (bolus 10-15 ml/kg) and/or catecholamines for hypotension and $NaHCO_3$ for acidosis. The IVH risk group also includes newborns with blood clotting disorders, thrombocytopenia, hypoglycemia, pneumothorax, bleeding of lungs, and those transported from another hospital [3,4,27]. Moreover, today increasing attention is being paid to genetic factors in the development of IVH, but their connection with IVH in the newborn has been confirmed by few clinical studies so far. The purpose of this paper is to discuss those genetic factors whose involvement in IVH pathogenesis has been confirmed in the highest number of reports and for which being a carrier plays an important role in their pathophysiology.

Congenital thrombophilias: factor V Leiden gene mutation, prothrombin G20210A mutation, factor XIII Val34Leu polymorphism

Congenital thrombophilias are a genetically conditioned predisposition for venous or arterial thrombosis. Activated protein C resistance (APCR), i.e. the resistance of factor V to the anti-coagulant action of APC, is the most prevalent type of congenital thrombophilia, and in over 90% of patients it is caused by a point mutation of the factor V gene on chromosome 1 (the Leiden mutation).

Factor V (FV) is synthesized by hepatocytes. It is also created in monocytes, macrophages and megakaryocytes, and is transformed by thrombin to its active form (factor Va, FVa). Factor V undergoes thrombin-dependent activation and APC-dependent inactivation. Thrombin cleaves FV at Arg709, Arg1018 and Arg1545 within the B domain of FV. The result is the active form (FVa) which, together with FXa and calcium ions, forms the prothrombinase complex that converts prothrombin into thrombin. Besides its pro-coagulant activity, FVa also plays an anti-coagulant role (APC-dependent). APC-mediated proteolysis of FVa to FVi occurs when APC is attached to FVa at Arg306, Arg506 and Arg679 of the heavy chain of FVa. The role of FVa is also to inactivate FVIIIa to FVIIIi, which is initiated by connecting APC to FVa at Arg506 and forming FVac, which inactivates FVIIIa [9,28,34].

Factor V Leiden mutation is an autosomal dominant genetic mutation affecting between 2% and 10% of the Caucasian race. This form of mutation is most often encountered in Cyprus, southern Sweden, Germany, Saudi Arabia and among the Jewish community in Israel, whereas it is extremely rare in Africa and in the Chinese and Japanese populations. In 90% of cases of factor V Leiden mutation, arginine at position 506 of the heavy chain is replaced with glutamine, which results in resistance to APC-dependent proteolysis and retained pro-coagulant activity of factor V. In addition, the mechanism of FVIIIa inactivation by FVac is switched off. In people with heterozygous mutation the risk of thromboembolic disease is 3-8 times higher than it is in the healthy population. In people with homozygous mutation the risk of developing venous thrombosis is even 80 times as high as the general population risk. The most frequently found symptoms of Leiden mutation are superficial thrombophlebitis and deep vein thrombosis of the legs and thrombosis in atypical locations: inferior vena cava, hepatic portal vein, hepatic veins [20,21].

Prothrombin (factor II, FII) is a vitamin K-dependent proenzyme produced in the liver and converting fibrinogen to fibrin. The prothrombin encoding gene is located on chromosome 11 (region: p11-q12). The F2 allelic variant – a mutation in the 3' untranslated region of the prothrombin gene (20210 – changing guanine to adenine) is associated with higher levels of prothrombin synthesis, increasing prothrombin plasma levels by over 10%. Its prevalence in the Polish population is estimated at approx. 1% [26]. In both child and adult populations an association has been found between the mutation of the prothrombin gene and the incidence of thrombosis in certain venous locations (portal vein, intracranial veins). Being a carrier of both factor V Leiden gene mutation and the prothrombin G20210A mutation increases the risk of thrombotic incidents approx. 3-fold, compared with the factor V Leiden gene mutation alone [31].

The association between the factor V Leiden gene mutation and IVH was first described in the literature in a group of 8 infants with hydrocephalus. Due to the immaturity of anti-coagulation mechanisms, including the C-protein system (comprising the C protein, S protein and thrombomodulin), the newborn shows a tendency to over-coagulate. The roles of factor V Leiden gene mutation and the prothrombin gene in IVH pathogenesis are probably a consequence of an increased risk of thrombosis in

the fine blood vessels in the region of the germinal matrix. Increased blood pressure in germinal matrix vessels may lead to vessel wall rupture and to IVH. As reported in the literature, congenital thrombophilia is associated with an increased IVH risk among newborns, but it may also play a protective role. Petäjä *et at*. [31] analyzed a group of 51 newborns with very low weight at birth (22 infants with grade 2 to 4 IVH and 29 in the control group), in which IVH was observed among carriers of the factor V Leiden gene mutation. Similar conclusions were reached by Komlósi *et al*. [18], who observed an increased IVH risk in newborns with congenital thrombophilia and birth weight below 2500 g. However, there are other studies which indicate that factor V Leiden and prothrombin G20210A gene mutations have a protective role against IVH. Data published by Göpel *et al*. [12] show that the risk of IVH above grade 2 among infants carrying factor V Leiden and prothrombin G20210A gene mutations is lower than among those not carrying these mutations. Härtel *et al*. [14] found no association between the prevalence of IVH in infants with body weight at birth < 1500 g and being the carrier of these mutations. Thus, the role of factor V Leiden and prothrombin G20210A gene mutations in the pathogenesis of IVH remains unclear. The heterogeneity, size and ethnic diversity of the groups of infants studied provide the most likely explanation of the differences in findings concerning the role of these two mutations in IVH pathogenesis.

The role of other genetic factors, such as factor XIII-Val34Leu polymorphism and factor VII-323 del/ins polymorphism, in the pathogenesis of neonatal IVH has not been fully confirmed. Factor XIII, whose role is to stabilize fibrin and create a clot, is coded by a gene located on chromosome 6. A point mutation in codon 34 at exon 2 of the factor XIII A subunit results in substituting leucine for valine at position 34 of the peptide. As reported in the literature, in the adult population the polymorphic variant of factor XIIIVal34Leu protects against myocardial infarction, ischemic stroke and venous thromboembolism while at the same time increasing the risk of intracranial hemorrhage [17]. Göpel *et al*. [11] confirmed an increased frequency of IVH grade 1 to 4 in very low birth weight infants carrying the Leu/Val or Leu/Leu allele (14.3%), compared to those with the Val/Val allele (10.1%). This association was not confirmed by Härtel *et al*. [14].

Gene polymorphisms in pro-inflammatory cytokines

There is no doubt that factors involved in inflammatory processes play a role in the pathogenesis of IVH. The role of a number of pro-inflammatory cytokines and polymorphic variants of IL-1β, ESR1 and TNF-α genes and their impact on damage to an immature central nervous system and the development of IVH in pre-term infants has been investigated in many studies [7,16,23,26,37].

Interleukin 1 (IL-1) is a family of cytokines comprising over 10 molecules including IL-1α, IL-1β, IL-1γ (IL-18), IL-1ε, IL-1δ, IL-1Ra, and IL-1H. Interleukine 1 plays a major role in regulating an inflammatory reaction and is produced mainly by monocytes and macrophages of various tissues in response to bacterial, viral and fungal antigens. The majority of IL-1 effects are associated with the presence of IL-1β. A significant association was confirmed between an increased IL-1β concentration in the amniotic fluid and umbilical cord blood and the development of IVH and periventricular leukomalacia in neonates [37]. Animal tests proved that administration of IL-1β causes damage to the central nervous system of newborn rats, yet the pathology mechanism is still unknown [7]. In 2013 Adén *et al*. [2] presented the results of a study in which genotypes of 224 premature infants with birth weight between 500 and 1250 g and with IVH grade 3 and 4 were analyzed. The analysis covered a number of gene polymorphisms for collagen 4A1 (COL4A1 Gly1580Arg); FII (97 G>A); FV (1601 G>A); interleukin IL-1β (87-511 T>C; 87-31 C>T); interleukin 6 (116-121 C>G); methylenetetrahydrofolate reductase (MTHFR) (677 C>T; 1298 A>C); TNF (169-319 G>A). In the study, of a number of the polymorphisms analyzed, the role in the pathogenesis of IVH was confirmed in carriers of the MTHFR 1298 A>C gene polymorphism, more frequently with the CC genotype. MTHFR is an enzyme which catalyzes the reduction of 5,10-methylenetetrahydrofolate to 5-methyltetrahydrofolate, a substrate in remethylation of homocysteine to methionine. Mutations in the MTHFR gene cause a reduction in the enzyme activity, which results in increased blood plasma homocysteine concentration. Raised homocysteine levels may cause damage to vascular endothelium, increase the risk of vessel rupture and lead to IVH.

Tumor necrosis factor (TNF) is produced mainly by active monocytes and macrophages and, in much lower quantities, by other tissues, and – together

with interleukins 1 and 6 – plays a role in the localized and systemic inflammatory response, using endo-, para- and autocrine signaling to communicate with immune system cells. Tumor necrosis factor is thought to play a role in the growth, differentiation and activities of various cells, both normal and modified by cancer. Among other things, it is responsible for damage to microcirculatory endothelium in the central nervous system, thereby increasing the risk of vessel rupture and IVH occurrence. The role of specific polymorphic gene variants for TNF-α and TNF-β in the pathogenesis of neonatal IVH is unclear. Adcock *et al*. [1] found a correlation between the development of IVH and being a carrier of the TNF-α 308 G/A (allele A) polymorphism. In a study investigating the role of polymorphic gene variants of 308 G/A TNF-α and NcoI TNF-β in a group of 27 infants born before week 32 of pregnancy, Heep *et al*. [15] confirmed higher incidence of severe (grade 3 or 4) IVH in carriers of the TNF-β2 allele, while a corresponding correlation in carriers of a polymorphism of the -308 promoter region of the TNF-α gene was not found.

Mutation of type IV collagen gene

The COL4A1 gene encodes the α chain of type IV collagen. Type IV collagen is the principal component of basement membrane. In mice studies the mutation in the COL4A1 gene resulted in intracranial hemorrhage, including IVH. The literature indicates that the 4582-4586dupCCCATG mutation of the COL4A1 gene is related to neonatal porencephaly and hemorrhagic stroke in adults. In 2009, Bilguvar *et al*. [5] published results which indicate the role of the 4582-4586dupCCCATG mutation of the COL4A1 gene in the pathogenesis of IVH in preterm infants. The 4582-4586dupCCCATG variant of the COL4A1 mutation leads to the insertion of two amino acids in the NC1 domain of type IV collagen, which results in destabilization of collagen IV and in perforation of the vascular basement membrane which affects, inter alia, cerebral vessels of newborn infants [5].

Polymorphisms of genes responsible for regulation of systemic blood pressure and cerebral blood flows

Cerebral blood flows through an infant's brain are controlled by four mechanisms: autoregulation and chemical, metabolic and neurogenic regulation. In healthy infants born at term the regulation of cerebral blood flow responds to stimuli in the same way as it does in an adult. Cerebral blood vessels, with their rich innervation (both sympathetic and parasympathetic), respond by contracting to neurotransmitters such as noradrenaline, serotonin and neuropeptide Y, and by relaxation to acetylcholine, vasoactive intestinal peptide and nitric oxide. In the pathogenesis of neonatal IVH in preterm infants, an important role is played by changes in venous and arterial cerebral flows. It has been shown that the ability of autoregulation of cerebral flows in response to variations in arterial blood pressure in preterm infants is impaired. This impaired autoregulation causes an increased risk of germinal matrix rupture and IVH occurrence [6].

It seems that endothelial nitric oxide synthase (eNOS) gene polymorphisms (Glu298Asp or –786 T>C) may increase the risk of IVH in preterm infants by significantly disrupting the regulation of cerebral flows [6,35]. Nitric oxide (NO) is continuously synthesized in the human body, inter alia in vascular endothelium. It is synthesized from the guanidine group of L-arginine with the release of L-citrulline in a reaction catalyzed by eNOS in the presence of molecular oxygen and cofactors: reduced nicotinamide adenine dinucleotide phosphate (NADPH), flavin adenine dinucleotide (FAD) and tetrahydrobiopterin (BH4). The eNOS enzyme, taking up cellular membrane microdomains in cells such as endothelium, myocytes, platelets and neurons, plays an important role in the transduction of signals reaching the cell from outside, e.g. by interaction with caveolin-1. The eNOS activity is controlled, inter alia, by phosphorylation and depalmitoylation, binding to the Ca^{2+}/calmodulin complex, and association with the Hsp90 protein. NO synthesis disorders may result from genetically conditioned disruptions in eNOS activity. The NOS3 gene (eNOS coding gene) comprises 26 exons and 25 introns; it codes 1203 amino acids with molecular mass of 133 kDa. The NOS3 gene polymorphism whereby guanine (G) is replaced with thymine (T) at nucleotide 894 (exon 7) results in a change of the amino acid sequence of Glu298Asp. The 786 T>C polymorphism of the NOS3 gene replaces thymine with cytosine in the NOS3 gene promoter at –786. It is thought that in the presence of Glu298Asp and –786T>C polymorphic variants, eNOS enzymatic activity may be impaired. The main NO receptor is guanyl cyclase. The effect of guanyl cyclase activation is an increase in cGMP

levels and the activation of protein kinase G (PKG). In endothelium NO plays a central role in the regulation of local blood pressure, by acting as a vasodilatory agent, whereby it ensures that blood flow through the tissues is adequate to the requirements. Moreover, it counteracts the factors acting as strong vasoconstrictive agents, such as endothelin-1 and angiotensin II, and it inhibits aggregation and adhesion of blood platelets by reducing the production of platelet activation factor (PAF) by the endothelium. It also acts protectively for vessel walls, by inhibiting oxidation of lipids and inactivating oxygen free radicals [10]. It has also been demonstrated that in pregnant women the activity of the NO synthesis system is high. This activity decreases as the delivery term approaches, which plays a major role in the mechanism of stimulating uterine contractions and the start of labor. Elevated levels of nitric oxide during pregnancy result from the stimulation of NO synthase in the uterine muscle and the syncytiotrophoblast by high estradiol concentrations. Maternal levels of NO also regulate the resistance in uteroplacental circulation vessels. NO deficiency in pregnancy may be related to arrested intrauterine fetus development and low birth weight. In infants carrying polymorphic variants of the eNOS gene a decreased concentration of nitric oxide synthase may lead to lower NO concentration in the perinatal period and to disruptions affecting neonatal cerebral blood flows [24,29,30].

The renin-angiotensin-aldosterone system (RAA system/RAAS) is a system that regulates blood volume and blood pressure, as well as the concentration of Na and K ions in systemic fluids.

Deletion/insertion variant for the angiotensin converting enzyme (ACE ins/del) and the 1166A/C polymorphism of 1 Ang II (ATR1166A/C) are related to a better prognosis in the course of acute respiratory distress syndrome. The role of these two polymorphisms in the IVH pathology in newborns still remains unclear. It is reported in the literature that the polymorphism of the ACE ins/del gene may act as either a good or a bad prognostic factor in the course of the infant respiratory distress syndrome. Newborn infants carrying the ACE ins/del polymorphism also carry a higher risk of retinopathy of prematurity (ROP), and those carrying ATR1166A/C polymorphism carry a risk of persistent ductus arteriosus (PDA) in premature infants [13]. In 2011 Spiegler *et al*. [32] published the results of a multi-center study carried out on 1209 infants born with body weight below 1500 g in 12 centers in Germany. No significant association between ACE-ins/del or ATR1166A/C genotype and neonatal death or other infant outcome parameters (such as IVH, bronchopulmonary dysplasia, ROP or PDA) was found [32,36].

Research to date has shown that the polymorphic variants of the ET-1 gene Lys198Asn and 134delA play a significant role in the pathogenesis of ischemic heart disease and arterial hypertension in adults, including in pregnancy, while their impact on the development of neonatal IVH is unclear. Endothelin 1 (ET-1) is the strongest known vasoconstrictor – the vasospasm effect lasts for 45-60 minutes. Endothelin 1 may play a role in maintaining hemodynamic homeostasis by changing the distribution of blood in the system [33]. It is also reported in the literature that childbirth is a stress factor leading to increased synthesis of ET-1 by umbilical vein endothelium. Endothelin 1 may play a significant role in the regulation of blood flow through the feto-placental unit. It is suggested that the fetus itself also synthesizes the hormone, as a result of hemodynamic and metabolic changes occurring during uterine contractions in childbirth. It is likely that an increased concentration of ET-1 in umbilical blood plasma during childbirth leads to the contraction of umbilical vessels after delivery, and it may be one of the mechanisms that prepare the fetus for taking the first breath [22].

Intraventricular hemorrhage represents a very significant complication in preterm infants. The role of genetic factors in IVH remains unclear. Further analysis of the role of genetic factors in the pathophysiology of IVH will make it possible to determine the group of newborns who are specifically at risk of developing IVH in the perinatal period.

Disclosure

Authors report no conflict of interest.

References

1. Adcock K, Hedberg C, Loggins J, Kruger TE, Baier RJ. The TNF-alpha-308, MCP-1 –2518 and TGF-beta-1 +polymorphisms are not associated with the development of chronic lung disease in very low birth weight infants. Genes Immun 2003; 4: 420-426.
2. Adén U, Lin A, Carlo W, Leviton A, Murray JC, Hallman M, Lifton RP, Zhang H, Ment LR; Gene Targets for Intraventricular Hemorrhage Study Group. Gene Targets for Intraventricular Hemorrhage Study Group. Candidate gene analysis: severe

intraventricular hemorrhage in inborn preterm neonates. J Pediatr 2013; 163: 1503-1506.
3. Allen KA. Treatment of hemorrhages in premature infants: where is the evidence? Adv Neonatal Care 2013; 13: 127-130.
4. Bassan H. Intracranial hemorrhage in the preterm infant: understanding it, preventing it. Clin Perinatol 2009; 36: 737-762.
5. Bilguvar K, DiLuna ML, Bizzarro MJ, Bayri Y, Schneider KC, Lifton RP, Gunel M, Ment LR; Pacifier and Breastfeeding Trial Group. COL4A1 mutation in preterm intraventricular hemorrhage. J Pediatr 2009; 155: 743-745.
6. Brinker T, Stopa E, Morrison J, Klinge P. A new look at cerebrospinal fluid circulation. Fluids Barriers CNS 2014; 11: 10.
7. Cai Z, Pang Y, Lin S, Rhodes PG. Differential roles of tumor necrosis factor-alpha and interleukin-1 beta in lipopolysaccharide-induced brain injury in the neonatal rat. Brain Res 2003; 975: 37-47.
8. Demirçubuk AG, Coşkun MY, Demiryürek Ş, Dokuyucu R, Öztuzcu S, Taviloğlu ZŞ, Arslan A, Sivaslı E. Endothelial NOS gene Glu298Asp polymorphism in preterm neonates with respiratory distress syndrome. Pediatr Pulmonol 2013; 48: 976-980.
9. Esmon CT. Crosstalk between inflammation and thrombosis. Maturitas 2008; 61: 122-131.
10. Galluccio E, Cassina L, Russo I, Gelmini F, Setola E, Rampoldi L, Citterio L, Rossodivita A, Kamami M, Colombo A, Alfieri O, Carini M, Bosi E, Trovati M, Piatti P, Monti LD, Casari G. A novel truncated form of eNOS associates with altered vascular function. Cardiovasc Res 2014; 101: 492-502.
11. Göpel W, Kattner E, Seidenberg J, Kohlmann T, Segerer H, Möller J; Genetic Factors in Neonatology Study Group. The effect of the Val34Leu polymorphism in the factor XIII gene in infants with a birth weight below 1500 g. Pediatr 2002; 140: 688-692.
12. Göpel W, Gortner L, Kohlmann T, Schultz C, Möller J. Low prevalence of large intraventricular hemorrhage in very low birth weight infants carrying the factor V Leiden or prothrombin G20210A mutation. Acta Paediatr 2001; 90: 1021-1024.
13. Harding D, Dhamrait S, Marlow N, Whitelaw A, Gupta S, Humphries S, Montgomery H. Angiotensin-converting enzyme DD genotype is associated with worse perinatal cardiorespiratory adaptation in preterm infants. J Pediatr 2003; 143: 746-749.
14. Härtel C, König I, Köster S, Kattner E, Kuhls E, Küster H, Möller J, Müller D, Kribs A, Segerer H, Wieg C, Herting E, Göpel W. Genetic polymorphisms of hemostasis genes and primary outcome of very low birth weight infants. Pediatrics 2006; 118: 683-689.
15. Heep A, Schueller AC, Kattner E, Kroll M, Sander J, Wisbauer M, Bartmann P, Stueber F. Association of two tumour necrosis factor gene polymorphisms with the incidence of severe intraventricular haemorrhage in preterm infants. J Med Genet 2005; 42: 604-608.
16. Kadhim H, Tabarki B, Verellen G, De Prez C, Rona AM, Sebire G. Inflammatory cytokines in the pathogenesis of periventricular leukomalacia. Neurology 2001; 56: 1278-1284.
17. Kohler HP, Stickland MH, Ossei-Gerning N, Carter A, Mikkola H, Grant PJ. Association of a common polymorphism in the factor XIII gene with myocardial infarction. Thromb Haemost 1998; 79: 8-13.
18. Komlósi K, Havasi V, Bene J, Storcz J, Stankovics J, Mohay G, Weisenbach J, Kosztolányi G, Melegh B. Increased prevalence of factor V Leiden mutation in premature but not in full-term infants with grade I intracranial hemorrhage. Biol Neonate 2005; 87: 56-59.
19. Kosińska-Kaczyńska K, Szymusik I, Kaczyński B. Jatrogenne i samoistne późne wcześniactwo wśród bliźniąt a ryzyko powikłań noworodkowych. Ginekol Pol 2013; 84: 430-435.
20. Laurent OM, Berislav VZ, Griffin JH. The cytoprotecive protein C pathway. Blood 2007; 109: 3161-3172.
21. Lewandowski K, Turowiecka Z, Rozek M, Markiewicz WT, Zawilska K. Mutacja punktów GàA nukleotydów 1691 genu czynnika V przyczyną powikłań zakrzepowych w rodzinie z opornością osocza na działanie aktywnego białka C. Pol Arch Med Wewn 1996; 4: 318-322.
22. Lisi V, Paternoster DM, Stecca A, Micciché F, Fantinato S, Leon A, Damante G, Fabbro D, Clementi M. Investigation of endothelin-1 type A receptor gene polymorphism (–231 G/A) in preeclampsia susceptibility. J Matern Fetal Neonatal Med 2007; 20: 145-149.
23. Liu XH, Kwon D, Schielke GP, Yang GY, Silverstein FS, Barks JD. Mice deficient in interleukin-1 converting enzyme are resistant to neonatal hypoxic-ischemic brain damage. J Cereb Blood Flow Metab 1999; 19: 1099-1108.
24. Pappa KI, Roubelakis M, Vlachos G, Marinopoulos S, Zissou A, Anagnou NP, Antsaklis A. Variable effects of maternal and paternal-fetal contribution to the risk for preeclampsia combining GSTP1, eNOS, and LPL gene polymorphisms. J Matern Fetal Neonatal Med 2011; 24: 628-635.
25. Payne AH, Hintz SR, Hibbs AM, Walsh MC, Vohr BR, Bann CM, Wilson-Costello DE; Eunice Kennedy Shriver National Institute of Child Health and Human Development Neonatal Research Network. Neurodevelopmental outcomes of extremely low-gestational-age neonates with low-grade periventricular-intraventricular hemorrhage. JAMA Pediatr 2013; 167: 451-459.
26. Petäjä J, Hiltunen L, Fellman V. Increased risk of intraventricular hemorrhage in preterm infants with thrombophilia. Pediatr Res 2001; 49: 643-646.
27. Rosendorff A, Dorfman DM. Activated Protein C Resistance and Factor V Leiden. Arch Pathol Lab Med 2007; 131: 866-871.
28. Ryckman KK, Dagle JM, Kelsey K, Momany AM, Murray JC. Replication of genetic associations in the inflammation, complement, and coagulation pathways with intraventricular hemorrhage in LBW preterm neonates. Pediatr Res 2011; 70: 90-95.
29. Seremak-Mrozikiewicz A, Drews K, Barlik M, Sieroszewski P, Grześkowiak E, Mrozikiewicz P. The significance of –786T > C polymorphism of endothelial NO synthase (eNOS) gene in severe preeclampsia. J Matern Fetal Neonatal Med 2011; 24: 432-436.
30. Seremak-Mrozikiewicz A, Drews K, Mrozikiewicz PM. The –786T/C polymorphism of the endothelial nitric oxide synthase gene in preeclampsia. Eur J Obstet Gynecol Reprod Biol 2008; 138: 118-119.
31. Skrzypczak J, Rajewski M, Wirstlein P, Goździewicz T, Breborowicz G, Leszczyńska-Gorzelak B, Ludwikowski G, Preis K, Wołczyński S, Zimmer M. Incidence of hereditary thrombophilia in women with pregnancy loss in multi-center studies in Poland. Ginekol Pol 2012; 83: 330-336.
32. Spiegler J, Gilhaus A, Konig IR, Kattner E, Vochem M, Kuster H, Moller J, Muller D, Kribs A, Segerer H, Wieg C, Nikischin W, von

der Wense A, Gebauer C, Herting E, Gopel W. Polymorphisms in the Renin-Angiotensin system and outcome of very-low-birth-weight infants. Neonatology 2010; 97: 10-14.
33. Su MT, Lin SH, Chen YC. Genetic association studies of angiogenesis- and vasoconstriction-related genes in women with recurrent pregnancy loss: a systematic review and meta-analysis. Hum Reprod Update 2011; 17: 803-812.
34. Szpecht D, Poprawski G, Mrówczyński W. The activity of protein C in infants undergoing cardiopulmonary bypass to correct a congenital heart defect – a pilot study. Adv Clin Exp Med 2009; 18: 163-168.
35. Vannemreddy P, Notarianni C, Yanamandra K, Napper D, Bocchini J. Is an endothelial nitric oxide synthase gene mutation a risk factor in the origin of intraventricular hemorrhage? Neurosurg Focus 2010; 28: E11.
36. Yanamandra K, Loggins J, Baier RJ. The Angiotensin Converting Enzyme Insertion/Deletion polymorphism is not associated with an increased risk of death or bronchopulmonary dysplasia in ventilated very low birth weight infants. BMC Pediatr 2004; 4: 26.
37. Yoon BH, Jun JK, Romero R, Park KH, Gomez R, Choi JH, Kim IO. Amniotic fluid inflammatory cytokines (interleukin-6, interleukin-1beta, and tumor necrosis factor-alpha), neonatal brain white matter lesions, and cerebral palsy. Am J Obstet Gynecol 1997; 177: 19-26.

Original article

Folia Neuropathologica

Erk activation as a possible mechanism of transformation of subependymal nodule into subependymal giant cell astrocytoma

Monika Siedlecka[1], Stanislaw Szlufik[1], Wieslawa Grajkowska[2,3], Marcin Roszkowski[4], Jarosław Jóźwiak[1]

[1]Department of Histology and Embryology, Medical University of Warsaw, [2]Department of Clinical and Experimental Neuropathology, Mossakowski Medical Research Centre, Polish Academy of Sciences, Warsaw, [3]Department of Pathology, The Children's Memorial Health Institute, Warsaw, [4]Department of Neurosurgery, The Children's Memorial Health Institute, Warsaw, Poland

Folia Neuropathol 2015; 53 (1): 8-14 DOI: 10.5114/fn.2015.49969

Abstract

Introduction: *Subependymal nodule (SEN) and subependymal giant cell astrocytoma (SEGA) are brain lesions frequently found in tuberous sclerosis (TS). As about 10-15% of SENs enlarge and transform into SEGAs, we examined here the possible mechanism of the phenomenon.*

Material and methods: *Using Western blot we studied 1 SEN and 3 SEGA samples; SEN and 1 SEGA came from the same TS patient. We evaluated e.g. the activation of the phosphorylated forms of proteins belonging to Akt, Erk and mTOR pathways.*

Results: *Differences in Erk pathway activation between SEN and SEGA were found. There was no upregulation of p-Erk, p-Mek or p-RSK1 in the SEN specimen, whilst we found these proteins to be significantly uptriggered in SEGA samples. Also, for the first time, we found p-Akt, p-GSK3β and p-PDK1 upregulated in both SEN and SEGA from the same TS patient.*

Conclusions: *Our current study shows for the first time the possible mechanism of SEN/SEGA transformation, where Erk pathway hyperactivation seems to be significant. We hypothesize that SEN/SEGA transformation may depend on Erk potentiation.*

Key words: *subependymal giant cell astrocytoma, subependymal nodule, Erk, tuberous sclerosis.*

Introduction

Tuberous sclerosis (TS) is a neurological autosomal dominant disorder, characterized by high variability of clinical presentation, as well as high penetrance, leading to an incidence estimated as 1 : 6000 [11]. Tuberous sclerosis may be associated with multiple hamartomas and neoplasms in several organs, mainly in the skin, brain, heart, kidneys and lungs [5,15]. The multisystem, usually benign, non-invasive lesions vary in size and number and are randomly distributed throughout the body. Thus, clinical manifestations can vary widely, even among close relatives. Major and minor clinical criteria serve to establish the diagnosis [15]. Recently, also genetic diagnostic criteria were postulated [17].

Brain-related manifestations are associated with the highest morbidity in TS patients. About 85% of patients suffer from neurological complications, such as epilepsy, intellectual disability or autism. Epilepsy

Communicating author:

Jarosław Jóźwiak, Department of Histology and Embryology, Center for Biostructure Research, Medical University of Warsaw, ul. Chalubinskiego 5, 02-004 Warsaw, Poland, fax: +48 22 629 52 82, e-mail: jaroslaw.jozwiak@gmail.com

is very often drug-resistant and has an early onset; seizures start during the first year of life in most patients [5]. Among neuropathological features of TS, the most frequent is the presence of cortical and subcortical tubers, a type of cortical dysplasia found in 90% of patients; subependymal nodules (SENs) are found in about 80% of TS patients and subependymal giant cell astrocytomas (SEGA; called subependymal giant cell tumors by some authors) occur in about 5-10% of TS patients.

Subependymal nodules are usually small, asymptomatic hamartomas, located in the lateral ventricles or adjacent to the caudate nucleus. Subependymal nodules usually develop during fetal life, and commonly calcify. The lesions can occur as single, irregular nodules, not exceeding 1 cm in diameter, or multiple lesions (forming "candle guttering"). On magnetic resonance imaging (MRI) scans, SENs are hyperintense on T1-weighted images, especially in neonates, whilst on T2-weighted images, because of their calcification, they exhibit an iso- or hypointense signal. Also variable enhancement after contrast injection is commonly seen, but this phenomenon is not considered to be of prognostic value [12]. In about 10-15% of cases SENs enlarge gradually and transform into SEGAs. This process is the fastest during the first 2 decades of life: SEGAs are rarely found in newborns, but their prevalence increases with age [5]. Histologically, the nodules consist of spindle glial cells and large cells, similar to giant cells in cortical tubers, positive for GFAP and sometimes for neuronal markers [10].

Subependymal giant cell tumors are low-grade (WHO grade 1) glial tumors, highly vascularised and located typically near the foramen of Monro, at the caudothalamic groove. The tumors consist of spindle cells, gemistocytic-like cells and giant cells. Immunohistochemical analysis reveals mainly glial, but also neuronal features. The dysmorphic glial cells in SEGA can form pseudorosettes or clusters. The giant cells are similar to those in cortical tubers. Also some foci of necrosis can be present, as well as some mitotic figures; the labeling index of Ki-67 is about 1% [1,2,4], although rare cases of higher mitotic index are also reported [3].

The diagnostic definition of SEGA includes caudothalamic groove lesions which exceed 1 cm in diameter or subependymal lesions growing consecutively, irrespective of the tumor size [15]. On CT, SEGAs are iso- or hyperattenuated and commonly calcified. On MRI they have mixed signal intensity and reveal strong enhancement after contrast administration [16]. Even though SEGAs grow slowly, eventually, because of their significant size, they can cause cerebrospinal flow obstruction, increase of intracranial pressure and hydrocephalus [10].

The clinical presentation results from mutation in the suppressor gene *TSC1* (tuberous sclerosis complex 1) or *TSC2* (tuberous sclerosis complex 2), encoding hamartin and tuberin, proteins forming a heterodimer. The hamartin-tuberin heterodimer acts in normal conditions as the suppressor of the mammalian target of rapamycin (mTOR), a serine-threonine kinase known as the central regulator of cellular growth, proliferation and protein synthesis. Mammalian target of rapamycin receives an input from various signals, such as growth factor stimulation, nutrient availability or the state of oxygenation. In TS, as the TSC1/TSC2 suppressor complex is nonfunctional, the upstream kinase cascades, such as protein kinase B (Akt) and extracellular signal-regulated kinase (Erk) pathways, are capable of mTOR upregulation through the phosphorylation of cell-cycle regulators as well as transcription factors [7].

In this study, we tried to determine why SENs start to grow and transform into SEGAs. First of all, we focused on mTOR kinase and its activators. It is already known that both Akt and Erk pathways can be upregulated in SEGAs [6,7]. However, we do not know any previous study on mTOR, Akt or Erk pathways on SEN specimens. For this reason, in the current study we examined for the first time the activation of the proteins belonging to the above-mentioned pathways in SEN and compared the results with the protein activation pattern in SEGAs.

Material and methods

Tissue samples

All studied SEN and SEGA samples, as well as control tissues, were retrieved from the Department of Pathology, Children's Memorial Hospital in Warsaw, Poland. Three studied SEGA samples and one SEN specimen from patients with TS complex, were classified by the neuropathologists, according to international criteria [14,15]. One of the SEGA samples came from the same TS patient from whom we obtained the SEN sample. As a positive control we used medulloblastoma, where Akt and Erk pathway activation was documented [17].

Sample preparation

Our research was performed by the Western blot method. All the lysates were prepared simultaneously, in order to avoid differences in conditions during sample processing. Tissues prepared for electrophoresis were homogenized in a tissue grinder with RIPA lysis buffer (20 mM Tris pH 7.5, 150 mM NaCl, 1% Nonident P-40, 0.5% sodium deoxycholate, 1 mM EDTA, 0.1% SDS) with 50 mM sodium fluoride and 1 mM sodium orthovanadate, supplemented with 1x Complete Protease Inhibitor (Roche, Indianapolis, IN) and Phosphatase Inhibitor Cocktail I (Sigma-Aldrich, St. Louis, MO). The storage temperature of prepared lysates was –80°C.

Western blot

Thawed tissue lysates were diluted in Bio-Rad's Laemmli Sample Buffer (62.5 mM Tris-HCl, pH 6.8; 25% glycerol; 2% SDS; 0.01% Bromophenol Blue; B-mercaptoethanol for a final concentration of 5% was added) in a 1 : 1 ratio. Subsequently the samples were heated for 5 minutes at 95°C. About 20 µg of protein tissue extract was put into each well of 10% polyacrylamide gel and subjected to SDS PAGE.

After completing SDS PAGE and electrophoretic transfer onto PVDF membrane, the blots were blocked with 5% non-fat dry milk in TBST (Tris buffered saline, 0.05% Tween). Afterwards, the membranes were incubated with the primary antibody (at 4°C, for 16 hours) and respective HRP-conjugated secondary antibody (for 30 minutes at room temperature; diluted with 2.5% non-fat dry milk in TBST). We used West Pico chemiluminescence substrate (Pierce, Rockford, IL) for protein detection. Equal protein loading was evaluated by Ponceau S and α-tubulin staining.

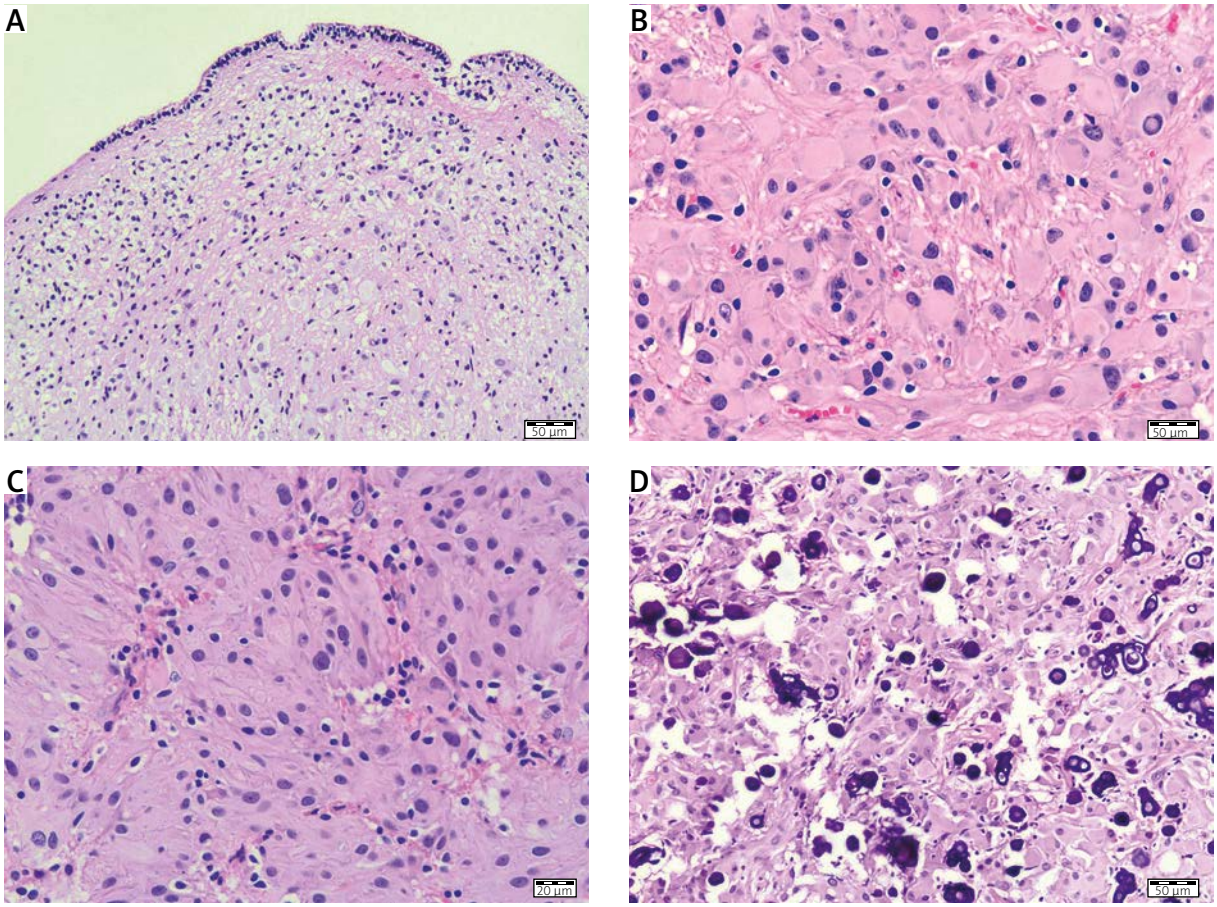

Fig. 1. A) Subependymal nodule covered by ependyma with largest cells in the central part of the lesion. **B)** Subependymal nodule showing large astrocytic cells with glassy cytoplasm. **C)** Subependymal nodule displaying spindle cell aggregate around blood vessels. **D)** Subependymal nodule with numerous calcifications. H&E staining.

Antibodies for Western blot

The following primary antibodies were purchased from Cell Signaling Technologies: PathScan PDGFR Activity Assay Multiplex Western Detection Cocktail; p-Akt/PKB Ser 473, p-GSK3β Ser 9, p-PDK1 Ser 24, p-S6rp Ser 235/236; p-MEK 1/2 Ser 221, p-p90-RSK Ser 380; p-Erk Thr 202/Tyr 204; total-Erk; Rheb; Raptor; eIF4E; p-SAPK/JNK Thr183/Tyr185.

The following primary antibodies were purchased from Santa Cruz Biotechnology: alpha-tubulin; cyclin D1; Bax; Bad; caspase 9.

Results

Neuropathological features

Histopathological features of both SEN and SEGAs were very similar (see Fig. 1A-D, Fig. 2A-D). They were composed of spindled, epithelioid and gemistocyte-like cells and gliovascular stroma. The SEN was covered by a layer of ependymal cells (Fig. 1A). In addition, the largest cells with abundant glassy cytoplasm were situated in the central portions and smaller cells at the periphery of the SEN (Fig. 1B and C). Subependymal nodule displayed several calcifications (Fig. 1D). No mitotic figures or necrosis were detected in either SEN or SEGAs.

Western blot results

In both types of samples (SEN and SEGA) we found increased activation of S6rp, a protein involved in translation and cell proliferation. Cyclin D1, a G1/S cell cycle phase transition regulator, appeared to be markedly increased in both types of tissues. Raptor protein (regulatory-associated protein of mTOR), interestingly, was expressed only in the SEN specimen (Fig. 3A).

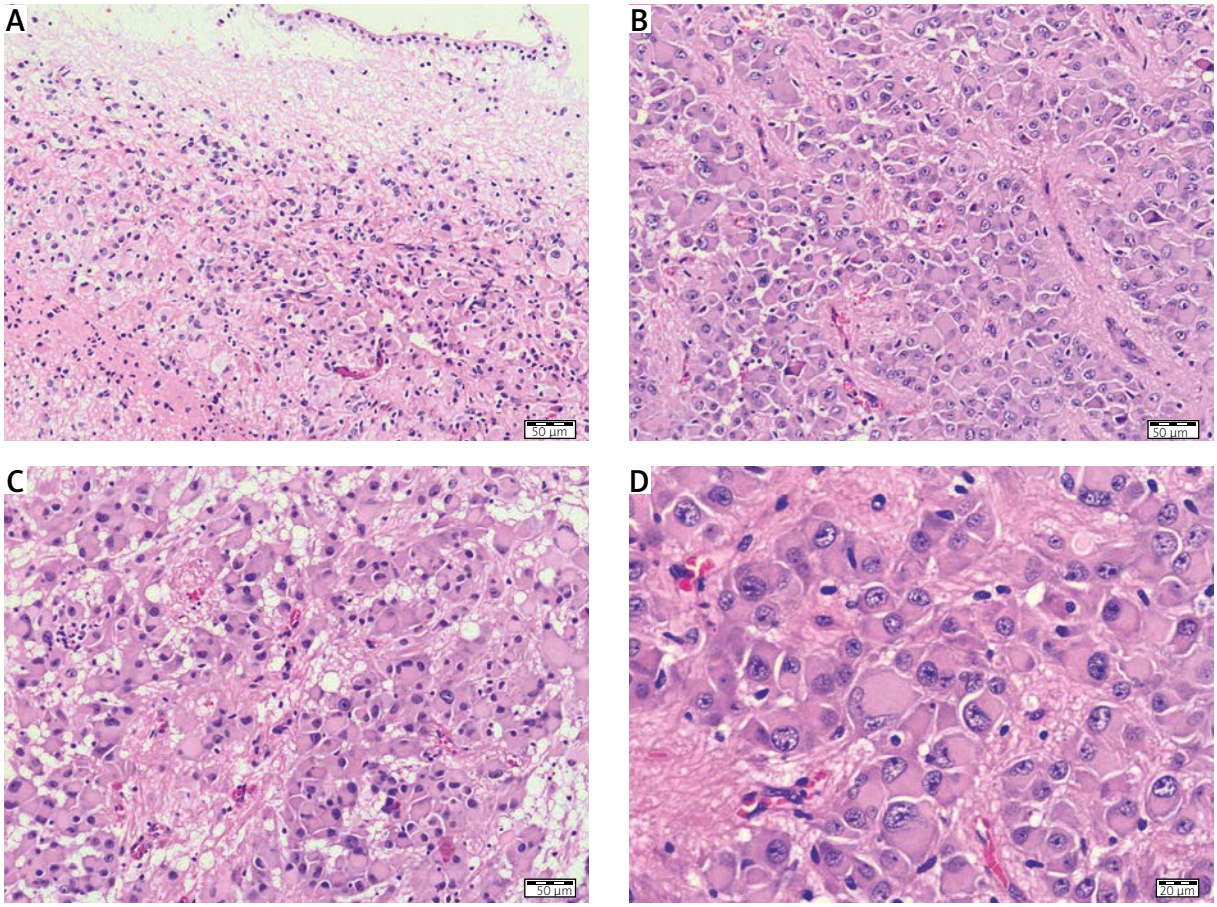

Fig. 2. Subependymal giant cell astrocytoma. **A)** Neoplastic cells covered by ependyma. **B)** Perivascular pseudorosettes. **C)** Gemistocytic-like cells in fibrillary background. **D)** Large, polygonal cells with abundant glassy cytoplasm and peripherally displaced nuclei. H&E staining.

Then, we focused on three proteins taking part in the Akt cascade: PDK1, Akt and GSK3β. We found that p-Akt, p-GSK3β (its effector) and p-PDK1, acting upstream of Akt, were upregulated in both SEN and SEGA from the same TS patient. The level of activation was similar in each sample and always significantly higher than in the control. Here, for the first time, we show Akt pathway activation in SEN (Fig. 3B).

As far as the Erk pathway is concerned, the results we obtained differ markedly for two types of lesions. Whilst there was no activation of p-Erk, p-Mek or p-RSK1 in the SEN specimen, these proteins were significantly uptriggered in SEGA samples. The level of total Erk in SEGA and SEN samples was increased, compared to the control.

Also phosphorylated forms of stress kinases SAPK/JNK (stress-activated protein kinase/c-Jun N-terminal kinases), other kinases from the Map kinase family, in both SEN and SEGA, were upregulated (Fig. 4).

We examined Bad and Bax proteins as well as caspase 9. Evaluation of these proteins, belonging to the apoptotic pathway, showed overactivation in

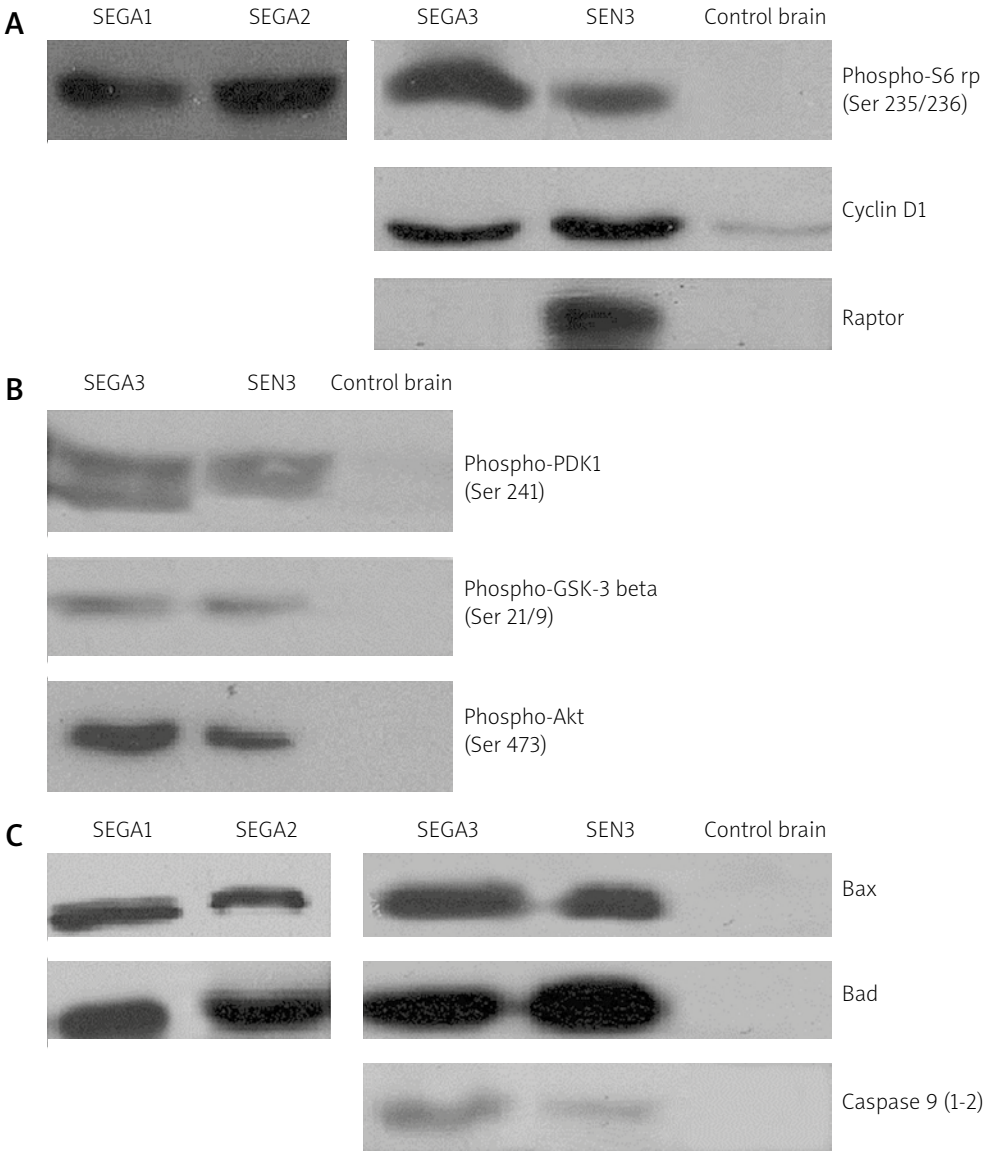

Fig. 3. Similarity of tumorigenic and apoptotic pathways in subependymal nodule (SEN) and subependymal giant cell astrocytoma (SEGA). **A)** Activation of mTOR effector, S6rp, cyclin D1 and raptor. **B)** Activation of Akt pathway. **C)** Activation of apoptosis.

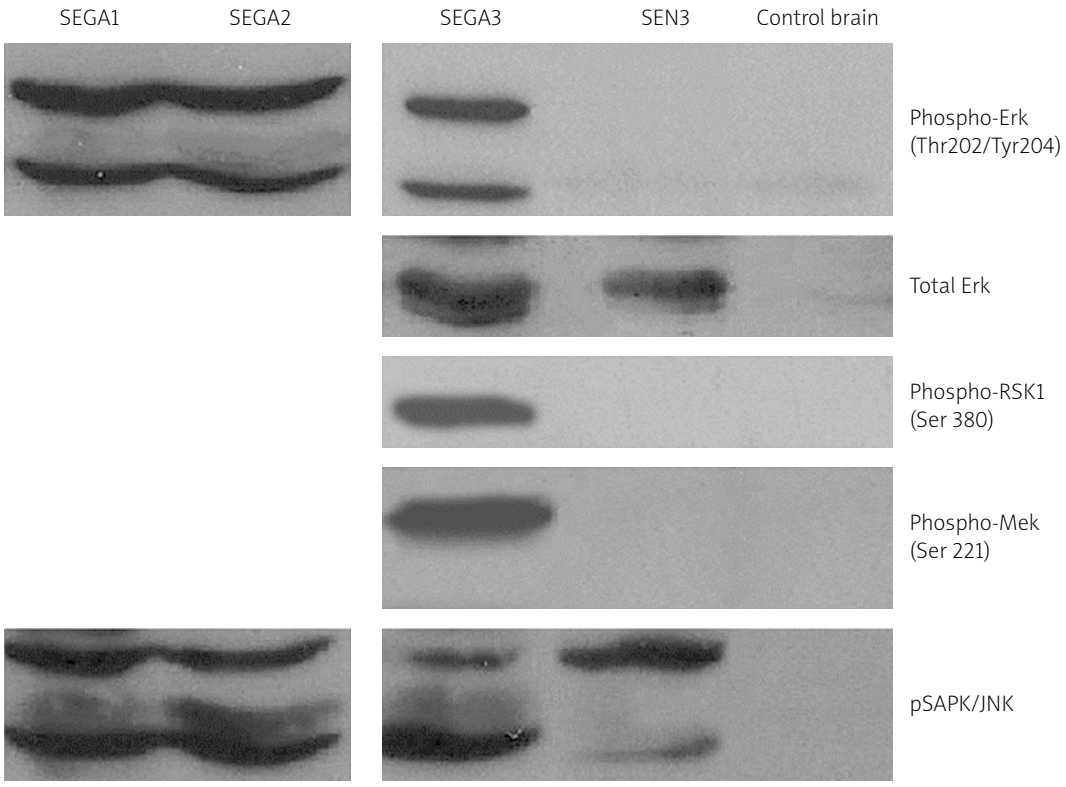

Fig. 4. Distinctive activation of Erk pathway in subependymal nodule (SEN), probably constituting the major difference between SEN and subependymal giant cell astrocytoma (SEGA).

both SEN and SEGA specimens, pointing to apoptosis activation (Fig. 3C).

Conclusions and discussion

Tumorigenesis is a complex phenomenon, involving disturbances of numerous signaling pathways: growth factor stimulation, cellular proliferation, apoptosis and cell death, DNA control, etc. The mammalian target of rapamycin pathway is located at the center of these events. Due to the fact that mTOR gathers signals associated with cellular well-being, such as the level of oxygen, nutrient availability or energy reserves, inhibiting cell proliferation if deficiency of any of these is detected, it is often a target of neoplastic transformation. Disturbances of pathways converging on mTOR are found in many epithelial tumors, including many CNS tumors of childhood [8,13].

Akt participation in mTOR pathway activation in TS has been quite well recognized so far. The effect of Erk on mTOR and, generally, its role in TS pathogenesis are still going through the stage of exploration. In general, the studies are performed on a few samples of SEGAs [5,6]. According to our knowledge, there are no previous investigations on SEN samples involving Akt, Erk or mTOR pathways.

In our earlier study [6] we observed both Akt and Erk hyperactivation in SEGA specimens. We also found that the Erk pathway plays a more important role in tumor formation in TS than Akt, as Erk hyperactivation without Akt was sufficient for tumor progression. The results of our current study appear to confirm this observation.

As we know, no single event results in tumorigenesis. Our current study sheds some light on the possible mechanism of SEN/SEGA transformation, for which Erk pathway hyperactivation in SEGA may be significant. Our study shows that activation of the "classical" Erk kinase cascade leading to mTOR activation through Mek and RSK1 is different in SEN and SEGA. Also, transcription upregulation, leading to cell growth, differentiation, survival or promotion of apoptosis by overactivation of the stress-activated protein kinases (SAPK)/Jun amino-terminal kinases (JNK), was observed. Although it is too early to demonstrate the exact mechanism leading to

SEGA appearance, one could suspect the following sequence of events: activation of PI3K/Akt, upregulation of mTOR (these two events leading to SEN formation, but too weak for the transformation of the cell into SEGA), and Erk activation (and thus appearance of SEGA). In view of the fact that SEN availability from human tissues is very scant, confirmation of this hypothesis may need some time. However, it may contribute to better future therapy of SEGA, as Erk inhibitors are already available on the market.

Disclosure

Authors report no conflict of interest.

References

1. Buccoliero AM, Franchi A, Castiglione F, Gheri CF, Mussa F, Giordano F, Gentori L, Taddei GL. Subependymal giant cell astrocytoma (SEGA): Is it an astrocytoma? Morphological, immunohistochemical and ultrastructural study. Neuropathology 2009; 29: 25-30.
2. Crino PB, Nathanson KL, Henske EP. The tuberous sclerosis complex. N Engl J Med 2006; 355: 1345-1356.
3. Grajkowska W, Kotulska K, Jurkiewicz E, Roszkowski M, Daszkiewicz P, Jóźwiak S, Matyja E. Subependymal giant cell astrocytomas with atypical histological features mimicking malignant gliomas. Folia Neuropathol 2011; 49: 39-46.
4. Gyure KA, Prayson RA. Subependymal giant cell astrocytoma: a clinicopathologic study with HMB45 and MIB-1 immunohistochemical analysis. Mod Pathol 1997; 10: 313-317.
5. Han S, Santos TM, Puga A, Roy J, Thiele EA, McCollin M, Stemmer-Rachamimov A, Ramesh V. Phosphorylation of tuberin as a novel mechanism for somatic inactivation of the tuberous sclerosis complex proteins in brain lesions. Cancer Res 2004; 64: 812-816.
6. Jozwiak J, Grajkowska W, Kotulska K, Jozwiak S, Zalewski W, Zajączkowska A, Roszkowski M, Slupianek A, Wlodarski P. Brain tumor formation in tuberous sclerosis depends on Erk activation. Neuromolecular Med 2007; 9: 117-127.
7. Jozwiak J, Jozwiak S, Wlodarski P. Possible mechanisms of disease development in tuberous sclerosis. Lancet Oncol 2008; 9: 73-79.
8. Jóźwiak J, Sontowska I, Bikowska B, Grajkowska W, Galus R, Roszkowski M. Favourable prognosis in medulloblastoma with extensive nodularity is associated with mitogen-activated protein kinase upregulation. Folia Neuropathol 2011; 49: 257-261.
9. Kalantari BN, Salamon N. Neuroimaging of tuberous sclerosis: spectrum of pathologic findings and frontiers in imaging. Am J Roentgenol 2008; 190: W304-W309.
10. Mizuguchi M, Takashima S. Neuropathology of tuberous sclerosis. Brain Dev 2001; 23: 508-515.
11. Northrup H, Krueger DA; International Tuberous Sclerosis Complex Consensus Group. Tuberous sclerosis complex diagnostic criteria update: recommendations of the 2012 International Tuberous Sclerosis Complex Consensus Conference. Pediatr Neurol 2013; 49: 243-254.
12. Osborne JP, Fryer A, Webb D. Epidemiology of tuberous sclerosis. Ann N Y Acad Sci 1991; 615: 125-127.
13. Rak B, Szlufik S, Grajkowska W, Perek D, Dembowska-Bagińska B, Filipek I, Daszkiewicz P, Włodarski P, Jóźwiak J. Upregulation of mitogen-activated protein kinase in ganglioglioma. Folia Neuropathol 2013; 51: 283-289.
14. Roach ES, Gomez MR, Northrup H. Tuberous sclerosis complex consensus conference: revised clinical diagnostic criteria. J Child Neurol 1998; 13: 624-628.
15. Roth J, Roach ES, Bartels U, Jóźwiak S, Koenig MK, Weiner HL, Franz DN, Wang HZ. Subependymal giant cell astrocytoma: diagnosis, screening, and treatment. Recommendations from the International Tuberous Sclerosis Complex Consensus Conference 2012. Pediatr Neurol 2013; 49: 439-444.
16. Rovira A, Ruiz-Falco ML, Garcia-Esparza E, Lopez-Laso E, Macaya A, Malaga I, Vazquez E, Vincente J. Recommendations for the radiological diagnosis and follow-up of neuropathological abnormalities associated with tuberous sclerosis complex. J Neurooncol 2014; 118: 205-223.
17. Włodarski P, Grajkowska W, Łojek M, Rainko K, Jóźwiak J. Activation of Akt and Erk pathways in medulloblastoma. Folia Neuropathol 2006; 44: 214-220.

Original article

Folia Neuropathologica

Laminar distribution of β-amyloid (Aβ) peptide deposits in the frontal lobe in familial and sporadic Alzheimer's disease

Richard A. Armstrong

Vision Sciences, Aston University, Birmingham, UK

Folia Neuropathol 2015; 53 (1): 15-23 DOI: 10.5114/fn.2015.49970

Abstract

To determine whether genetic factors influence frontal lobe degeneration in Alzheimer's disease (AD), the laminar distributions of diffuse, primitive, and classic β-amyloid (Aβ) peptide deposits were compared in early-onset familial AD (EO-FAD) linked to mutations of the amyloid precursor protein (APP) or presenilin 1 (PSEN1) gene, late-onset familial AD (LO-FAD), and sporadic AD (SAD). The influence of apolipoprotein E (Apo E) genotype on laminar distribution was also studied. In the majority of FAD and SAD cases, maximum density of the diffuse and primitive Aβ deposits occurred in the upper cortical layers, whereas the distribution of the classic Aβ deposits was more variable, either occurring in the lower layers, or a double-peaked (bimodal) distribution was present, density peaks occurring in upper and lower layers. The cortical layer at which maximum density of Aβ deposits occurred and maximum density were similar in EO-FAD, LO-FAD and SAD. In addition, there were no significant differences in distributions in cases expressing Apo E ε4 alleles compared with cases expressing the ε2 or ε3 alleles. These results suggest that gene expression had relatively little effect on the laminar distribution of Aβ deposits in the frontal lobe of the AD cases studied. Hence, the pattern of frontal lobe degeneration in AD is similar regardless of whether it is associated with APP and PSEN1, mutation, allelic variation in Apo E, or with SAD.

***Key words*:** *laminar distribution, β-amyloid (Aβ) peptide deposits, gene mutation.*

Introduction

The neuropathology of Alzheimer's disease (AD) is characterised by the formation of extracellular senile plaques (SP) and intracellular neurofibrillary tangles (NFT) [5,34]. The most important molecular constituent of the SP is β-amyloid (Aβ) [28], an approximately 4 kDa peptide arising by constitutive cleavage of a trans-membrane amyloid precursor protein (*APP*). A variety of Aβ peptides are formed as a result of secretase cleavage of *APP* [40]. The most common of these peptides is Aβ42, found largely in discrete Aβ deposits, whereas the more soluble Aβ40 is also found in association with blood vessels [37] and may develop later in the disease [21]. The discovery of Aβ led to the formulation of the 'amyloid cascade hypothesis' (ACH), one of the most important models of the molecular pathology of AD developed over the last 25 years [28]. Essentially, the ACH proposes that the deposition of Aβ is the initial pathological event in AD leading to the formation of NFT, cell death, and cortical degeneration [28].

At least four genetic loci are associated with AD: the *APP* gene on chromosome 21 [17,26], the prese-

Communicating author:

Dr Richard A. Armstrong, Vision Sciences, Aston University, Birmingham B4 7ET, UK, phone: 0121-204-4102, fax: 0121-204-4048, e-mail: R.A.Armstrong@aston.ac.uk

nilin *PSEN* genes on chromosome 14 (*PSEN1*) [47] and chromosome 1 (*PSEN2*) [32], and the apolipoprotein E (*Apo E*) gene on chromosome 19 [44]. *APP* and *PSEN* mutation may alter APP metabolism, resulting in increased deposition of Aβ peptide, while allelic polymorphism of *Apo E*, and especially the expression of allele ε4, may influence the proportion of the more fibrillogenic Aβ42 formed in the tissue [32,47]. These genetic factors, however, may not explain the majority of AD cases [27]. Hence, early-onset cases linked to *APP* and *PSEN* mutations may account for less than 5% of total AD [29]. Additional susceptibility genes and environmental factors are therefore likely to be involved, especially in sporadic AD (SAD) [38,39,41]. In isolated Amish communities, for example, 24 markers have been linked to dementia [33] and several other linkage studies have shown the presence of AD susceptibility genes on chromosomes 9, 10, and 12 [48]. Hence, a small number of AD cases have been linked recently to the chromosome 9 open reading frame 72 (*C9ORF72*) gene [55].

Three morphological subtypes of Aβ deposit are commonly observed in AD: 1) diffuse ('pre-amyloid') deposits, in which the Aβ is not in a fibrillar form with a β-pleated conformation, dystrophic neurites (DN) and paired helical filaments (PHF) being largely absent, 2) primitive ('neuritic') deposits, in which the Aβ is in a fibrillar form and is associated with DN and PHF, and 3) classic ('dense-cored') deposits, in which Aβ is highly aggregated to form a central amyloid plaque 'core' surrounded by a 'ring' of DN [3,8,10-12,20]. In the cerebral cortex in AD, Aβ deposits [2] and NFT [54] often exhibit significant variation in density across the cortex from pia mater to white matter, maximum density occurring within different layers [2,54]. The laminar distribution of Aβ deposits may be a consequence of degeneration of neural pathways that have their neurons of origin or axon terminals located within particular layers [22]. The main objective of this study was to determine whether genetic factors influence the laminar distribution of Aβ deposits and therefore result in a specific type of cortical degeneration in the frontal cortex in AD. Hence, laminar distributions of diffuse, primitive, and classic Aβ deposits were studied in three groups of cases: 1) early-onset familial Alzheimer's disease (EO-FAD) linked to mutations of either amyloid precursor protein (*APP717*) or presenilin 1 (*PSEN1: G209V*, *E280A*) genes, 2) late-onset familial AD (LO-FAD), and 3) sporadic AD (SAD). In addition, the influence of *Apo E* genotype on the distribution of Aβ deposits was studied.

Material and methods

Cases

Alzheimer's disease cases (N = 20; details in Table I) were obtained from the Brain Bank, Department of Neuropathology, Institute of Psychiatry, King's College, London, UK. Informed consent was given for the removal of all brain tissue according to the 1996 Declaration of Helsinki (as modified Edinburgh, 2000). Patients were clinically assessed and all fulfilled the 'National Institute of Neurological and Communicative Disorders and Stroke and the Alzheimer Disease and Related Disorders Association' (NINCDS/ADRDA) criteria for probable AD [52]. The histological diagnosis of AD was established by the presence of widespread neocortical SP consistent with the 'Consortium to Establish a Registry of Alzheimer Disease' (CERAD) criteria [34] and 'National Institute on Aging (NIA)-Reagan Institute' criteria [30,34]. The cases were divided into three groups: 1) EO-FAD (onset ≤ 65 years) (n = 4), 2) LO-FAD (≥ 65 years) (n = 6), and 3) SAD (n = 10) with no evidence of familial involvement.

Tissue preparation

A block of the frontal cortex was taken at the level of the genu of the corpus callosum to study the superior frontal gyrus (SFG). Tissue was fixed in 10% phosphate-buffered formal saline and embedded in paraffin wax. Both immunostaining and thioflavin S have been used to stain SP in AD [14,45]. Thioflavin S staining indicates that amyloid in these plaques contains fibrillar material with a β-pleated sheet conformation [14]. By contrast, immunohistochemistry generally reveals more plaques including diffuse Aβ deposits which are mainly thioflavin S-negative [14]. Hence, to label all types of plaque 7 µm coronal sections were immunolabelled with a rabbit polyclonal antibody (Gift of Prof. B.H. Anderton, Institute of Psychiatry, King's College London) raised to the 12-28 amino acid sequence of the Aβ protein and first used to identify Aβ deposit subtypes in Down's syndrome (DS) [50] but which also effectively distinguishes the major types of Aβ deposit in AD [4,6,7,10,50]. The antibody was used at a dilution of 1 in 1200 and the sections incubated at 4°C overnight. Sections were pretreated with

Table I. Demographic and genetic data of the Alzheimer's disease (AD) cases studied

Case	Sex	Age	Onset of disease	Group	Genetics	*Apo E*
1	M	65	–	EO-FAD	*APP717*	3/3
2	F	59	–	EO-FAD	*APP717*	3/3
3	F	61	–	EO-FAD	*PSEN1*	3/3
4	F	45	40	EO-FAD	*PSEN1*	2/3
5	F	72	66	LO-FAD	ND	2/3
6	F	86	80	LO-FAD	ND	3/4
7	F	77	72	LO-FAD	ND	3/3
8	F	79	68	LO-FAD	ND	3/4
9	F	85	76	LO-FAD	ND	3/3
10	F	89	–	LO-FAD	ND	3/3
11	M	80	77	SAD	–	3/3
12	F	87	82	SAD	–	3/4
13	F	64	59	SAD	–	4/4
14	F	91	83	SAD	–	3/4
15	M	73	66	SAD	–	2/3
16	F	82	75	SAD	–	ND
17	F	91	85	SAD	–	3/4
18	F	86	83	SAD	–	3/4
19	F	90	–	SAD	–	ND
20	M	82	78	SAD	–	3/3

Apo E – apolipoprotein E, APP – amyloid precursor protein, EO-FAD – early-onset familial Alzheimer's disease, LO-FAD – late-onset familial Alzheimer's disease, SAD – sporadic Alzheimer's disease, PSEN1 – presenilin 1, M – male, F – female, ND – not determined

98% formic acid for 6 minutes, which enhances Aβ immunoreactivity. Aβ was visualised using the streptavidin-biotin horseradish peroxidase procedure with diaminobenzidine as the chromogen. Sections were also stained with haematoxylin. Aβ deposits were identified in the sections using criteria published by Delaere *et al*. [20]: 1) diffuse deposits were 10-200 µm in diameter, lightly stained, irregular in shape, and with diffuse boundaries, 2) primitive deposits were 20-60 mm, well demarcated, symmetrical in shape, and strongly stained, and (3) classic deposits were 20-100 mm and had a distinct central amyloid core surrounded by a 'corona' of DN [20].

Morphometric methods

The distribution of the Aβ deposits in the SFG of each case was studied from the pia mater to white matter using methods described previously [23]. Five traverses from the pia mater to the edge of the white matter were located at random within each gyrus [9]. All deposits were then counted in 200 x 1000 µm sample fields arranged contiguously, the larger dimension of the field parallel with the surface of the pia mater. An eye-piece micrometer was used as the sample field and was moved down each traverse one step at a time from the pia mater to the edge of the white matter. Histological features of the section were used to correctly position the field. The mean of the counts from the five traverses was calculated to study variations in density of histological features across each cortical gyrus.

Data analysis

No attempt was made to locate precisely the boundaries between individual cortical layers. First, the degree of cortical degeneration present in many

gyri made laminar identification difficult. Second, identification was especially difficult in the frontal cortex because it exhibits a heterotypical structure, i.e., six layers cannot always be clearly identified and vary in prominence from case to case. Third, Aβ deposits appeared to exhibit complex patterns of distribution across the cortex rather than being confined to specific layers. Hence, variations in density of Aβ deposits with distance across the cortex were analysed using a polynomial curve-fitting procedure (STATISTICA software, StatSoft Inc., 2300 East 14th St, Tulsa, OK, 74104, USA) [2,49]. For each gyrus, polynomials of order 1, 2, 3 up to the 4th order were fitted successively to the data. Hence, second-order curves are parabolic, third-order curves are 'S' shaped, and fourth-order curves are double-peaked (bimodal). With each fitted polynomial, the correlation coefficients (Pearson's '*r*'), regression coefficients, standard errors of the mean (SEM), values of *t*, and the residual mean square were obtained. At each stage, the reduction in the sums of squares (*SS*) was tested for significance. A polynomial was accepted as the best fit using the procedure described by Snedecor and Cochran [49], viz. when either a non-significant value of *F* was obtained or there was little gain in explained variance. The distributions of the Aβ deposits across the cortex were classified initially into three groups: 1) a single density peak was present (unimodal distribution), peak density being located in either upper or lower layers, 2) two density peaks were present (bimodal distribution), density peaks occurring in upper and lower layers, and 3) there was no significant change in density across the cortex, Aβ deposits not being confined to particular layers. Bimodal distributions were then classified further according to whether the density peaks in the upper and lower layers were of similar or different magnitude. To study the effect of *Apo E* genotype, cases were classified into two groups: those not expressing allele ε4, i.e., genotypes ε2/3 and ε3/3, and those expressing at least one allele ε4, i.e., genotypes ε3/4 and ε4/4. In addition, the location of peak density and the maximum density of deposits were compared in EO-FAD, LO-FAD, and SAD. Hence, the point of maximum density (peak density) was identified for each deposit type for each gyrus while location of the peak was determined as the distance from the pia mater to that of the maximum density of Aβ deposits, expressed as a percentage of the total distance from the pia mater to the edge of the white matter.

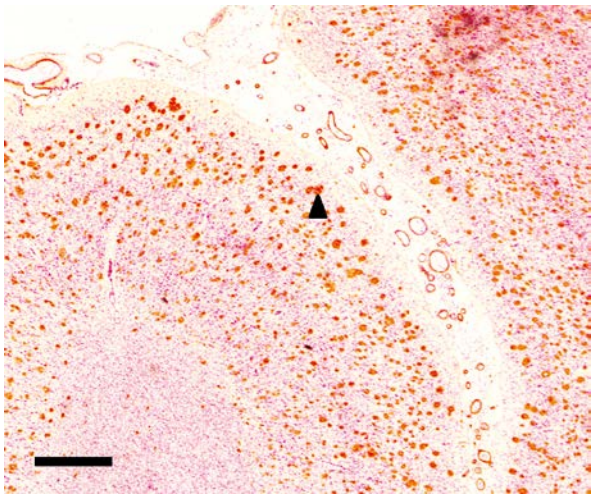

Fig. 1. Distribution of β-amyloid (Aβ) peptide deposits (arrowhead) in the superior frontal gyrus (SFG) in a case of early-onset familial Alzheimer's disease (EO-FAD) (*PSEN1* mutation). Aβ deposits occur across the cortex in all layers but with a greater density of larger-sized deposits in the upper layers. Aβ immunohistochemistry, haematoxylin, bar = 0.75 mm.

Results

Examples of the distribution of Aβ peptide deposits across the SFG are shown in Figures 1 and 2. In a case of EO-FAD (Fig. 1) (*PSEN1* mutation), Aβ deposits occurred across the cortex with a greater density of larger deposits in the upper layers. By contrast, in a case of SAD (Fig. 2), Aβ deposits occur largely in the lower layers.

Examples of the laminar distribution of the diffuse, primitive, and classic Aβ deposits in the SFG of a single EO-FAD case (case 2, *APP* mutation) is shown in Figure 3. The distribution of the diffuse deposits was fitted by a first-order (linear) regression ($r = 0.82$, $p < 0.01$) consistent with greater densities of diffuse deposits in the upper layers and a linear decrease in density across the cortex from pia mater to white matter. The distribution of the primitive Aβ deposits was fitted by a third-order polynomial ($r = 0.91$, $p < 0.001$) with a large density peak in the upper layers, while the classic deposits were also fitted by a third-order polynomial ($r = 0.82$, $p < 0.01$) with slightly higher densities adjacent to the pia mater and in the lower layers.

A comparison of the laminar distributions is shown in Table II. In FAD, diffuse Aβ deposits exhib-

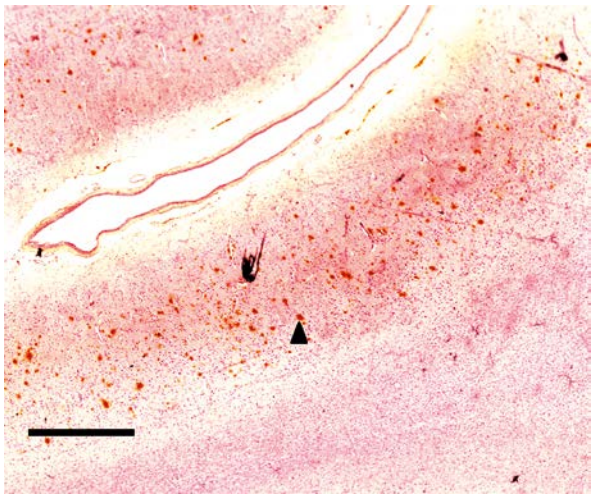

Fig. 2. Distribution of β-amyloid (Aβ deposits) (arrowhead) across the superior frontal gyrus (SFG) in a case of sporadic Alzheimer's disease (SAD). Aβ deposits occur largely in the lower layers. Aβ immunohistochemistry, haematoxylin, bar = 0.75 mm.

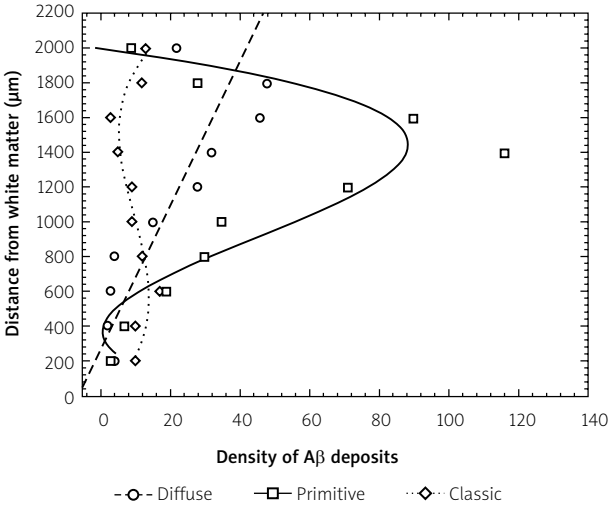

Fig. 3. Examples of the laminar distribution of the diffuse, primitive, and classic β-amyloid (Aβ deposits) in frontal lobe of a case of early-onset familial Alzheimer's disease (EO-FAD) (case 2, amyloid precursor protein (*APP*) gene mutation).

ited a density peak in the upper layers in 6/10 cases, and the primitive deposits did so in 9/10 cases. The distribution of the classic deposits was more variable; in 6/10 cases there was either a density peak in lower cortex or a bimodal distribution was present with density peaks in upper and lower layers. In SAD, diffuse and primitive Aβ deposits exhibited a density peak in the upper cortex in 7/10 cases and 9/10 cases respectively. Distribution of the classic Aβ deposits was more variable, a density peak in the lower layers or a bimodal distribution being present in 5/10 cases. The frequency of the various types of distribution of the diffuse (χ^2 = 3.74, p > 0.05), primitive (χ^2 = 0.71, p > 0.05), and classic (χ^2 = 11.18, p > 0.05) Aβ deposits was similar in EO-FAD, LO-SAD, and SAD.

Comparison of the mean location of maximum density and peak density of deposits among the three groups of cases is shown in Table III. Although there were significant differences in the layers at which peak density occurred among Aβ deposit subtypes (F = 4.44, p < 0.01), there were no significant differences among EO-FAD, LO-FAD, or SAD (F = 0.89, p > 0.05). In addition, there were no significant differences in peak density of Aβ deposits (F = 3.28, p > 0.05) among patient groups.

A comparison of the distributions exhibited by the Aβ deposits in cases classified according to *Apo E* genotype groups is shown in Table IV. There were no significant differences in distribution of diffuse (χ^2 = 2.55, p < 0.05), primitive (χ^2 = 0.003, p < 0.05), or classic (χ^2 = 3.41, p < 0.05) Aβ deposits in cases expressing *Apo E* genotypes ε2/3 and ε3/3, compared with those expressing genotypes ε3/4 and ε4/4.

Discussion

The objective of this study was to determine whether genetic factors were associated with a specific pattern of cortical degeneration, as revealed by the deposition of Aβ deposits in the frontal cortex in AD. The data confirm the need for quantitative assessment of Aβ deposition in different layers of cortex as deposits often occur over many layers with variation in abundance across the cortex. This study demonstrated: 1) laminar distributions of diffuse, primitive, and classic Aβ deposit subtypes were essentially similar in EO-FAD, LO-FAD, and SAD, 2) within FAD, laminar distributions were similar in *APP/PSEN1* cases compared with LO-FAD, and 3) laminar distributions were similar in cases expressing *Apo E* ε4 alleles compared with cases expressing ε2 or ε3 alleles.

The data suggest no significant differences in Aβ deposit density in EO-FAD, LO-FAD, and SAD or when cases were classified according to *Apo E* genotype. Previous quantitative studies comparing SP or Aβ

Table II. Comparison of the frequencies of different types of laminar distribution of β-amyloid (Aβ) deposits in superior frontal gyrus (SFG) in three groups of cases: early-onset familial Alzheimer's disease (EO-FAD), late-onset familial AD (LO-FAD), and sporadic AD (SAD). Data are the number of cases in which a particular type of laminar distribution is present

Group	Deposit type	Type of laminar distribution			
		UL	LL	B	NS
EO-FAD	Diffuse	3	0	1	0
	Primitive	4	0	0	0
	Classic	2	0	2	0
LO-FAD	Diffuse	3	1	1	1
	Primitive	5	0	0	1
	Classic	0	4	0	2
SAD	Diffuse	7	1	0	2
	Primitive	9	0	0	1
	Classic	2	4	1	3

Comparison of frequencies between groups: χ^2 contingency tables: diffuse deposits $\chi^2 = 5.09$ (6 DF, $p > 0.05$), primitive deposits $\chi^2 = 0.74$ (2 DF, $p > 0.05$), classic deposits $\chi^2 = 11.26$ (6 DF, $p > 0.05$)
UL – maximum Aβ deposit density occurred in upper cortical layers, LL – maximum Aβ deposit density occurred in lower cortical layers, B – bimodal distribution with peaks of density in upper and lower layers, NS – no significant change in density of Aβ deposits across the cortex

Table III. Comparison of mean peak location, i.e., percentage distance from the pia mater at which maximum density of β-amyloid (Aβ) deposits occurred expressed as a percentage of the width of the gray matter, and mean peak density, i.e., the actual density of deposits at the peak (mm^2) in the superior frontal gyrus (SFG) in three groups of cases: early-onset familial Alzheimer's disease (EO-FAD), late-onset familial AD (LO-FAD), and sporadic AD (SAD). Standard errors of the mean (SEM) are in parentheses

Group		Aβ deposit subtype		
		Diffuse	Primitive	Classic
EO-FAD	Peak location	32.5 (12.11)	21.3 (5.98)	40.0 (12.54)
	Peak density	36.5 (6.39)	86.5 (21.85)	12.3 (2.19)
LO-FAD	Peak location	39.5 (9.89)	31.7 (4.88)	51.7 (10.24)
	Peak density	28.0 (5.22)	70.3 (17.84)	8.17 (1.79)
SAD	Peak location	32.0 (9.66)	27.20 (3.69)	55.10 (6.09)
	Peak density	20.8 (3.20)	38.3 (10.76)	10.3 (1.50)

Analysis of variance (ANOVA): 1) Peak location: patient group $F = 0.89$ ($p > 0.05$), deposit type $F = 4.44$ ($p < 0.01$), interaction $F = 0.22$ ($p > 0.05$); 2) Peak density: patient group $F = 3.28$ ($p > 0.05$), deposit type $F = 18.73$ ($p < 0.001$), interaction $F = 1.36$ ($p > 0.05$)

deposit abundance in FAD and SAD have been controversial [16,18,24,36]. Hence, no significant differences in severity scores of SP were observed in FAD and SAD [36], and Aβ 'load' in the frontal cortex and temporal isocortex was similar in SAD and FAD cases linked to the APP_{717} mutation [16]. Nevertheless, cultured cells expressing a double mutation in *APP* produced six times more Aβ than normal cells [18]. In addition, other studies have reported increased amyloid deposition in individuals expressing allele ε4 [24]. However, it is possible that Aβ deposition could be more widely distributed across the cortical layers of the SFG in FAD, but with similar peak densities.

In the SFG of both SAD and FAD, maximum density of the diffuse and primitive Aβ deposits occurred most frequently in the upper layers. By contrast, the distribution of the classic deposits was more variable, peak densities occurring either in the lower lay-

Table IV. Comparison of frequencies of different types of laminar distribution of Aβ deposits in superior frontal gyrus (SFG) of Alzheimer's disease (AD) cases divided into two groups according to apolipoprotein (*Apo E*) genotype, i.e., those expressing genotypes ε2/3 and ε3/3 compared with those expressing genotypes ε3/4 and ε4/4. Data are the number of cases in which a particular type of laminar distribution is present

Group	Aβ deposit subtype	Laminar distribution			
		UL	LL	B	NS
ε2/3, ε3/3	Diffuse	8	0	2	1
	Primitive	10	0	0	1
	Classic	3	4	2	2
ε3/4, ε4/4	Diffuse	7	0	0	0
	Primitive	7	0	0	0
	Classic	1	5	0	1

Chi-square (χ^2) contingency tables: diffuse deposits $\chi^2 = 2.29$ (2 DF, $p > 0.05$), primitive deposits $\chi^2 = 0.006$ (1 DF, $p > 0.05$), classic deposits $\chi^2 = 2.69$ (3 DF, $p > 0.05$) UL – maximum Aβ deposit density occurred in upper cortical layers, LL – maximum Aβ deposit density occurred in lower cortical layers, B – bimodal distribution with peaks of density in upper and lower layers, NS – no significant change in density of Aβ deposits across the cortex

ers, or in both upper and lower layers. Similar results have been reported in studies of the laminar distribution of SP [15,19], Apo E-immunoreactive SP [53], neuritic plaques (NP) [42], and Aβ deposits in AD [2], which are frequently abundant in layers II and III. In addition, in a transgenic mouse model expressing the APP_{717} mutation, Aβ deposits were most abundant in layers II and III, similar to AD [51]. However, aged dogs often show a different distribution of Aβ deposits to humans, being usually abundant in the deep cortical layers but with evidence of spread to superficial cortical layers with increasing age [43].

Various hypotheses could explain the laminar distribution of Aβ deposits in the SFG in AD. First, mRNA of APP is preferentially expressed by the large pyramidal neurons in layers III and V [13]. Degeneration of these neurons could then result in increased secretion of APP and formation of Aβ deposits within these layers [4]. Second, interleukin-immunoreactive microglia (IL-Mg) have a similar laminar distribution as APP-immunoreactive NP [46]. Hence, the laminar distribution of microglia could be a factor determining the distribution of the Aβ deposits. Third, the laminar distribution of the classic deposits could be spatially related to blood vessels [2,37]. Large blood vessels often exhibit a bimodal distribution in the cortex, whereas smaller capillaries occur at maximum density in the deeper layers [2]. In addition, Akiyama *et al*. [1] found that Aβ deposits accumulated vertically in columns, with blood vessels often occurring perpendicular to the column and penetrating its centre. Previous studies suggest, however, that although classic Aβ deposits are clustered around blood vessels in SAD [6], there are fewer spatial associations with blood vessels in FAD [7].

Laminar distributions of Aβ deposits in frontal lobe AD are essentially similar in the FAD and SAD cases examined and similar whether *Apo E* allele ε4 was present or not [31]. In addition, among FAD cases, there was no evidence that a specific type of laminar distribution was influenced by genetic subtype. Hence, neither *APP/PSEN1* mutations nor the presence of *Apo E* allele ε4 uniquely determines Aβ deposition and therefore the pattern of frontal lobe degeneration in AD. Uchihara *et al*. [53] found that Apo E labelled a subset of deposits in lamina III with more Apo E-immunoreactive diffuse deposits in the deeper layers. However, only a proportion of the diffuse deposits were Apo E-immunoreactive, suggesting that Apo E was not involved in the process of cortical degeneration but immunoreactivity was acquired by certain deposits later in the disease. Hence, pathological changes initiated by the various genetic changes in FAD and, by other causes in SAD, appear to follow a parallel course resulting in very similar patterns of cortical degeneration in the SFG.

In conclusion, there were no essential differences in the laminar distribution of the Aβ deposits in the SFG between FAD and SAD, or between different subtypes of FAD. Hence, *APP* and *PSEN1* mutations and the presence of *Apo E* genotype ε4 appear to have little influence on laminar distribution. Although the

mechanism of generating fibrillogenic species of Aβ may differ among disease subtypes, gene expression appears to have little effect on the pattern of degeneration of the frontal lobe in AD.

Acknowledgments

Brain tissue sections for this study were kindly provided by the Brain Bank, Department of Neuropathology, Institute of Psychiatry, King's College London, UK. Mrs Mavis Kibble and Mr Alan Brady are thanked for technical help with tissue preparation.

Disclosure

Author reports no conflict of interest.

References

1. Akiyama H, Yamada T, McGeer PL, Kawamata T, Tooyama I, Ishii T. Columnar arrangement of beta-amyloid deposits in the cerebral cortex of patients with Alzheimer's disease. Acta Neuropathol 1993; 85: 400-403.
2. Armstrong RA. β-amyloid (Aβ) deposits and blood vessels: laminar distribution in frontal cortex of patients with Alzheimer's disease. Neurosci Res Comms 1996; 18: 19-28.
3. Armstrong RA. β-amyloid plaques: stages in life history or independent origin? Dement Geriatr Cogn Disord 1998; 9: 227-238.
4. Armstrong RA. Diffuse β-amyloid (Aβ) deposits and neurons: in situ secretion or diffusion of Aβ? Alz Rep 2001; 3: 289-294.
5. Armstrong RA. Plaques and tangles and the pathogenesis of Alzheimer's disease. Folia Neuropathol 2006; 44: 1-11.
6. Armstrong R. Classic β-amyloid deposits cluster around large diameter blood vessels rather than capillaries in sporadic Alzheimer's disease. Curr Neurovasc Res 2006; 3: 289-294.
7. Armstrong RA. Spatial correlations between β-amyloid (Aβ) deposits and blood vessels in familial Alzheimer's disease. Folia Neuropathol 2009; 46: 241-248.
8. Armstrong RA. A spatial pattern analysis of β-amyloid (Aβ) deposition in the temporal lobe in Alzheimer's disease. Folia Neuropathol 2010; 48: 67-74.
9. Armstrong RA. Quantitative methods in neuropathology. Folia Neuropathol 2010; 48: 217-230.
10. Armstrong RA. Spatial patterns of β-amyloid (Aβ) deposits in familial and sporadic Alzheimer's disease. Folia Neuropathol 2011; 49: 153-161.
11. Armstrong RA. β-amyloid (Aβ) deposition in cognitively normal brain, dementia with Lewy bodies, and Alzheimer's disease. Folia Neuropathol 2012; 50: 130-139.
12. Armstrong RA. Size frequency distributions of β-amyloid (Aβ) deposits: a comparative study of four neurodegenerative disorders. Folia Neuropathol 2012; 50: 240-249.
13. Bahmanyar S, Higgins GA, Goldgaber D. Localization of amyloid β protein messenger RNA in brains from patients with Alzheimer's disease. Science 1987; 237: 77-80.
14. Bussiere T, Bard F, Barbour R, Grajeda H, Guido T, Khan K, Schenk D, Games D, Seubert P, Buttini M. Morphological characterization of thioflavin-S-positive plaques in transgenic Alzheimer mice and effect of passive Aβ immunotherapy on their clearance. Am J Pathol 2004; 165: 987-995.
15. Braak H, Braak E, Kalus P. Alzheimer's disease: areal and laminar pathology in the occipital isocortex. Acta Neuropathol 1989; 77: 494-506.
16. Cairns NJ, Chadwick A, Lantos PL, Levy R, Rossor M. βA4 protein load in familial Alzheimer's disease with the mutation in codon 717 of the βA4 amyloid precursor protein gene and sporadic Alzheimer's disease. Neurosci Lett 1993; 149: 137-140.
17. Chartier-Harlin MC, Crawford F, Houlden H, Warren A, Hughes D, Fidani L, Goate A, Rossor M, Rocques P, Hardy J, Mullan M. Early onset Alzheimer's disease caused by mutations at codon 717 of the β-amyloid precursor protein gene. Nature 1991; 353: 844-846.
18. Citron M, Oltersdorf T, Haass C, McCoulogue L, Hung AY, Seubert P, Vigo-Pelfrey C, Lieberburg I, Selkoe DJ. Mutation of β-amyloid precursor protein in familial Alzheimer's disease increases β-protein production. Nature 1992; 360: 672-674.
19. Delaere P, Duyckaerts C, Brion JP, Poulain V, Hauw JJ. Tau, paired helical filaments and amyloid in the neocortex: A morphometric study of 15 cases with graded intellectual status in aging and senile dementia of the Alzheimer type. Acta Neuropathol 1989; 77: 645-653.
20. Delaere P, Duyckaerts C, He Y, Piette F, Hauw JJ. Subtypes and differential laminar distribution of β/A4 deposits in Alzheimer's disease: relationship with the intellectual status of 26 cases. Acta Neuropathol 1991; 81: 328-335.
21. Delacourte A, Sergeant N, Champain D. Wattez A, Maurage CA, Lebert F, Pasquier F, David JP. Nonoverlapping but synergetic tau and amyloid precursor protein pathologies in sporadic Alzheimer's disease. Neurology 2002; 59: 398-407.
22. De Lacoste M, White CL III. The role of cortical connectivity in Alzheimer's disease pathogenesis: a review and model system. Neurobiol Aging 1993; 14: 1-16.
23. Duyckaerts C, Hauw JJ, Bastenaire F, Piette F, Poulain C, Rainsard V, Javoy-Agid F, Berthaux P. Laminar distribution of neocortical senile plaques in senile dementia of the Alzheimer type. Acta Neuropathol 1986; 70: 249-256.
24. Gearing M, Schneider JA, Robins RS, Hollister RD, Mori H, Games D, Hyman BT, Mirra SS. Regional variations in the distribution of Apolipoprotein E and Aβ in Alzheimer's disease. J Neuropath Exp Neurol 1995; 54: 833-841.
25. Glenner GG, Wong CW. Alzheimer's disease and Down's syndrome: sharing of a unique cerebrovascular amyloid fibril protein, Biochem Biophys Res Commun 1984; 122: 1131-1135.
26. Goate R, Chartier-Harlin M-C, Mullan M, Brown J, Crawford F, Fidani L, Giuffra L, Haynes A, Irving N, James L, Mant R, Newton P, Rooke K, Roques P, Talbot C, Pericak-Vance, Roses A, Williamson R, Rossor M, Owen M, Hardy J. Segregation of a missense mutation in the amyloid precursor protein gene with familial Alzheimer's disease. Nature (London) 1991; 349: 704-706.
27. Grazini M, Prabas J, Silva F, Oliveira S, Santana I, Oliveira C. Genetic basis of Alzheimer's dementia: role of mitochondrial DNA mutations. Genes, Brain, and Behaviour 2006; 5 (Suppl 2): 92-107.

28. Hardy JA, Higgins GA. Alzheimer's disease: The amyloid cascade hypothesis. Science 1992; 256: 184-185.
29. Hoenicka J. Genes in Alzheimer's disease. Revista de Neurolgia 2006; 42: 302-305.
30. Jellinger KA, Bancher C. Neuropathology of Alzheimer's disease: a critical update. J Neural Transm 1998; 54: 77-95.
31. Kida E, Pluta R, Lossinsky AS, Golabek AA, Choimiura NH, Wisniewski HM, Mossakowski MJ. Complete cerebral ischemia with short-term survival in rat induced by cardiac-arrest. II. Extracellular and intracellular accumulation of apolipoproteins E and J in the brain. Brain Res 1995; 674: 341-346.
32. Levy-Lahad E, Wijsman EM, Nemens E, Anderson L, Goddard KA, Weber JL, Bird TD, Schellenberg GD. A familial Alzheimer's disease locus on chromosome 1. Science 1995; 269: 970-973.
33. McCauley JL, Hahs DW, Jiang L, Scott WK, Welsh-Bohmer KA, Jackson CE, Vance JM, Pericak-Vance MA, Haines JL. Combinatorial Mismatch Scan (CMS) for loci associated with dementia in the Amish. BMC Med Genet 2006; 7: 19.
34. Mirra SS, Heyman A, McKeel D, Sumi SM, Crain BJ, Brownlee LM, Vogel FS, Hughes JP, van Belle G, Berg L, et al. The Consortium to Establish a Registry for Alzheimer's Disease (CERAD). Part II. Standardization of the neuropathological assessment of Alzheimer's disease. Neurology 1991; 41: 479-486.
35. Newell KL, Hyman BT, Growden JH, Hedley-Whyte ET. Application of the National Institute on Aging (NIA)-Reagan Insitute criteria for the neuropathological diagnosis of Alzheimer's disease. J Neuropathol Exp Neurol 1999; 58: 1147-1155.
36. Nochlin D, Van Belle G, Bird TD, Sumi SM. Comparison of the severity of neuropathologic changes in familial and sporadic Alzheimer's disease. Alz Dis Assoc Dis 1993; 7: 212-222.
37. Pluta R, Barcikowska M, Januszewski S, Misicka A, Lipkowski AW. Evidence of blood-brain barrier permeability/leakage for circulating human Alzheimer's beta-amyloid-(1-42)-peptide. Neuroreport 1996; 7: 1261-1265.
38. Pluta R, Jabloński M, Czuczwar SJ. Postischemic dementia with Alzheimer phenotype: selectively vulnerable versus resistant areas of the brain and neurodegeneration versus β-amyloid peptide. Folia Neuropathol 2012; 50: 101-109.
39. Pluta R, Kocki J, Maciejewski R, Ulamek-Koziol M, Jabloński M, Bogucka-Kocka A, Czuczwar SJ. Ischemia signalling to Alzheimer-related genes. Folia Neuropathol 2012; 50: 322-329.
40. Pluta R, Furmaga-Jablonska W, Maciejewski R, Ulamek-Koziol M, Jablonski M. Brain ischaemia activates beta- and gamma-secretase cleavage of amyloid precursor protein: Significance in sporadic Alzheimer's disease. Mol Neurobiol 2013; 47: 425-434.
41. Pluta R, Jablonski M, Ulamek-Koziol M, Kocki J, Brzozowska J, Januszewski S, Furmaga-Jablonska W, Bogucka-Kocka A, Maciejewski R, Czuczwar S. Sporadic Alzheimer's disease begins as episodes of brain ischemia and ischemically dysregulated Alzheimer's disease genes. Mol Neurobiol 2013; 48: 500-515.
42. Rafalowska J, Barcikowska M, Wen GY, Wisniewski HM. Laminar distribution of neuritic plaques in normal aging, Alzheimer's disease and Downs syndrome. Acta Neuropathol 1988; 77: 21-25.
43. Satou T, Cummings BJ, Head E, Nielson KA, Hahn FF, Milgram NW, Velaquez P, Cribbs DH, Tenner AJ, Cotman CW. The progression of beta-amyloid deposition in the frontal cortex of the aged canine. Brain Res 1997; 774: 35-43.
44. Saunders A, Strittmatter W, Schmechel D, St. George-Hyslop P, Pericak-Vance M, Joo S, Rose B, Gasella J, Crapper-MacLachan D, Albersts M, Hulette C, Crain B, Goldgaber D, Roses A. Association of apolipoprotein E allele e4 with late-onset familial and sporadic Alzheimer's disease. Neurology 1993; 43: 1467-1472.
45. Serrano-Pozo A, Mielke ML, Muzitansky A, Gomez-Isla T, Growdon JH, Bacskai BJ, Betensky RA, Frosch MP, Hyman BT. Stable size distribution of amyloid plaques over the course of Alzheimer's disease. J Neuropath Exp Neurol 2012; 71: 694-701.
46. Sheng JG, Griffin VST, Roystan MC, Mrak RE. Distribution of interleukin-1-immunoreactive microglia in cerebral cortical layers: implications for neuritic plaque formation in Alzheimer's disease. Neuropath Appl Neurobiol 1998; 24: 278-283.
47. Sherrington R, Rogaev E, Liang Y, Rogaeva E, Levesque G, Ikeda M, Chi H, Lin C, Li G, Holman K, Tsuda T, Mar L, Foncin J, Bruni A, Moulese M, Sorbi S, Rainero I, Pinessi L, Nee L, Chumakov I, Pollen D, Brookes A, Sauseau P, Polinski R, Wasco, R, Dasilva H, Haines J, Pericak-Vance M, Tanzi R, Roses A, Fraser P, Rommens J, St George-Hyslop P. Cloning of a gene bearing missense mutations in early onset familial Alzheimer's disease. Nature 1993; 375: 754-760.
48. Sillén A, Forsell C, Lilius L, Axwlman K, Björk B, Onkamo P, Kere J, Winblad B, Graff C. Genome scan on Swedish Alzheimer disease families. Mol Psychiatry 2006; 11: 182-186.
49. Snedecor GW, Cochran WG. Statistical Methods. Iowa State University Press, Ames 1980.
50. Spargo E, Luthert PJ, Anderton BH, Bruce M, Smith D, Lantos PL. Antibodies raised against different proteins of A4 protein identify a subset of plaques in Down's syndrome. Neurosci Lett 1990; 115: 345-350.
51. Su Y, Ni BH. Selective deposition of amyloid-beta protein in the entorhinal-dentate projection of a transgenic mouse model of Alzheimer's disease. J Neurosci Res 1998; 53: 177-186.
52. Tierney MC, Fisher RH, Lewis AJ, Zorzitto ML, Snow WG, Reid DW, Nieuwstraten P. The NINCDS-ADRDA work group criteria for the clinical diagnosis of probable Alzheimer's disease. Neurology 1988; 38: 359-364.
53. Uchihara T, Duyckaerts C, Lazarini F, Mokhtari K, Seilhean D, Amouyel P, Hauw JJ. Inconsistent apolipoprotein (Apo E)-like immunoreactivity in amyloid beta protein deposits: relationship with Apo E genotype in aging brain and Alzheimer's disease. Acta Neuropathol 1996; 92: 180-185.
54. Van Hoesen GW, Parvizi J, Chu CC. Orbitofrontal cortex/pathology in Alzheimer's disease. Cerebral Cortex 2000; 10: 243-251.
55. Wallon D, Rovelet-Lecrux A, Deramecourt V, Pariente J, Auriacombe S, Le Ber I, Schraen S, Pasquier F, Campion D, Hannequin D. Definite behavioural variant of frontotemporal dementia with C9ORF72 expansions despite positive Alzheimer's disease cerebrospinal fluid biomarkers. J Alz Dis 2012; 32: 19-22.

Original paper

Folia Neuropathologica

Association of the rs1801133 variant in the *MTHFR* gene and sporadic Parkinson's disease

Silvia García[1], Ramón Mauricio Coral-Vázquez[2], Martha P. Gallegos-Arreola[3], Luis Ángel Montes-Almanza[1,4], Patricia Canto[1], Froylan Arturo García-Martínez[1,4], Gerardo Chavira-Hernández[1,5], Carlos Palma-Flores[1], Luis Dávila-Maldonado[6], Carlos F. Cuevas-García[7], Luz Berenice López Hernández[1]

[1]Centro Médico Nacional "20 de Noviembre", Instituto de Seguridad y Servicios Sociales de los Trabajadores del Estado, México, D.F., [2]Sección de Investigación y Estudios de Posgrado, Escuela Superior de Medicina, Instituto Politécnico Nacional, México, D.F., [3]Centro de Investigación Biomédica de Occidente, Jalisco, [4]Universidad Nacional Autónoma de México, México, D.F., [5]Universidad de Guadalajara, Centro Universitario de Ciencias de la Salud, México, [6]Instituto de Ciencias Médicas y de la Nutrición Salvador Zubirán, México, D.F., [7]Centro Médico Nacional Siglo XXI, Instituto Mexicano del Seguro Social, México, D.F., México

Folia Neuropathol 2015; 53 (1): 24-28 DOI: 10.5114/fn.2015.49971

Abstract

The MTHFR gene has been reported as a susceptibility locus for sporadic Parkinson's disease (sPD). The functional variant rs1801133 has been linked to hyperhomocysteinemia and dopaminergic cell death. Among different populations, Mexican-Mestizos (most present-day Mexicans) have the highest frequency of this variant. Therefore, we sought to determine a possible association of rs1801133 with SPD. In total, 356 individuals were included: 140 patients with PD, diagnosed according to the Queen Square Brain Bank criteria, and 216 neurologically healthy controls. Genotyping was performed using TaqMan probes for rs1801133 and real-time PCR. Logistic regression analysis with adjustment for smoking and gender was used to test for an association between genotype and SPD. The CC genotype was associated with SPD; exp(β) = 2.06; 95% CI: 1.101-3.873, p = 0.024. No association with age at onset, cognitive impairment or gender was found in our study group. Our data suggest an important role of MTHFR gene variants in SPD.

Key words: *rs1801133, MTHFR, Parkinson's disease, common variants, C677T, Mexico.*

Introduction

Parkinson's disease (PD) is a multifactorial neurodegenerative disease that affects about 1-2% of people older than 65 years [23], sporadic cases (sPD) being more frequent than familial ones. Among genetic factors influencing PD, rare variants in *PARK* genes such as *LRRK2* (PARK8) and *SNCA* (PARK1) [2,5] are known to play a major role in PD pathogenesis (rare variant common disease hypothesis) [3,14]. However, it is possible that common variants in other genes account for part of the unrevealed heritability of PD (the common variant common disease hypothesis) [16]. In this regard, the *MTHFR* gene has been

Communicating author:
Luz Berenice López Hernández, PhD, Subdirección de Enseñanza e Investigación, Centro Médico Nacional 20 de Noviembre, Instituto de Seguridad y Servicios Sociales de los Trabajadores del Estado, San Lorenzo 502, C.P. 03100, México, D.F., México, phone: 01 52 55 52 00 50 03, fax: 01 52 33 36 32 62 00, e-mail: lblhmedgen@gmail.com

recently proposed as a candidate risk gene for PD by two independent meta-analyses [24,25].

The enzyme MTHFR (EC 1.5.1.20) catalyzes the transformation of 5,10-methylenetetrahydrofolate to 5-methyltetrahydrofolate, a co-substrate for homocysteine remethylation to methionine. The T allele of the functional rs1801133 variant in this gene generates a thermolabile enzyme with reduced activity. The homozygous state of this variant (TT) has been linked to elevated plasma homocysteine (Hcy) levels [9], although optimal folate and vitamin B_{12} intake can counteract the effect of genotype [12]. Elevated Hcy may hasten dopaminergic cell death through oxidative stress and excitotoxicity [7,18].

Variants in the *MTHFR* gene may also influence the response to treatment, since impaired transmethylation potential has been detected in hyperhomocysteinemic L-dopa-treated PD patients [6].

Among different populations, Mexican-Mestizos (most present-day Mexicans) have the highest frequency of the T allele [20]; therefore we sought to determine whether rs1801133 is associated with SPD in our population.

Material and methods

Patients and controls

We conducted a case-control study that included 140 SPD patients and 216 neurologically healthy controls. Institutional Committees approved the study and informed written consent was obtained from participants. Patients were recruited from February 2009 to June 2010, from four tertiary-care level hospitals in Mexico (Neurology Departments from Centro Médico Nacional "20 de Noviembre" – ISSSTE, Centro Médico Nacional Siglo XXI-IMSS, Instituto de Ciencias Médicas y de la Nutrición "Salvador Zubirán", Mexico City; and División de Genética, Centro de Investigación Biomédica de Occidente-IMSS, Jalisco, Mexico). Diagnosis was performed according to Queen Square Brain Bank criteria [15]. The threshold for early-onset Parkinson's disease (EOPD) was considered as onset earlier than 40 years old. Cognitive impairment was assessed using the Folstein Mini Mental State Examination Test. We did not measure plasma Hcy levels because most PD patients could show elevated levels derived from pharmacological therapy with L-dopa. Controls were healthy blood bank donors or patients' spouses who agreed to participate in an additional neurological evaluation; they were Mexican-Mestizos without family history of neurodegenerative disorders.

DNA isolation and genotyping

DNA was extracted from peripheral blood samples by the DTAB CTAB method [13]. Genotyping was performed by real-time PCR using TaqMan probes (Hydrolysis probes) using the C_1202883_20 assay (Applied Biosystems, Foster City, CA, USA). Real-time PCR was performed on a LightCycler 480 II (Roche Diagnostics GmbH, Switzerland); PCR reactions were conducted according to the manufacturer's instructions. Random samples were confirmed by high resolution melting curves (Fig. 1). The samples were previously screened for common variants in six *PARK* genes, including A30P of *SNCA* and G2019S and G2385R of *LRRK2*; the prevalence of DNA changes was low [10].

Statistical analysis

Statistical analysis was performed using SPSS software v. 18.0 (SPSS Inc., Chicago, IL, USA) for the χ^2 test, logistic regression and ANOVA. Hardy-Weinberg equilibrium (HWE) was estimated in both groups using the χ^2 test (http://ihg.gsf.de/cgi-bin/hw/hwa1.pl [20/08/2013]). Statistical power was calculated *a posteriori* using Quanto Software Version 1.2.

Results

In total, 356 individuals were genotyped, 140 patients with SPD (95 males and 45 females, aged:

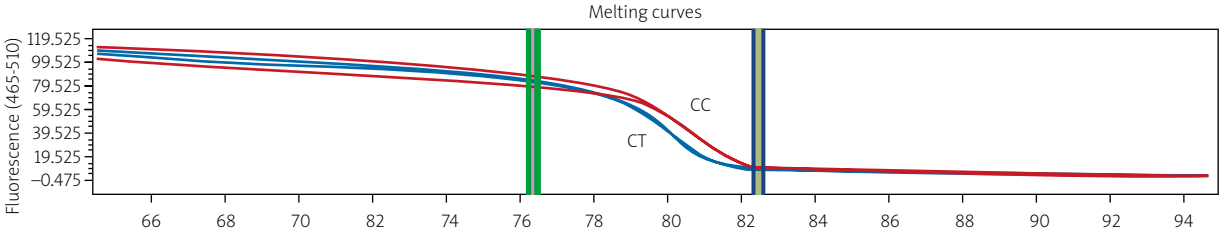

Fig. 1. Melting curves for the MTHFR rs1801133 showing CC and CT genotypes.

Table I. Genotype frequencies of rs1801133 in cases and controls

Genotypes	Controls *n* = 216	Patients *n* = 140	OR (95% CI)	*p*-value*
CC	37 (0.17)	38 (0.27)	2.02 (1.081-3.779)	0.026
TC	118 (0.55)	71 (0.51)		
TT	61 (0.28)	31 (0.22)		

65.46 ± 11.5 [mean ± standard deviation] years old), age at onset 58 ± 13.66), whereas 216 healthy individuals constituted the control group (140 males and 76 females, aged: 63.68 ± 8.8 years old). Hardy-Weinberg equilibrium test showed that alleles were distributed according to expected frequencies in both groups (corrected *p*-values, controls $p = 0.13$, cases $p = 1.00$). Distribution of genotypes between groups is shown in Table I.

The association test showed that the C allele was associated with PD only under the recessive model (OR = 2.02, CI: 1.08-3.77, $p = 0.02$); after logistic regression for known confounding factors, the association remained significant ($\exp(\beta) = 2.06$, CI: 1.101-3.873, $p = 0.024$). There was no association of any allele and cognitive impairment ($p = 0.33$). One-way ANOVA showed no differences between genotypes and age at onset ($p > 0.05$). Additionally, when age at onset was categorized (EOPD), the χ^2 test did not show an association of any allele or genotype and EOPD ($p > 0.05$) (TT group $n = 31$).

Discussion

In contrast to the hypothesis that the TT genotype of rs1801133 in the *MTHFR* gene leads to elevated levels of Hcy, cell death and therefore a higher risk of neurodegeneration [25], our data suggest that the CC genotype is associated with PD. This may be explained by the fact that the TT genotype has the greatest influence on Hcy levels in populations with low folate and high B_{12} vitamin plasma concentration such as Africans but not Mexican-Mestizos, in whom folate and B_{12} levels were high and moderate respectively [11]. Thus the TT genotype does not always imply high Hcy levels; in fact, a protective effect of the TT genotype against preeclampsia was reported in Maya-Mestizo women [1].

Others have also suggested that homozygosis of the T allele may confer a survival advantage in populations with sufficient dietary folate consumption [11,17,19]. Therefore, it is expected that in some populations such as Mexican-Mestizos, the T allele even when linked to an impaired biochemical function (elevated Hcy) may represent the wild-type allele, since an advantage may fix an allele within a population under particular environmental conditions. A presumptive advantage may exist, as described previously in an intervention where folate sources and dosages where controlled [4]. In contrast to its counterpart, the TT genotype showed only a slight decrease in global DNA methylation after folate depletion; conversely, under low folate basal levels, the TT genotype has shown significantly diminished global DNA methylation [8]. Thus, the finding that the derived CC genotype has the greatest decrease in DNA methylation after folate depletion may represent a different mechanism linked to neurodegeneration, besides the known effect of hyperhomocysteinemia on neuronal cytotoxicity [4].

The ancestral C allele may be considered the risk variant for PD in the Mexican-Mestizo population. Although it is speculative, hypomethylation as observed with the CC genotype under folate depletion may potentially impact epigenetic regulation of other genes such as *LRRK2* and *SNCA* [21]. SNCA protein is also involved in the arrest of DNMT1 (a major element in epigenetic regulation) in postmortem brains of PD patients, worsening in this way the hypomethylation phenomenon [21]. Interestingly, another study found this same genotype (CC of rs1801133) related to earlier age at onset of PD [22]. Our data do not replicate the observation, probably because in our group patients with EOPD were uncommon. Larger studies documenting age at onset and MTHFR genotype may confirm this finding. To our knowledge this is the first report on association of the CC genotype of MTHFR and SPD. Other studies in different populations with larger samples may add support to our hypothesis in which convergent pathways between common and rare variants may potentially affect complex neurodegenerative disorders such as PD.

Limitations of the study

Some of the limitations of the present study were that since a considerable proportion of patients were treated with L-dopa among other anti-parkinsonian drugs, homocysteine levels or global methylation were not measured and therefore the genotype-phenotype correlation could not be explored to support our hypothesis. The presence of essential hypertension could not be assessed accurately, since the study was not intended to do so. The statistical power reached was 72% (lower than the expected 80%).

Acknowledgments

This project was financed by the E-015 institutional program (ISSSTE).

We are also grateful to Luis Javier Cano Martínez and Benjamín Gómez Díaz for useful suggestions and comments.

Disclosure

Authors report no conflict of interest.

References

1. Canto P, Canto-Cetina T, Juarez-Velazquez R, Rosas-Vargas H, Rangel-Villalobos H, Canizales-Quinteros S, Velazquez-Wong AC, Villarreal-Molina MT, Fernandez GCoral-Vazquez R. Methylenetetrahydrofolate reductase C677T and glutathione S-transferase P1 A313G are associated with a reduced risk of preeclampsia in Maya-Mestizo women. Hypertens Res 2008; 31: 1015-1019.
2. Cardo LF, Coto E, de Mena L, Ribacoba R, Lorenzo-Betancor O, Pastor P, Samaranch L, Mata IF, Diaz M, Moris G, Menendez M, Corao AIAlvarez V. A search for SNCA 3' UTR variants identified SNP rs356165 as a determinant of disease risk and onset age in Parkinson's disease. J Mol Neurosci 2012; 47: 425-430.
3. Clark LN, Wang Y, Karlins E, Saito L, Mejia-Santana H, Harris J, Louis ED, Cote LJ, Andrews H, Fahn S, Waters C, Ford B, Frucht S, Ottman RMarder K. Frequency of LRRK2 mutations in early- and late-onset Parkinson disease. Neurology 2006; 67: 1786-1791.
4. Crider KS, Quinlivan EP, Berry RJ, Hao L, Li Z, Maneval D, Yang TP, Rasmussen SA, Yang Q, Zhu JH, Hu DJ, Bailey LB. Genomic DNA methylation changes in response to folic acid supplementation in a population-based intervention study among women of reproductive age. PLoS One 2011; 6: e28144.
5. Chung SJ, Armasu SM, Biernacka JM, Lesnick TG, Rider DN, Lincoln SJ, Ortolaza AI, Farrer MJ, Cunningham JM, Rocca WA, Maraganore DM. Common variants in PARK loci and related genes and Parkinson's disease. Mov Disord 2011; 26: 280-288.
6. De Bonis ML, Tessitore A, Pellecchia MT, Longo K, Salvatore A, Russo A, Ingrosso D, Zappia V, Barone P, Galletti P, Tedeschi G. Impaired transmethylation potential in Parkinson's disease patients treated with L-Dopa. Neurosci Lett 2010; 468: 287-291.
7. Duan W, Ladenheim B, Cutler RG, Kruman, II, Cadet JL, Mattson MP. Dietary folate deficiency and elevated homocysteine levels endanger dopaminergic neurons in models of Parkinson's disease. J Neurochem 2002; 80: 101-110.
8. Friso S, Choi SW, Girelli D, Mason JB, Dolnikowski GG, Bagley PJ, Olivieri O, Jacques PF, Rosenberg IH, Corrocher R, Selhub J. A common mutation in the 5,10-methylenetetrahydrofolate reductase gene affects genomic DNA methylation through an interaction with folate status. Proc Natl Acad Sci U S A 2002; 99: 5606-5611.
9. Frosst P, Blom HJ, Milos R, Goyette P, Sheppard CA, Matthews RG, Boers GJ, den Heijer M, Kluijtmans LA, van den Heuvel LP et al. A candidate genetic risk factor for vascular disease: a common mutation in methylenetetrahydrofolate reductase. Nat Genet 1995; 10: 111-113.
10. García S, López-Hernández LB, Suarez-Cuenca JA, Solano-Rojas M, Gallegos-Arreola MP, Gama-Moreno O, Valdez-Anguiano P, Canto P, Dávila-Maldonado L, Cuevas-García CF, Coral-Vázquez RM. Low prevalence of most frequent pathogenic variants of six PARK genes in sporadic Parkinson's disease. Folia Neuropathol 2014; 52: 22-29.
11. Gueant-Rodriguez RM, Gueant JL, Debard R, Thirion S, Hong LX, Bronowicki JP, Namour F, Chabi NW, Sanni A, Anello G, Bosco P, Romano C, Amouzou E, Arrieta HR, Sanchez BE, Romano A, Herbeth B, Guilland JC, Mutchinick OM. Prevalence of methylenetetrahydrofolate reductase 677T and 1298C alleles and folate status: a comparative study in Mexican, West African, and European populations. Am J Clin Nutr 2006; 83: 701-707.
12. Gueant JL, Chabi NW, Gueant-Rodriguez RM, Mutchinick OM, Debard R, Payet C, Lu X, Villaume C, Bronowicki JP, Quadros EV, Sanni A, Amouzou E, Xia B, Chen M, Anello G, Bosco P, Romano C, Arrieta HR, Sanchez BE, Romano A, Herbeth B, Anwar W, Namour F. Environmental influence on the worldwide prevalence of a 776C->G variant in the transcobalamin gene (TCN2). J Med Genet 2007; 44: 363-367.
13. Gustincich S, Manfioletti G, Del Sal G, Schneider C, Carninci P. A fast method for high-quality genomic DNA extraction from whole human blood. Biotechniques 1991; 11: 298-300, 302.
14. Healy DG, Falchi M, O'Sullivan SS, Bonifati V, Durr A, Bressman S, Brice A, Aasly J, Zabetian CP, Goldwurm S, Ferreira JJ, Tolosa E, Kay DM, Klein C, Williams DR, Marras C, Lang AE, Wszolek ZK, Berciano J, Schapira AH, Lynch T, Bhatia KP, Gasser T, Lees AJ, Wood NW. Phenotype, genotype, and worldwide genetic penetrance of LRRK2-associated Parkinson's disease: a case-control study. Lancet Neurol 2008; 7: 583-590.
15. Hughes AJ, Daniel SE, Ben-Shlomo Y, Lees AJ. The accuracy of diagnosis of parkinsonian syndromes in a specialist movement disorder service. Brain 2002; 125: 861-870.
16. Manolio TA, Collins FS, Cox NJ, Goldstein DB, Hindorff LA, Hunter DJ, McCarthy MI, Ramos EM, Cardon LR, Chakravarti A, Cho JH, Guttmacher AE, Kong A, Kruglyak L, Mardis E, Rotimi CN, Slatkin M, Valle D, Whittemore AS, Boehnke M, Clark AG, Eichler EE, Gibson G, Haines JL, Mackay TF, McCarroll SA, Visscher PM. Finding the missing heritability of complex diseases. Nature 2009; 461: 747-753.

17. Mayor-Olea A, Callejon G, Palomares AR, Jimenez AJ, Gaitan MJ, Rodriguez A, Ruiz M, Reyes-Engel A. Human genetic selection on the MTHFR 677C>T polymorphism. BMC Med Genet 2008; 9: 104.
18. Miller JW. Homocysteine, folate deficiency, and Parkinson's disease. Nutr Rev 2002; 60: 410-413.
19. Munoz-Moran E, Dieguez-Lucena JL, Fernandez-Arcas N, Peran-Mesa S, Reyes-Engel A. Genetic selection and folate intake during pregnancy. Lancet 1998; 352: 1120-1121.
20. Mutchinick OM, Lopez MA, Luna L, Waxman J, Babinsky VE. High prevalence of the thermolabile methylenetetrahydrofolate reductase variant in Mexico: a country with a very high prevalence of neural tube defects. Mol Genet Metab 1999; 68: 461-467.
21. Tan YY, Wu L, Zhao ZB, Wang Y, Xiao Q, Liu J, Wang G, Ma JF, Chen SD. Methylation of alpha-synuclein and leucine-rich repeat kinase 2 in leukocyte DNA of Parkinson's disease patients. Parkinsonism Relat Disord 2014; 20: 308-313.
22. Vallelunga A, Pegoraro V, Pilleri M, Biundo R, De Iuliis A, Marchetti M, Facchini S, Formento Dojot P, Antonini A. The MTHFR C677T polymorphism modifies age at onset in Parkinson's disease. Neurol Sci 2014; 35: 73-77.
23. Wickremaratchi MM, Perera D, O'Loghlen C, Sastry D, Morgan E, Jones A, Edwards P, Robertson NP, Butler C, Morris HR, Ben-Shlomo Y. Prevalence and age of onset of Parkinson's disease in Cardiff: a community based cross sectional study and meta-analysis. J Neurol Neurosurg Psychiatry 2009; 80: 805-807.
24. Wu YL, Ding XX, Sun YH, Yang HY, Sun L. Methylenetetrahydrofolate reductase (MTHFR) C677T/A1298C polymorphisms and susceptibility to Parkinson's disease: a meta-analysis. J Neurol Sci 2013; 335: 14-21.
25. Zhu ZG, Ai QL, Wang WM, Xiao ZC. Meta-analysis supports association of a functional SNP (rs1801133) in the MTHFR gene with Parkinson's disease. Gene 2013; 531: 78-83.

Original article

Folia Neuropathologica

Cabergoline protects dopaminergic neurons against rotenone-induced cell death in primary mesencephalic cell culture

Jörn Meinel[1,2*], Khaled Radad[3*], Wolf-Dieter Rausch[4], Heinz Reichmann[2], Gabriele Gille[2]

[1]Department of Pathology, Technical University, Dresden, Germany, [2]Department of Neurology, Technical University, Dresden, Germany, [3]Department of Pathology, Faculty of Veterinary Medicine, Assiut University, Assiut, Egypt, [4]Institute of Medical Biochemistry, Department of Biomedical Sciences, University for Veterinary Medicine, Vienna, Austria

*Authors contributed equally to the publication. They share the first authorship.

Folia Neuropathol 2015; 53 (1): 29-40 DOI: 10.5114/fn.2015.49972

Abstract

In the present study, primary mesencephalic cell cultures prepared from embryonic mouse mesencephala were used to investigate the neuroprotective effect of cabergoline, an ergoline D_2 receptor agonist, against the pesticide and neurotoxin rotenone relevant to Parkinson disease (PD). Treatment of cultures with cabergoline alone significantly increased the number of tyrosine hydroxylase immunoreactive (THir) neurons and reduced the release of lactate dehydrogenase (LDH) into the culture medium compared to untreated controls. Against rotenone toxicity, cabergoline significantly rescued degenerating THir neurons, reduced the release of LDH into the culture medium and improved the morphology of surviving THir neurons. The neuroprotective effects afforded by cabergoline were independent of dopaminergic stimulation as blocking of dopamine receptors by the dopamine receptor antagonist sulpiride did not prevent them. Furthermore, rotenone-induced formation of reactive oxygen species (ROS) was significantly reduced by cabergoline. Although cabergoline increased the glutathione (GSH) content in the culture, the protective effect for dopaminergic neurons seemed not to be predominantly mediated by increasing GSH, as depletion of GSH by L-buthionine-(S,R)-sulfoximine (BSO), a GSH biosynthesis inhibitor, did not prevent cabergoline-mediated neuroprotection of THir neurons in rotenone-treated cultures. Moreover, cabergoline significantly increased the ATP/protein ratio in primary mesencephalic cell cultures when added alone or prior to rotenone treatment. These results indicate a neuroprotective effect of cabergoline for dopaminergic neurons against rotenone toxicity. This effect was independent of dopamine receptor stimulation and was at least partially mediated by reducing ROS production and increasing the ATP/protein ratio.

Key words: *cabergoline, dopamine agonist, rotenone, dopaminergic cell culture, neuroprotection, Parkinson's disease.*

Introduction

Parkinson disease (PD) as the second most common neurodegenerative disease affects up to 10 million people worldwide [8]. Its specific symptomatology results primarily from progressive degeneration of dopaminergic neurons in the substantia nigra pars compacta (SNpc) and subsequent depletion in striatal dopamine levels [3]. Thus dopamine denervation leads to the classic motor symptoms of PD, most notably tremor, rigidity, bradykinesia and postural instability [30].

Communicating author:
Ass. Prof. Gabriele Gille, Department of Neurology, Technical University, Fetscherstr. 74, 01307 Dresden, Germany,
e-mail: Gabriele.Gille@uniklinikum-dresden.de

Since the 1960s, dopamine replacement therapy using levodopa has been the most effective choice for treatment of PD. However, as the disease progresses, the medication becomes increasingly inadequate in controlling motor complications such as dyskinesia, wearing off and on-off motor fluctuation [31]. In addition to these disabling side effects, there is also serious concern about possible toxic actions of levodopa on the remaining dopaminergic neurons [13].

Dopamine receptor agonists are clinically indicated in PD to postpone the onset of levodopa therapy, and to delay and minimize levodopa-related motor complications [20]. They exert their antiparkinsonian effects through direct activation of dopamine receptors mimicking the endogenous neurotransmitter dopamine [21]. Unlike levodopa, dopamine receptor agonists are not metabolized by an oxidative pathway and so do not lead to the cytotoxic free radical formation that is associated with the metabolism of dopamine [25]. Besides providing symptomatic relief of PD, data from *in vitro* and *in vivo* studies indicated potential neuroprotective effects of some dopamine agonists [24].

Cabergoline is an ergot-derived dopamine agonist with high affinity for the dopamine D_2 receptor, but also possesses significant affinity for the D_3 and D_4 receptor. It has the longest half-life among related dopamine agonists [15]. Although physicians will nowadays avoid prescribing cabergoline as first-line therapy, since it has been shown to cause valvular heart disease in a subset of patients [34], there is still a considerable amount of patients treated with the agonist. Cabergoline was reported to elicit neuroprotection in *in vitro* and *in vivo* models of neurodegeneration. In this context, Ohta *et al*. found that cabergoline increased concentrations of nerve growth factor (NGF), brain-derived neurotrophic factor (BDNF), and glial cell line-derived neurotrophic factor (GDNF) in primary cultured mouse astrocytes [19]. Miglio *et al*. reported that cabergoline protected SH-SY5Y cells from ischemia-induced cell death [16]. Yoshioka *et al*. reported that cabergoline normalized the dopamine turnover in the striatum of 6-OHDA-treated mice [32]. Finally, in cultures of cortical neurons cabergoline prevented H_2O_2-induced neuronal cell death by reducing excitotoxicity [18].

To date, there are no investigations exploring the direct neuroprotective effect of cabergoline towards dopaminergic neurons. Accordingly, in the current study primary mesencephalic cell cultures were used to investigate the potential neuroprotective effects of cabergoline for dopaminergic neurons in a rotenone toxicity model.

Material and methods

Preparation of primary mesencephalic cell culture

Mice (C57Bl/6 mice from Charles River Wiga, Sulzfeld, Germany) were cared for and handled in accordance with the guidelines of the European Union Council (86/609/EU) for the use of laboratory animals. The killing of mice for scientific purposes was officially approved by the Landesdirektion Dresden (State Directorate)/Free State of Saxony. Primary mesencephalic cell cultures were prepared according to Gille *et al*. [6] with some modifications. Cultures were not sex-segregated. In brief, embryonic mouse mesencephala were dissected on the 14th day of gestation and cut into small pieces in a drop of Dulbecco's Phosphate Buffered Saline (DPBS; Invitrogen, Germany), 2 ml of 0.2% trypsin solution (Invitrogen, Germany) and 2 ml of 0.02% DNase I solution (Roche, Germany) were added, and the tissue was subsequently incubated in a water bath at 37°C for 7 min. Then, 2 ml of trypsin inhibitor (0.25 mg/ml) (Invitrogen, Germany) were added, the tissue was centrifuged at 100 g for 4 min and the supernatant was aspirated. The tissue pellet was triturated 2-3 times with a fire-polished Pasteur pipette in 3 ml of Dulbecco's Modified Eagle's Medium (DMEM; Invitrogen, Germany) containing 0.02% DNase I. Dissociated cells were plated in 4-well culture dishes (NUNC, Germany) at a density of 257,000 cells/cm^2 in DMEM supplemented with 4 mM glutamine (Sigma, Germany), 10 mM HEPES buffer (Sigma, Germany), 30 mM glucose (Sigma, Germany), 100 IU/ml penicillin, 0.1 mg/ml streptomycin (Roche, Germany) and 10% heat-inactivated Fetal Calf Serum (FCS; Sigma, Germany). When 8-well glass chamber slides (BD Biosciences, Germany) were used for fluorescence microscopy, cells were plated at a density of 365,600 viable cells/cm^2. Two thirds of medium was changed on the 1st day *in vitro* (DIV). On the 3rd DIV the medium was changed completely. On the 5th DIV half of the medium was replaced by serum-free DMEM containing 2% B-27 supplement (Invitrogen, Germany). Serum-free supplemented DMEM was used for feeding from the 6th DIV and was subsequently replaced every 2nd day.

Treatment of cultures with cabergoline

A 4 mM stock solution of cabergoline (kindly provided by Pfizer) was prepared and further diluted in ethanol and DMEM. Each final cabergoline concentration used for treatment contained 0.25% ethanol. To investigate the effect of cabergoline on the survival of dopaminergic neurons, cultures were treated with cabergoline (0.001, 0.01, 0.1, 1, 10 µM) from the 6th DIV for eight consecutive days. During the treatment period, culture medium containing cabergoline was changed every two days. On the 14th DIV cultures were fixed and stained.

Treatment of cultures with cabergoline and rotenone

To investigate the neuroprotective effect of cabergoline against rotenone (Sigma, Germany) toxicity, cultures were treated with cabergoline (0.001, 0.01, 0.1, 1, 10 µM) on the 6th DIV for 6 consecutive days. During the treatment period, culture medium containing cabergoline was changed every two days. On the 10th DIV rotenone (80 or 100 nM) was concomitantly added to the cultures for 48 h. On the 12th DIV cultures were fixed and stained.

Treatment of cultures with sulpiride, cabergoline and rotenone

Sulpiride (Tocris, UK), a dopamine D_2/D_3 receptor antagonist, was diluted to 10 mM in ethanol. On the 8th DIV, culture medium was completely removed and cultures were incubated with 40 µM sulpiride in 375 µl of fresh culture medium for 10 min. After 10 min, 375 µl of fresh medium containing different concentrations of cabergoline (0.001, 0.02, 2 µM) were additionally added to the cultures, so that the final concentration of sulpiride was 20 µM and that of cabergoline 0.0005, 0.01 and 1 µM, respectively. On the 9th DIV, the culture medium was replaced with medium containing 80 nM rotenone and the cultures were grown to the 11th DIV.

Identification of tyrosine hydroxylase immunoreactive neurons

Dopaminergic neurons were identified immunocytochemically by tyrosine hydroxylase staining. Cultures were rinsed carefully with phosphate buffered saline (PBS, pH 7.2) at the end of each treatment, placed on ice and fixed for 30 s in Accustain (Sigma, Germany) pre-cooled to 4°C. After washing with PBS, cells were permeabilized with 0.4% Triton X-100 (Fluka, Switzerland) for 15 min at room temperature. Then, 30% H_2O_2 (Merck, Germany) was diluted with 50% methanol (Merck, Germany) to 1% and added for 15 min to the cultures in order to saturate endogenous peroxidases. Cultures were washed 3 times with PBS and incubated with 5% horse serum (Vectastain ABC Elite kit; Vector Laboratories, USA) for 60 min to block nonspecific binding sites. To determine the number of tyrosine hydroxylase immunoreactive (THir) neurons in cultures, cells were sequentially incubated with anti-TH primary antibody (Chemicon, UK) overnight at 4°C, biotinylated secondary antibody (Vectastain ABC Elite kit) and avidin-biotin-horseradish peroxidase complex (Vectastain ABC Elite kit) for 90 min each at room temperature and washed with PBS between stages. The reaction product was developed with a peroxidase substrate kit (Vector VIP purple; Vector Laboratories, USA). Stained cells were counted with an inverted microscope (Axiovert 35, Carl Zeiss AG, Germany) in 20 randomly selected fields per well at 100x magnification (1.302 mm^2/field). The average number of THir cells in controls on the 12th DIV was 1000-1200 cells/well.

Measurement of lactate dehydrogenase activity

Cellular injury was quantitatively assessed by measuring the activity of LDH released from damaged cells into the culture medium. Lactate dehydrogenase (LDH) activity was measured with the Cytotoxicity Detection Kit (Roche, Germany) according to the manufacturer's instructions. Briefly, LDH catalyses the conversion of lactate to pyruvate with a concomitant reduction of NAD^+ to NADH + H^+. The protons of NADH + H^+ are transferred to the yellow tetrazolium salt 2-[4-iodophenyl]-3-[4-nitrophenyl]-5-phenyltetrazolium chloride (INT) by diaphorase, resulting in red formazan, which was measured spectrophotometrically (ELISA-reader Tecan Sunrise, Germany) at 490 nm with a reference at 688 nm. Supplemented medium was used as a blank and subtracted as background.

Measurement of reactive oxygen species with CM-H_2DCFDA fluorescent dye

To investigate the effect of cabergoline on reactive oxygen species (ROS) production following rote-

none treatment, cultures were treated with 0.01 µM cabergoline from the 8th to the 9th DIV and 80 nM rotenone on the 9th DIV. Production of ROS was detected using 5-(and-6)-chloromethyl-2',7'-dichlorodihydrofluorescein diacetate acetyl ester (CM-H_2DCFDA; Molecular Probes, Invitrogen, Germany). Stock solutions of CM-H_2DCFDA (1 mM) were prepared in dimethylsulfoxide (DMSO) and further diluted in PBS. Cultures were loaded with a final concentration of 0.75 µM CM-H_2DCFDA for 15 min, washed and further incubated in colorless M 199 (GIBCO, Germany) with low autofluorescence. CM-H_2DCFDA is believed to diffuse passively into cells, where its acetate groups are cleaved by intracellular esterases and subsequent oxidation by ROS yields a green fluorescent adduct that is trapped inside the cells. Images were taken with a computer-driven digital camera (Leica DC350 FX, Wetzlar, Germany) on an inverted microscope (Leica DM IRE2 HC FLUO, Wetzlar, Germany) equipped with an incubator and temperature control for live cell experiments. The green fluorescence was visualized with the MS 2 filter [excitation 430–510 Band Pass (BP)/emission 482–562 Band Pass (BP)]. Visualization of nuclei was performed with Hoechst 33342 with the DAPI filter [excitation 340–380 Band Pass (BP)/emission 425 Long Pass]. The fluorescence intensity of ROS was always normalized to the density of nuclei representing cellular density. Semi-quantitative image analysis was performed densitometrically with Adobe Photoshop (Munich, Germany).

Glutathione measurement

To investigate the effect of cabergoline on glutathione (GSH) synthesis in cultured cells, cultures were treated with cabergoline (0.001, 0.01, 0.1, 1, 10 µM) on the 8th DIV for 24 h. On the 9th DIV, GSH concentrations were determined using a GSH detection kit (Chemicon International, Temecula, CA, USA) following the protocol of the manufacturer. Cultures were grown in 4-well culture dishes as usual and two wells of lysed cells were pooled for measurement. After centrifugation the supernatant was transferred into a 96-well plate (flat bottom, black) and monochlorobimane (MCB), a dye with high affinity for GSH that fluoresces in its bound state, was added. The fluorescence intensity was analyzed using a Tecan Genios plate reader with excitation at 380 nm and emission at 460 nm. To investigate whether increasing GSH concentrations played a role in cabergoline's neuroprotective effect against rotenone, cultures were treated with 10 µM buthionine sulfoximine (BSO; Sigma, Steinheim, Germany), a GSH biosynthesis inhibitor, on the 8th DIV for 2 h. Then, cabergoline (0.0005, 0.01, 1 µM) was additionally added to the cultures for 24 h and rotenone (80 nM) on the 9th DIV for 48 h. On the 11th DIV, cultures were fixed and stained immunohistochemically against TH antibody.

ATP measurement

The total ATP content of individual wells was determined with the CellTiter-Glo Luminescent Cell Viability Assay (Promega, WI, USA) according to the manufacturer's instructions. The test principle is based on the ATP-dependent mono-oxygenation of luciferin to oxyluciferin by firefly luciferase leading to a luminescent signal that is directly proportional to the quantity of ATP. The luminescence signal was measured with a microplate reader (TECAN GENios, Crailsheim, Germany) and a run with PBS was subtracted as background.

ATP was measured in cultures that were treated either with cabergoline or cabergoline and rotenone, respectively. In the former case cabergoline (0.0005, 0.01, 1 µM) was added on the 8th DIV for 24 h. Then, cultures were kept in fresh medium from the 9th to the 11th DIV. Alternatively, cabergoline (0.0005, 0.01, 1 µM) was added on the 8th DIV for 24 h and rotenone (80 nM) on the 9th DIV for 2 consecutive days. The measured ATP values were correlated with the protein contents in the treated cultures.

Protein measurement

Cellular protein was measured using the BCA protein assay reagent kit (Pierce, Rockford, IL, USA). Briefly, the assay is based on the reduction of Cu^{2+} to Cu^{1+} by protein in an alkaline medium (biuret reaction) and the formation of a red-violet chelate complex of 2 molecules of bicinchoninic acid (BCA) with one Cu^{1+} ion. The photometrically measured absorbance of the formed complex at 562 nm is directly proportional to the total protein concentration (µg/ml). A run with PBS instead of a sample was used as a blank. Absorbance was measured with a Tecan Sunrise absorbance reader (Crailsheim, Germany).

Statistics

Data were expressed as mean values ± standard error of the mean (SEM). Statistical differences were

determined using the Mann-Whitney *U*-test or Kruskal-Wallis (*H*) test followed by the χ^2 test. Differences with $p < 0.05$ were regarded as statistically significant.

Results

Cabergoline increased the survival of tyrosine hydroxylase immunoreactive neurons in primary mesencephalic cell culture and protected against rotenone-induced cell death

Treatment of cultures with cabergoline on the 6th DIV for 8 consecutive days significantly increased the number of THir neurons by up to 31% (0.1 µM cabergoline) (Fig. 1A). On the other hand, at an unphysiological high concentration of 10 µM, cabergoline reduced the number of THir neurons by 26% (Fig. 1A).

Treatment of cultures with 100 nM rotenone on the 10th DIV for 48 h reduced the number of THir neurons by 71% compared to control cultures (Fig. 1B). Surviving neurons after rotenone treatment showed fewer, shortened and dysmorphic neurites (Fig. 2C,D) compared to control cells (Fig. 2A,B). Treatment with cabergoline from the 6th DIV for 6 consecutive days rescued THir neurons from degeneration when rotenone (100 nM) was concomitantly added on the 10th DIV for 48 h. The number of THir neurons was increased significantly by up to 20% (0.001 and 0.01 µM cabergoline) (Fig. 1B). Moreover, the morphologic deteriorations induced by rotenone were also ameliorated by cabergoline treatment (Fig. 2E,F).

Cabergoline reduced lactate dehydrogenase release in primary mesencephalic cell culture

Cabergoline significantly reduced the release of LDH when mesencephalic cell cultures were treated with cabergoline alone or together with rotenone. Treatment with cabergoline from the 6th DIV for six consecutive days significantly reduced the release of LDH into the culture medium by 66-50% at concentrations of 0.001-10 µM as measured on the 12th DIV (Fig. 3). When control cultures were incubated with 80 nM rotenone on the 10th DIV for 48 h, the release of LDH was increased by 73% compared to untreated cultures (Fig. 3). Concomitant addition of rotenone on the 10th DIV for 48 h during cabergoline treatment revealed that cabergoline significantly reduced the release of LDH by 60-36% at concentra-

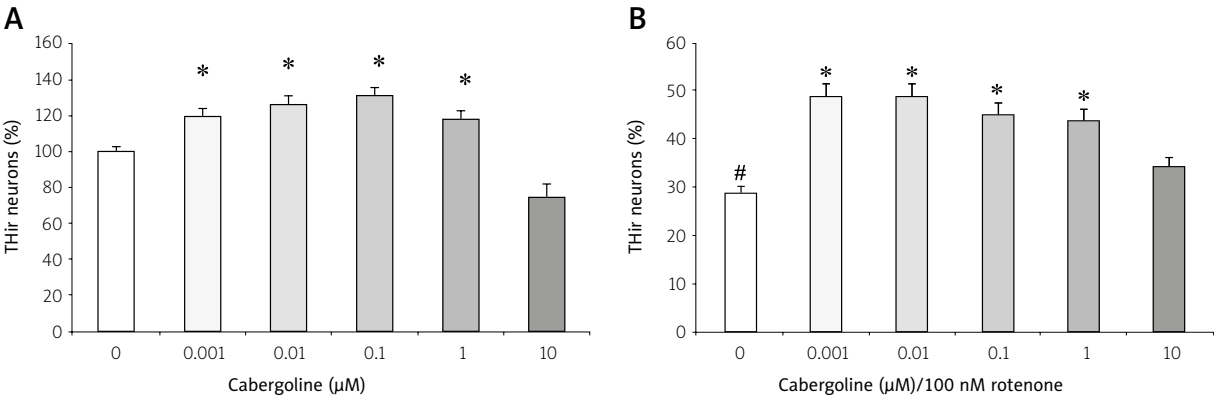

Fig. 1. A) Effect of cabergoline treatment on the number of tyrosine hydroxylase immunoreactive (THir) neurons. One hundred percent corresponds to the total number of THir neurons after 14 days *in vitro* (DIV) in untreated control cultures. Values represent the mean ± SEM of three independent experiments with four wells in each treatment. In each well 10 randomly selected fields were counted for tyrosine hydroxylase (TH) immunocytochemistry. $^*p < 0.0001$, significance compared with untreated controls using Kruskal-Wallis test followed by χ^2 test. **B)** Effect of cabergoline on the survival of rotenone-treated THir neurons. One hundred percent corresponds to the total number of THir neurons after 12 DIV in untreated control culture. Values represent the mean ± SEM of three independent experiments with four wells in each treatment. In each well 10 randomly selected fields were counted for TH immunocytochemistry. $^\#p < 0.0001$, significance compared with untreated controls using Mann-Whitney test; $^*p < 0.001$, significance compared with rotenone-treated control cultures using Kruskal-Wallis test followed by χ^2 test.

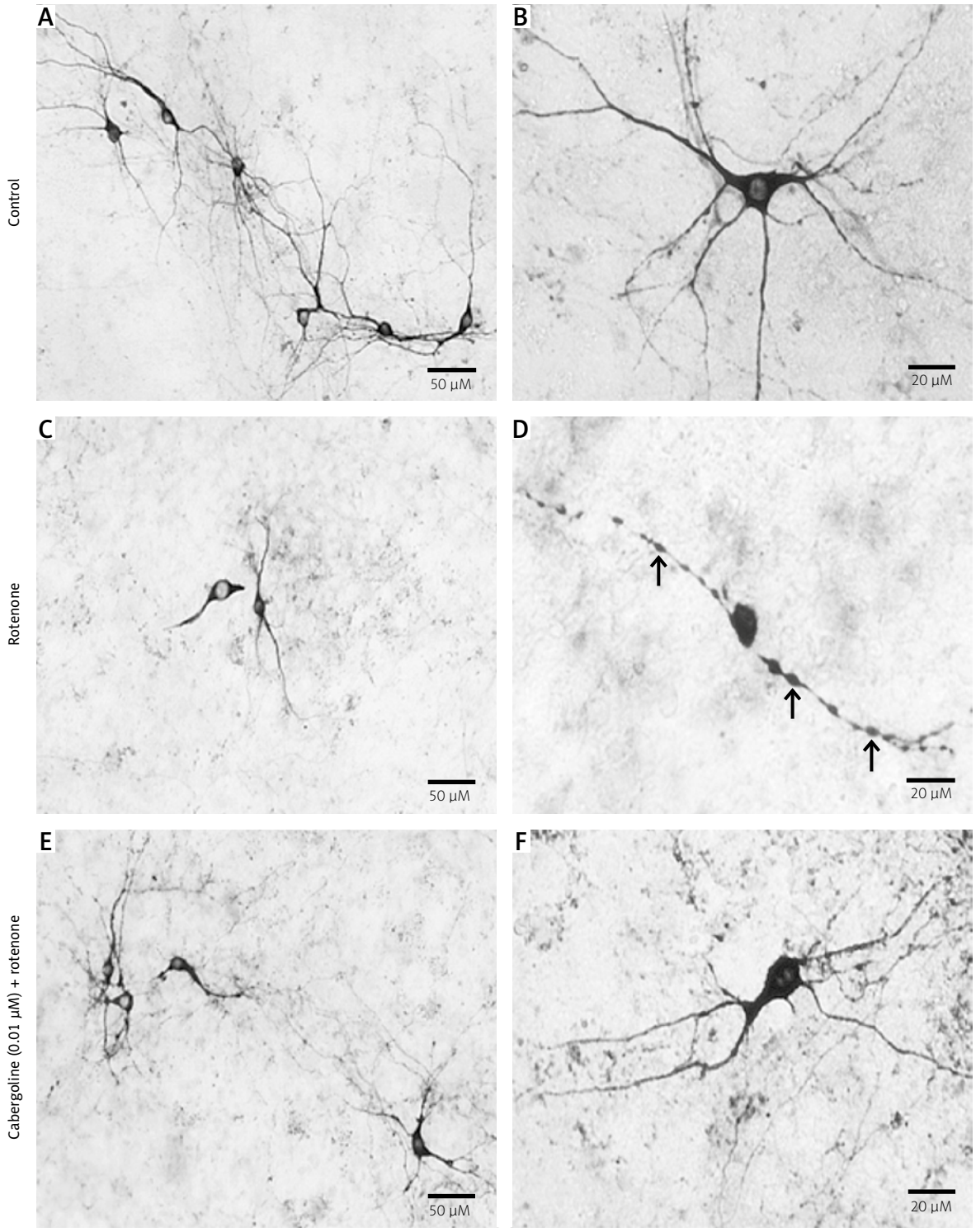

Fig. 2. Representative micrographs of tyrosine hydroxylase immunoreactive (THir) neurons in primary mesencephalic cell cultures after 12 days *in vitro* (DIV). **A, B)** Untreated control cultures show intact THir neurons with long and branched processes. **C, D)** Surviving neurons after rotenone exposure appear few in number with shortened and dysmorphic neurites with bead-like structures (arrows). **E, F)** Cabergoline improves the number and morphology of THir neurons compared to rotenone-treated cultures.

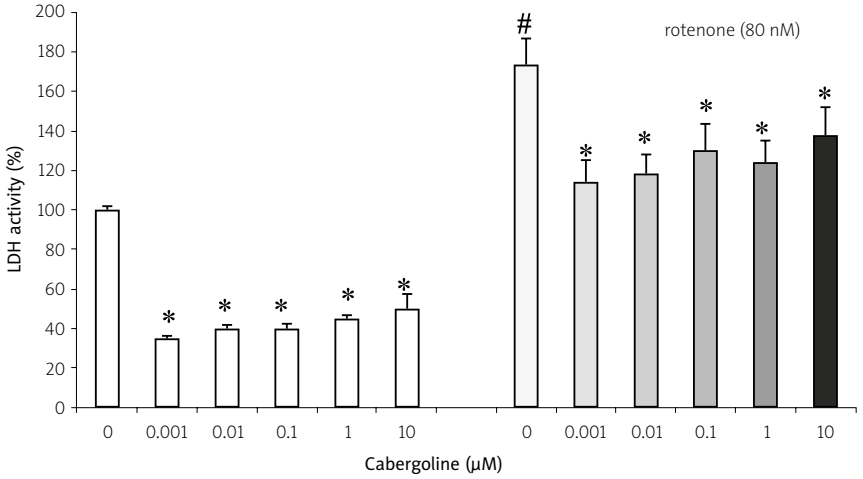

Fig. 3. Release of lactate dehydrogenase (LDH) in primary mesencephalic cell cultures. One hundred percent corresponds to the amount of LDH in the culture medium after 12 days *in vitro* (DIV). Values represent the mean ± SEM of three independent experiments with four wells in each treatment. $^{\#}p < 0.0001$, significance compared with untreated controls using Mann-Whitney test; $^{*}p < 0.001$, significance compared with untreated and rotenone-treated control cultures using Kruskal-Wallis test followed by χ^2 test.

tions of 0.001-10 μM, compared to cultures treated with rotenone only (Fig. 3).

The protective effect of cabergoline against rotenone was not dopamine receptor-dependent

The dopamine receptor antagonist sulpiride did not antagonize the neuroprotection afforded by cabergoline in rotenone-treated cultures. When cultures were treated with cabergoline together with sulpiride on the 8th DIV for 24 h and treatment with 80 nM rotenone was started on the 9th DIV for 48 h, no reduction in the protective effect of cabergoline on the number of THir neurons could be detected (Fig. 4). Treatment with sulpiride alone had no effect on the number of dopaminergic neurons (data not shown).

Cabergoline inhibited the production of reactive oxygen species in primary mesencephalic cell culture

Since the production of ROS is a central mechanism of rotenone toxicity, it was tested whether cabergoline could counteract the effect of rotenone-induced ROS production. The treatment of cultures with 80 nM rotenone on the 9th DIV significantly elevated overall ROS production by 224% after 24 h as measured by CM-H_2DCFDA fluorescence compared to untreated control cultures (Fig. 5A). Pre-treatment with cabergoline (0.01 μM) significantly reduced

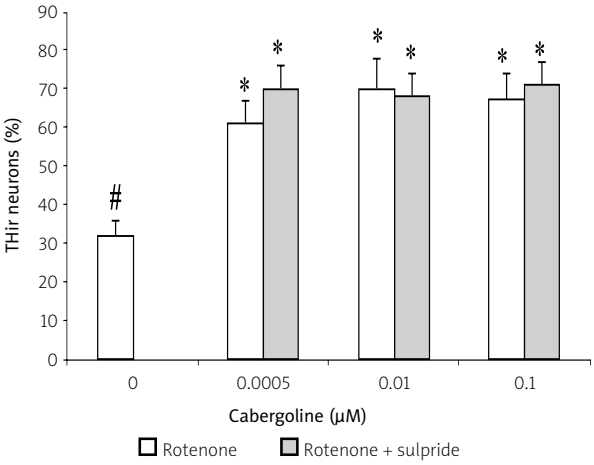

Fig. 4. Effect of different concentrations of cabergoline with and without sulpiride on the survival of rotenone-treated tyrosine hydroxylase immunoreactive (THir) neurons. One hundred percent corresponds to the total number of dopaminergic neurons after 11 days *in vitro* (DIV) in untreated control cultures. Values represent the mean ± SEM of three independent experiments with four wells in each treatment. In each well 10 randomly selected fields were counted for tyrosine hydroxylase (TH) immunocytochemistry. $^{\#}p < 0.0001$, significance compared with untreated controls using Mann-Whitney test; $^{*}p < 0.001$, significance compared with rotenone-treated control cultures using Kruskal-Wallis test followed by χ^2 test.

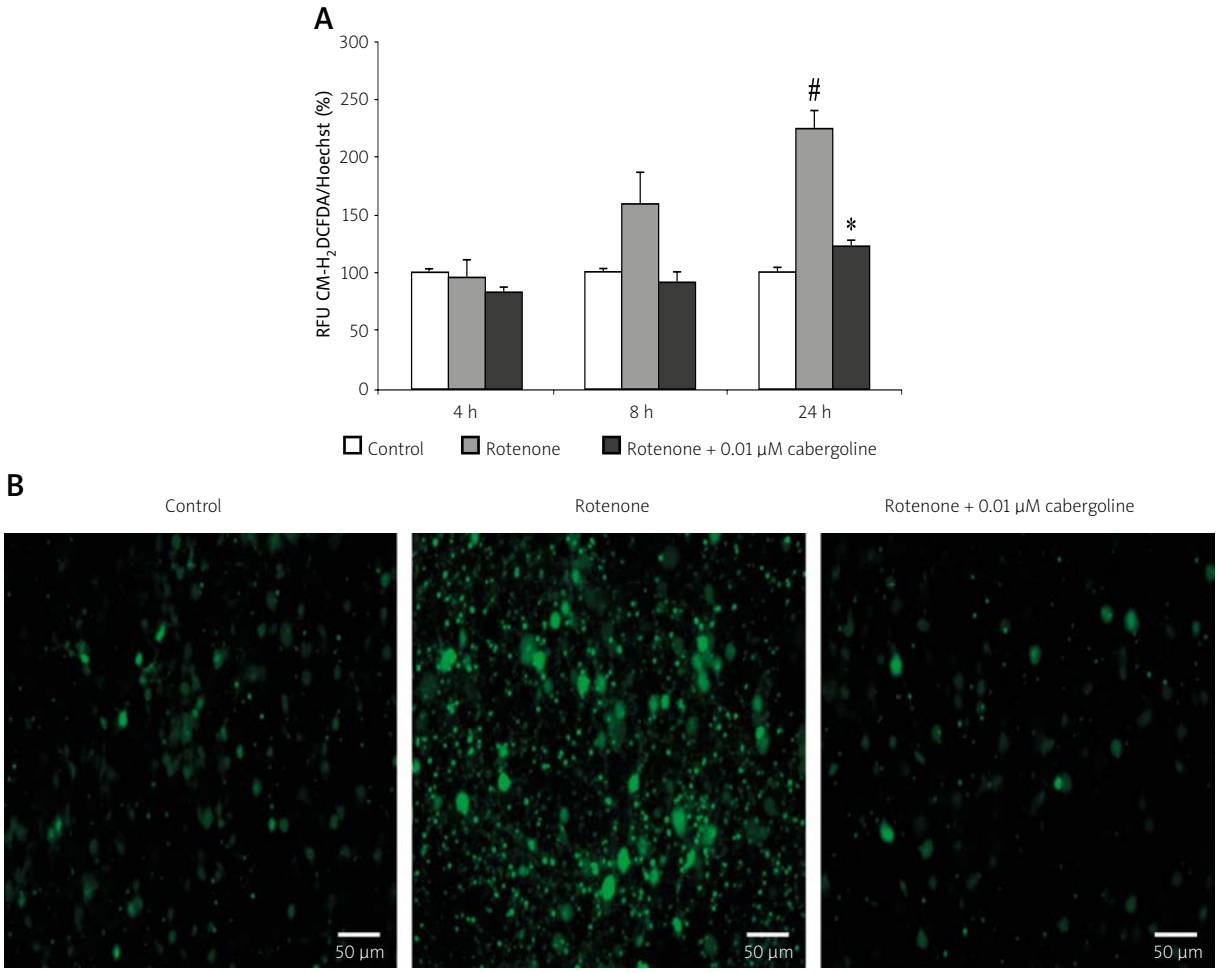

Fig. 5. A) Measurement of reactive oxygen species (ROS) production in primary mesencephalic cell cultures using CM-H_2DCFDA fluorescence staining. One hundred percent corresponds to the fluorescence intensity after 10 days *in vitro* (DIV) in untreated control cultures. Values represent the mean ± SEM of four independent experiments. Fluorescence intensity was determined densitometrically from a total of 80 randomly selected micrographs (20 photos in each experiment). $^{\#}p < 0.0001$, significance compared with untreated controls using Mann-Whitney test; $^{*}p < 0.0001$, significance compared with rotenone-treated control cultures. **B)** Representative micrographs of primary mesencephalic cell cultures after staining with CM-H_2DCFDA fluorescence dye on the 10th DIV.

rotenone-induced ROS production by about 100% when added on the 8th DIV for 24 h (Fig. 5A). Different fluorescence intensities could be detected microscopically in control, rotenone-treated and rotenone-cabergoline-treated cultures (Fig. 5B).

Cabergoline increased the content of glutathione in primary mesencephalic cell culture

The antioxidant GSH is essential for the cellular detoxification of reactive oxygen species in brain cells. Therefore, it was investigated whether cabergoline might confer protection for dopaminergic neurons against rotenone toxicity by increasing the production of GSH. Treating the cultures with cabergoline from the 8th DIV for 24 h stimulated the content of GSH by up to 35% (0.01 µM cabergoline) when measured on the 9th DIV (Fig. 6A). When cultures were treated with the GSH synthesis inhibitor BSO on the 8th DIV for 24 h, GSH was significantly reduced to 44% (from 2.57 µmol/mg protein to 1.13 µmol/mg protein) of control values (data not

shown). However, when 80 nM rotenone was added to the GSH depleted cultures from the 9th to the 11th DIV, the protective effect for dopaminergic neurons afforded by cabergoline was not prevented (Fig. 6B), indicating that GSH increase is not decisive in cabergoline-induced neuroprotection.

Cabergoline significantly increased the content of ATP in primary mesencephalic cell culture

As an inhibitor of the mitochondrial respiratory chain, rotenone is known to reduce the intracellular content of ATP. It was therefore studied whether cabergoline influenced the content of ATP in the culture with and without rotenone treatment. The treatment of cultures with cabergoline from the 8th DIV for 24 h significantly increased the content of ATP by 37% at 0.0005 µM compared to control cultures when measured on the 11th DIV (Fig. 7). Addition of 80 nM rotenone significantly reduced the ATP content by 53% when added on the 9th DIV for 48 h (Fig. 7). On the other hand, pretreatment of cultures with cabergoline significantly increased the ATP content by 33 and 28% at concentrations of 0.0005 and 0.01 µM, respectively, compared to rotenone-treated control cultures (Fig. 7).

Discussion

In the present study, cabergoline was found to promote the survival of THir neurons when added to primary mesencephalic cell cultures (Fig. 1A). Such a stimulatory effect is not exhibited by all ergoline dopamine agonists, since it was for example demonstrated for lisuride [6], but not for pergolide [5] or α-dihydroergocryptine [4] when analogously used under the same treatment conditions. Similarly to these ergoline agonists, cabergoline reduced the number of dopamine neurons at an unphysiological high concentration (10 µM).

Remarkably, cabergoline was able to protect THir neurons against the potent mitochondrial complex I inhibitor rotenone (Fig. 1B). The pesticide is well known to increase the risk for PD during long-term use [27]. In the tested concentration range, cabergoline rescued a significant number of THir neurons and improved their morphology under rotenone

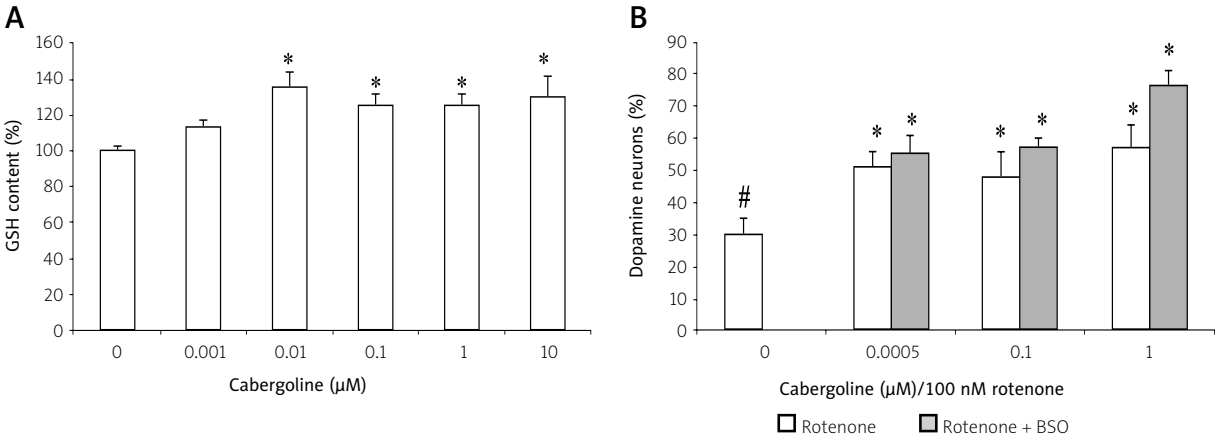

Fig. 6. A) Effect of cabergoline on glutathione (GSH) synthesis in primary mesencephalic cell cultures. One hundred percent corresponds to GSH content after 9 days *in vitro* (DIV) in untreated control cultures and amounts to 2.57 µmol/mg protein. Values represent the mean ± SEM of three independent experiments with four wells in each treatment. $^{*}p < 0.001$, significance compared with untreated control cultures using Kruskal-Wallis test followed by χ^2 test. **B)** Effect of cabergoline with and without L-buthionine-(S,R)-sulfoximine (BSO) on the survival of rotenone-treated tyrosine hydroxylase immunoreactive (THir) neurons. One hundred percent corresponds to the total number of dopaminergic neurons after 11 DIV in untreated control culture. Values represent the mean ± SEM of three independent experiments with four wells in each treatment. In each well, 10 randomly selected fields were counted for tyrosine hydroxylase (TH) immunocytochemistry. $^{\#}p < 0.0001$, significance compared with untreated controls using Mann-Whitney test; $^{*}p < 0.05$, significance compared with rotenone-treated control cultures using Kruskal-Wallis test followed by χ^2 test.

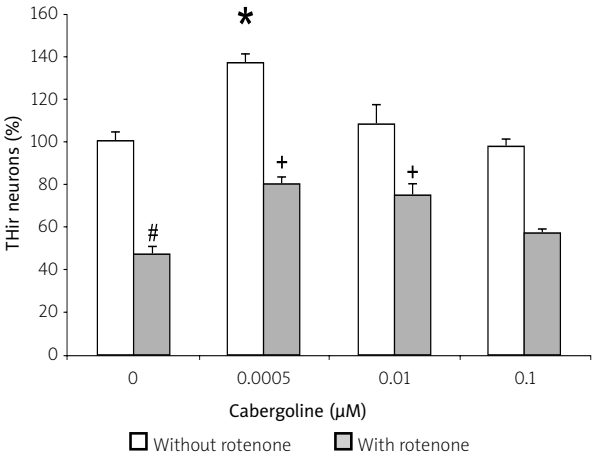

Fig. 7. Effect of cabergoline on ATP content in primary mesencephalic cell cultures. One hundred percent corresponds to the ATP content after 11 days *in vitro* (DIV) in untreated control cultures and amounts to 3.5 nmol/mg protein. Values represent the mean ± SEM of three independent experiments with four wells in each treatment. $^{*}p < 0.01$, significance compared with untreated control cultures using Kruskal-Wallis test followed by χ^2 test; $^{\#}p < 0.0001$, significance compared with untreated control cultures using Mann-Whitney test; $^{+}p < 0.01$, significance compared with rotenone-treated control cultures using Kruskal-Wallis test followed by χ^2 test.

treatment (Fig. 2). Protection against rotenone toxicity by dopamine agonists has been only sparsely reported in the literature. In mice treated with rotenone the non-ergoline agonist pramipexole saved dopaminergic neurons in the substantia nigra from degeneration [11]. Ropinirole, also belonging to the non-ergoline agonists, prevented rotenone-induced apoptosis in the dopaminergic cell line SH-SY5Y via caspase- and JNK-dependent pathways [2]. Recently, we detected protective properties of the non-ergoline dopamine agonist rotigotine for dopaminergic neurons in primary mesencephalic culture [22]. To our knowledge, this is the first report of neuroprotective properties of an ergot agonist against rotenone toxicity for dopaminergic neurons.

Neuroprotection by cabergoline has been reported previously in different cellular and animal models of neurodegeneration. For instance, Lombardi *et al*. [14] and Miglio *et al*. [16] reported that cabergoline protected SH-SY5Y human neuroblastoma cells against tert-butylhydroperoxide (t-BOOH)- and ischemia-induced cell death, respectively. *In vivo*, Yoshioka *et al*. [32] found that cabergoline reduced the cell death of striatal dopaminergic neurons provoked by 6-hydroxydopamine (6-OHDA) in mice. In our study we found an overall protective effect of cabergoline on the primary mesencephalic cell culture. Cabergoline significantly reduced the release of LDH when applied either alone or together with rotenone (Fig. 3). Cabergoline was similarly reported to reduce LDH release induced by ischemia in SH-SY5Y cells [16].

Neuroprotective effects exerted by dopamine agonists are often mediated via stimulation of dopamine receptors. For instance, blocking of dopamine D_2 receptors by the dopamine receptor antagonist sulpiride prevented dopaminergic neuroprotection by lisuride and α-dihydroergocryptine against glutamate and dopamine, respectively [4,17]. Sulpiride also abolished the protection of dopaminergic neurons by ropinirole against 6-OHDA [9]. In SHSY-5Y cells expressing D_2 receptors the protective effect of cabergoline against paraquat toxicity was partially reduced by inhibition of the D_2 receptor with clozapine [1], and recently it was shown that in cortical neurons cabergoline prevented cell death induced by H_2O_2 through a D_2 receptor-mediated mechanism [18]. In contrast, the protection of THir neurons against rotenone toxicity by cabergoline appears independent of dopamine receptor stimulation. The pretreatment of cultures with sulpiride did not attenuate the rescuing effect of cabergoline for THir neurons in primary mesencephalic cell culture (Fig. 4). Since sulpiride has almost equal affinity to dopamine D_2 and D_3 receptors (Ki~15 nM for the dopamine D_2 receptor and Ki~13 nM for the dopamine D_3 receptor) [26], stimulation of the D_3 receptor is not decisive for the neuroprotective effect of cabergoline either. In this respect cabergoline resembles the non-ergot dopamine agonist pramipexole, which has been shown to protect SHSY-5Y cells against apoptotic cell death induced by rotenone or 1-methyl-4-phenylpyridinium (MPP^+) independent of dopamine receptor stimulation [7]. In contrast, neuroprotective effects against oxidative stress in rat mesencephalic cultures provided by the ergot agonist bromocriptine depended on dopamine receptor stimulation and the synthesis of radical scavenging proteins [23].

Recently, it was shown that male dopaminergic neurons were slightly more sensitive towards rotenone, and estrogen exerted a moderate protective

effect towards both genders [28]. Therefore, it might be of interest in future experiments to investigate the neuroprotective efficacy of cabergoline towards male and female dopaminergic neurons.

Oxidative stress is believed to contribute to the degeneration of dopaminergic neurons in PD [29]. We therefore tested whether cabergoline was able to reduce rotenone-induced oxidative stress in the cultures. Pre-treatment of the cultures with cabergoline was found to reduce overall ROS production elicited by subsequent rotenone addition as measured by CM-H_2DCFDA fluorescence (Fig. 5). Similarly, cabergoline was reported to relieve oxidative stress in different experimental models of PD and in PD patients. For example, Chau *et al*. reported that cabergoline diminished dihydroethidium (DHE) oxidation in SHSY-5Y cells exposed concomitantly to paraquat [1]. Since DHE is predominantly a superoxide indicator, we detected that cabergoline is also able to reduce general oxidative stress induced by rotenone even when the culture is only pre-incubated with the agonist. Isobe *et al*. found that cabergoline scavenged peroxynitrite induced by levodopa in PD patients [12]. Although cabergoline increased GSH synthesis in mesencephalic cell cultures, its neuroprotective effect against rotenone toxicity was not dependent on GSH synthesis, as pre-treatment of mesencephalic cell cultures with the GSH biosynthesis inhibitor BSO did not prevent protection of dopaminergic neurons afforded by cabergoline (Fig. 6). In contrast, Chau *et al*. postulated that the increased GSH level induced by cabergoline in SHSY-5Y cells may at least partially explain the protection against paraquat [1].

Depletion of ATP was reported to be among the major consequences of complex I inhibition in different *in vitro* and *in vivo* PD models. For instance, Im *et al*. [10] and Zaitone *et al*. [33] found that rotenone reduced ATP levels in PC12 cells and Sprague-Dawley rats, respectively. In accordance with these results, treatment of primary mesencephalic cell culture with rotenone resulted in a significant decrease in the ATP/protein ratio compared to untreated cultures (Fig. 7). On the other hand, cabergoline not only significantly increased the ATP content in the culture, but even attenuated rotenone-induced ATP depletion, which might contribute to cabergoline's neuroprotective effect. To our knowledge, this is the first report demonstrating protection against rotenone-induced ATP loss by a dopamine agonist. These results imply that cabergoline might exert its neuroprotective properties also at and via the mitochondrial level.

Conclusions

Cabergoline protected dopaminergic neurons against rotenone-induced cell death in primary mesencephalic cell culture. This effect was independent of dopaminergic stimulation and did not predominantly depend on increased GSH production. Cabergoline could reduce excessive ROS formation and restore the ATP/protein ratio. Moreover, its beneficial effect for the whole culture was detected by reduced LDH release. These results undermine the neuroprotective potential of dopamine agonists and demonstrate that ergot agonists may exert their protective action independently of dopamine receptor stimulation.

Disclosure

The authors report no conflict of interest.

References

1. Chau KY, Korlipara LV, Cooper JM, Schapira AH. Protection against paraquat and A53T alpha-synuclein toxicity by cabergoline is partially mediated by dopamine receptors. J Neurol Sci 2009; 278: 44-53.
2. Chen S, Zhang X, Yang D, Du Y, Li L, Li X, Ming M, Le W. D2/D3 receptor agonist ropinirole protects dopaminergic cell line against rotenone-induced apoptosis through inhibition of caspase- and JNK-dependent pathways. FEBS Lett 2008; 582: 603-610.
3. Dauer W, Przedborski S. Parkinson's disease: mechanisms and models. Neuron 2003; 39: 889-909.
4. Gille G, Radad K, Reichmann H, Rausch WD. Synergistic effect of alpha-dihydroergocryptine and L-dopa or dopamine on dopaminergic neurons in primary culture. J Neural Transm 2006; 113: 1107-1118.
5. Gille G, Rausch WD, Hung ST, Moldzio R, Janetzky B, Hundemer HP, Kolter T, Reichmann H. Pergolide protects dopaminergic neurons in primary culture under stress conditions. J Neural Transm 2002; 109: 633-643.
6. Gille G, Rausch WD, Hung ST, Moldzio R, Ngyuen A, Janetzky B, Engfer A, Reichmann H. Protection of dopaminergic neurons in primary culture by lisuride. J Neural Transm 2002; 109: 157-169.
7. Gu M, Irvani M, Cooper JM, King D, Jenner P, Schapira AH. Pramipexole protects against apoptotic cell death by non-dopaminergic mechanisms. J Neurochem 2004; 91: 1075-1081.
8. Hickey P, Stacy M. Adenosine A2A antagonists in Parkinson's disease: what's next? Curr Neurol Neurosci Rep 2012; 12: 376-385.
9. Iida M, Miyazaki I, Tanaka K, Kabuto H, Iwata-Ichikawa E, Ogawa N. Dopamine D2 receptor-mediated antioxidant and neuro-

protective effects of ropinirole, a dopamine agonist. Brain Res 1999; 838: 51-59.
10. Im AR, Kim YH, Uddin MR, Chae S, Lee HW, Kim YH, Kim YS, Lee MY. Betaine protects against rotenone-induced neurotoxicity in PC12 cells. Cell Mol Neurobiol 2013; 33: 625-635.
11. Inden M, Kitamura Y, Tamaki A, Yanagida T, Shibaike T, Yamamoto A, Takata K, Yasui H, Taira T, Ariga H, Taniguchi T. Neuroprotective effect of the antiparkinsonian drug pramipexole against nigrostriatal dopaminergic degeneration in rotenone-treated mice. Neurochem Int 2009; 55: 760-767.
12. Isobe C, Abe T, Kikuchi T, Murata T, Sato C, Terayama Y. Cabergoline scavenges peroxynitrite enhanced by L-DOPA therapy in patients with Parkinson's disease. Eur J Neurol 2006; 13: 346-350.
13. Lipski J, Nistico R, Berretta N, Guatteo E, Bernardi G, Mercuri NB. L-DOPA: a scapegoat for accelerated neurodegeneration in Parkinson's disease? Prog Neurobiol 2011; 94: 389-407.
14. Lombardi G, Varsaldi F, Miglio G, Papini MG, Battaglia A, Canonico PL. Cabergoline prevents necrotic neuronal death in an in vitro model of oxidative stress. Eur J Pharmacol 2002; 457: 95-98.
15. Marco AD, Appiah-Kubi LS, Chaudhuri KR. Use of the dopamine agonist cabergoline in the treatment of movement disorders. Expert Opin Pharmacother 2002; 3: 1481-1487.
16. Miglio G, Varsaldi F, Francioli E, Battaglia A, Canonico PL, Lombardi G. Cabergoline protects SH-SY5Y neuronal cells in an in vitro model of ischemia. Eur J Pharmacol 2004; 489: 157-165.
17. Moldzio R, Radad K, Duvigneau JC, Kranner B, Krewenka C, Piskernik C, Rausch WD. Glutamate-induced cell death and formation of radicals can be reduced by lisuride in mesencephalic primary cell culture. J Neural Transm 2006; 113: 1095-1105.
18. Odaka H, Numakawa T, Adachi N, Ooshima Y, Nakajima S, Katanuma Y, Inoue T, Kunugi H. Cabergoline, dopamine D2 receptor agonist, prevents neuronal cell death under oxidative stress via reducing excitotoxicity. PLoS One 2014; 9: e99271.
19. Ohta K, Fujinami A, Kuno S, Sakakimoto A, Matsui H, Kawahara Y, Ohta M. Cabergoline stimulates synthesis and secretion of nerve growth factor, brain-derived neurotrophic factor and glial cell line-derived neurotrophic factor by mouse astrocytes in primary culture. Pharmacology 2004; 71: 162-168.
20. Perez-Lloret S, Rascol O. Dopamine receptor agonists for the treatment of early or advanced Parkinson's disease. CNS Drugs 2010; 24: 941-968.
21. Quinn N. Drug treatment of Parkinson's disease. BMJ 1995; 310: 575-579.
22. Radad K, Scheller D, Rausch WD, Reichmann H, Gille G. Neuroprotective effect of rotigotine against complex I inhibitors, MPP+ and rotenone in primary mesencephalic cell culture. Folia Neuropathol 2014; 52: 179-186.
23. Sawada H, Ibi M, Kihara T, Urushitani M, Akaike A, Kimura J, Shimohama S. Dopamine D2-type agonists protect mesencephalic neurons from glutamate neurotoxicity: mechanisms of neuroprotective treatment against oxidative stress. Ann Neurol 1998; 44: 110-119.
24. Schapira AH. Dopamine agonists and neuroprotection in Parkinson's disease. Eur J Neurol 2002; 9 Suppl 3: 7-14.
25. Schapira AH. Neuroprotection in PD-A role for dopamine agonists? Neurology 2003; 61: S34-S42.
26. Seeman P, Van Tol HH. Dopamine receptor pharmacology. Trends Pharmacol Sci 1994; 15: 264-270.
27. Tanner CM, Kamel F, Ross GW, Hoppin JA, Goldman SM, Korell M, Marras C, Bhudhikanok GS, Kasten M, Chade AR, Comyns K, Richards MB, Meng C, Priestley B, Fernandez HH, Cambi F, Umbach DM, Blair A, Sandler DP, Langston JW. Rotenone, paraquat, and Parkinson's disease. Environ Health Perspect 2011; 119: 866-872.
28. Tao Q, Fan X, Li T, Tang Y, Yang D, Le W. Gender segregation in gene expression and vulnerability to oxidative stress induced injury in ventral mesencephalic cultures of dopamine neurons. J Neurosci Res 2012; 90: 167-178.
29. Tripanichkul W, Jaroensuppaperch EO. Ameliorating effects of curcumin on 6-OHDA-induced dopaminergic denervation, glial response, and SOD1 reduction in the striatum of hemiparkinsonian mice. Eur Rev Med Pharmacol Sci 2013; 17: 1360-1368.
30. Utsumi H, Okuma Y, Kano O, Suzuki Y, Iijima M, Tomimitsu H, Hashida H, Kubo S, Suzuki M, Nanri K, Matsumura M, Murakami H, Hattori N. Evaluation of the efficacy of pramipexole for treating levodopa-induced dyskinesia in patients with Parkinson's disease. Intern Med 2013; 52: 325-332.
31. Worth PF. When the going gets tough: how to select patients with Parkinson's disease for advanced therapies. Pract Neurol 2013; 13: 140-152.
32. Yoshioka M, Tanaka K, Miyazaki I, Fujita N, Higashi Y, Asanuma M, Ogawa N. The dopamine agonist cabergoline provides neuroprotection by activation of the glutathione system and scavenging free radicals. Neurosci Res 2002; 43: 259-267.
33. Zaitone SA, Abo-Elmatty DM, Shaalan AA. Acetyl-L-carnitine and alpha-lipoic acid affect rotenone-induced damage in nigral dopaminergic neurons of rat brain, implication for Parkinson's disease therapy. Pharmacol Biochem Behav 2012; 100: 347-360.
34. Zanettini R, Antonini A, Gatto G, Gentile R, Tesei S, Pezzoli G. Valvular heart disease and the use of dopamine agonists for Parkinson's disease. N Engl J Med 2007; 356: 39-46.

Original article

Folia Neuropathologica

Subdural infusion of dexamethasone inhibits leukomyelitis after acute spinal cord injury in a rat model

Jacek M. Kwiecien[1], Bozena Jarosz[2], Lucia Machova Urdzikova[3], Radoslaw Rola[2], Wojciech Dabrowski[4]

[1]Department of Pathology and Molecular Medicine, Michael G. deGroote School of Medicine, McMaster University, Hamilton, Canada, [2]Department of Neurosurgery and Paediatric Neurosurgery, Medical University of Lublin, Lublin, Poland, [3]Department of Stem Cells and Tissue Repair, Institute of Experimental Medicine, Academy of Sciences of the Czech Republic, Prague, Czech Republic, [4]Department of Anaesthesiology and Intensive Therapy, Medical University of Lublin, Lublin, Poland

Folia Neuropathol 2015; 53 (1): 41-51 DOI: 10.5114/fn.2015.49973

Abstract

Trauma in spinal cord injury often results in massive damage to the white matter and in damage to myelin that results in a severe phagocyte-rich infiltration apparently directed at removing immunologically toxic myelin debris. In the epidural balloon crush injury to the rat cranial thoracic spinal cord, the dorsal column was crushed, which at one week post-op resulted in its obliteration by a severe infiltration by a virtually pure population of macrophages that internalized all damaged myelin. A week-long subdural infusion of dexamethasone, a stable synthetic corticosteroid, resulted in remarkable inhibition of the macrophage infiltration of the crush cavity and in the lack of removal of myelin debris by phagocytosis. In this study we demonstrated that spinal cord injury results in a severe inflammatory response directed at massively damaged myelin, and we inhibited this response with a subdural infusion of a powerful anti-inflammatory drug, dexamethasone.

Key words: *spinal cord injury, leukomyelitis, macrophages, subdural infusion, dexamethasone.*

Introduction

Acute damage to the tissue in spinal cord injury (SCI) results in mechanical disruption, haemorrhages and ischaemia, which after 48 h (Kwiecien, unpublished) are followed by a severe inflammatory infiltration [57] that soon becomes directed primarily against damaged myelin and is primarily represented by macrophages [11,12,27,49,58]. This secondary inflammation in the spinal cord white matter is known as leukomyelitis, and is a well-recognized pathological process whose mechanisms are not well understood. Neuropathological evidence indicates that leukomyelitis is a chronic, tissue destructive process, probably sustained by a mechanism of a vicious cycle where massively damaged myelin acts in a potently pro-inflammatory fashion [33], attracting a large number of blood-borne macrophages which when activated, phagocytise damaged myelin and, in the process release a variety of pro-inflammatory factors that cause additional tissue damage involving more myelin damage and macrophage chemotaxis [3,18,19,29,30,39,48,50,56,60]. Although actively expanding leukomyelitis in the rat

Communicating author:

Dr Jacek M. Kwiecien, Department of Pathology and Molecular Medicine, Michael G. deGroote School of Medicine, McMaster University, 1280 Main Street West, Hamilton, Ontario, Canada L8S 4K1, phone: 905-525-9140, fax: 905-522-3580ext. 22827, e-mail: Kwiecien@mcmaster.ca

runs well beyond 2 months [33], its total duration is not known in experimental animals and in human patients, but this severe inflammatory process is self-limiting, indicating unknown anti-inflammatory factors in the surrounding tissue. Since the long duration of leukomyelitis is associated with an expanding volume of irreversibly destroyed tissue of the spinal cord [18] and with progressive loss of neurologic function, the inhibition of this process was attempted in this study.

Methylprednisolone succinate (MPS), a powerful synthetic glucocorticoid derivative, is currently the only approved treatment of spinal cord injury patients. In the standard treatment, an SCI patient follows the National Acute Spinal Cord Injury Study (NASCIS) recommendation and is given an intravenous bolus injection of 30 mg/kg body weight (b.w.) of MPS that is followed by 24-48 hours of intravenous infusion at 5.4 mg/kg b.w./hour [6,7]. This treatment is widely considered as not successful in improving the outcome in the treated SCI patients versus non-treated individuals [17,45]. Severe side effects related to very high doses of MPS have been described in human patients; they include wound infection, pneumonia, sepsis and steroid myopathy and add to the problematic therapeutic value of this treatment [40]. In a study performed on cats, a 30 mg/kg b.w. intravenous (i.v.) bolus of MPS was found to translate into 1.3 μg/g (or 0.004% of total injected) of wet tissue of the spinal cord [8]. The authors of this study determined that the half life of MPS in the spinal cord tissue was 3 h and recommended a 15 mg/kg b.w. injection i.v. every 3 hours to maintain this tissue level. These data indicate that intravenous administration of large quantities of MPS may not translate into its therapeutic effectiveness in the SCI at the tissue level. In addition, since leukomyelitis is a chronic inflammatory process, for an anti-inflammatory therapy to be effective, it should likely be administered in a sustained fashion, well beyond a single intraperitoneal (i.p.) injection of 30 mg/kg b.w. [32,42,53-55], or multiple i.p. injections over 48 h [24], or single intravenous (i.v.) injection of 30 mg/kg b.w. [13,15,23,28,41] or multiple i.v. injections within 24 h [43], or 30 mg/kg b.w. bolus i.v. followed by maintenance 5.4 mg/kg b.w. per hour for 24 h [25]. A short-term intrathecal administration [62] as performed in some experiments on SCI rats or a single i.v. injection of 30 mg/kg b.w. [64] or a bolus i.v. injection of 30 mg/kg b.w. followed by i.v. injections of 5.4 mg/kg b.w. every 2.5 h [37] in rabbit models of SCI, or single or multiple doses of 15-60 mg/kg b.w. i.v. in a cat model of SCI [1,9], were also attempted. The NASCIS 24-48-hour intravenous protocol is available to human patients [6,7,63], but it is not considered efficacious.

In the present study we adopted an epidural spinal cord injury method with a crush effected by a temporarily inflated balloon [61] to create an injury and initiate leukomyelitis. We infused the crush lesion subdurally with dexamethasone, a stable and more powerful substitute for MPS, delivered over a period of 1 week, which resulted in a virtually absent infiltration by macrophages that we interpret as inhibition of leukomyelitis.

Material and methods

Experiments on rats were conducted at the Central Animal Facility, McMaster University, after approval by the Animal Research Ethics Board according to the guidelines by the Canadian Council on Animal Care.

Balloon compression spinal injury

A total of 13 mature Long Evans rats of both sexes were induced and maintained under isoflurane anaesthesia. Balloon crush injury was adopted from Vanicky *et al*. [61,62]. Laminectomy was performed over the lumbar region of the spinal cord and a 3F embolectomy catheter (ZTS Hagmed, Poland) was inserted epidurally over the dorsal spinal cord to place the balloon in the rostral thoracic segment of the spinal cord. The sleeve of the catheter was filled with saline, and the balloon was inflated with 0.2 ml of saline using a Hamilton syringe (VWR International) for 5 s. After the compression evidenced by sudden movement of the hind legs, the balloon was deflated and the catheter carefully removed.

Subdural infusion

Immediately after the balloon crush, in the laminectomy site in the lumbar spine the dura was cut with a 25 gauge needle and a rat intrathecal catheter (Alzet, Durect Corporation, Cupertino, CA) was carefully inserted into the subdural space over the dorsal spinal cord to approximate the end of the catheter with the site of the balloon crush. After the steel wire was removed from the catheter, the free end was attached to a 2 ml osmotic pump with infu-

sion time of 1 week (Alzet) that was pre-loaded with 2 ml of dexamethasone (Dexamethasone 2, 2 mg/ml, Vetoquinol N-A. Inc, Lavartrie, Quebec, Canada) in 5 rats (dexamethasone treatment group, $n = 5$) or 2 ml of phosphate buffered saline (PBS) pH 7.2 in 5 rats (control treatment group, $n = 5$). The attached pump was placed subcutaneously on the flank of the rat. The surgery rats were injected subcutaneously with 5 ml of saline and 0.3 ml of ketoprofen (10 mg/ml, Anafen, Merial Canada, Inc., Baie d'Urfe, Quebec, Canada) for analgesia prior to recovery from anaesthesia. The injections of analgesic were repeated once daily for 2 more days, and administration of saline was performed 1-2 times daily as indicated by the hydration status. Three additional rats were subjected to the balloon crush and perfused at 2 h post-surgery to serve as acute controls.

Clinical observations

All 13 rats with the balloon crush injury recovered well and had marked paresis or complete paralysis of the hind end throughout the 1 week of survival. Rats treated with dexamethasone were doing progressively poorly after post-op day 4. They were lethargic, dehydrated, the food intake was markedly reduced or nil, and the body condition was deteriorated. Rats treated with PBS remained in good health except for motor neurologic deficits. At post-op day 6, open field behavioural testing was attempted on the rats, but it was deemed inconclusive due to pronounced weakness in dexamethasone-treated rats.

Perfusions

At post-op day 7, the surgery rats were overdosed with 100 mg/kg b.w. sodium barbital (Ceva, France), the chest was opened and 100 IU sodium heparin intracardiac injection was administered. The blood was washed out by lactated Ringer's solution (Baxter, Canada) via the left cardiac ventricle with the outflow created by cutting the right heart auricle [34]. The animals were perfusion-fixed in 10% buffered formalin, carcasses post-fixed at 4°C for 1-3 hours and the spinal cord removed carefully and post-fixed in 10% formalin. Other routine tissues – the brain, mandibular salivary glands, thyroid glands, trachea, oesophagus, lung, heart, diaphragm, liver, spleen, kidney, pancreas, duodenum, caecum, colon, testis, epididymis, sexual glands, ovary, uterus, cervix and urinary bladder – were also sampled for histological analysis.

Histology, immunohistochemistry

The length of the spinal cord was sectioned transversely into 2 mm thick segments with the cranial face placed down in the tissue cassette. The tissues were treated by raising concentrations of ethyl alcohol and xylene, embedded in paraffin, cut 4 μm thick and mounted on glass slides. Histochemical stains used included the routine haematoxylin and eosin (H&E) stain, periodic acid-Schiff (PAS) to stain intracellular carbohydrates indicative of active phagocytosis [59] and Luxol fast blue (LFB) for myelin [59]. For immune stains, the glass-mounted sections were heated at 58°C overnight and deparaffinised in a Target Retrieval Solution, pH buffer (DAKO) at 97°C for 20 min in a DAKO PT Link Pre-Treatment Module for Tissue Specimens PT101 apparatus. Antibodies against the CD68 antigen and against the glial fibrillary acidic protein (GFAP) were obtained from DAKO Corp., were applied at a 1 : 50 dilution, and the positive reaction was visualized with DAKO EnVision+System-HRP (DAB+). The histological analysis was performed under a Nikon Eclipse 50i microscope and the abnormalities in the spinal cord and in other tissues photographed.

Results

Clinical observations

All rats recovered well from the surgery and had hind end paralysis. Some of the rats developed paralysis of the urinary bladder requiring manual expression of urine from a distended bladder 3-4 times a day. Although the untreated rats did well until the end of the study, rats treated with dexamethasone did poorly after day 4 post-op and were treated with subcutaneous saline 10 ml, 1-2 times a day until the sacrifice.

Although open field testing of the rats was attempted at post-op day 6, it was inconclusive, since the dexamethasone rats were remarkably weak and the motor function could not be assessed in relation to the spinal cord injury.

Histology, immunohistochemistry

In rats perfused 2 hours after the balloon crush surgery there was a tear of a large proportion of

the dorsal column (Fig. 1) resulting in its separation from the surrounding tissue of the spinal cord. The separation contained discontinuous haemorrhages, but there was no evidence of active demyelination (Fig. 1B,E) or of infiltration by phagocytic cells (Fig. 1C,F).

In untreated rats at 1 week post-op the dorsal column was obliterated by a severe inflammatory exudate directly connected with the subdural space (Fig. 2A-C) composed predominantly of mononuclear cells containing an oval or round nucleus surrounded by abundant, often microvacuolated cytoplasm (Fig. 2D) staining positively with LFB (Fig. 2E) for internalized myelin debris and often staining positively with PAS (Fig. 2F), which indicates active phagocytosis [59]. Free, un-phagocytized red blood cells and LFB-positive debris were not apparent in the inflammatory exudate (Fig. 2D-E). The phagocytic cells were interpreted as macrophages, some of which stained or stained weakly with anti-CD68 antibody (Fig. 2G) even though this antibody labelled well numerous monocytes in the lumen of blood vessels in the adjacent tissue (Fig. 2H). The area of inflammation was called leukomyelitis, inflammation of the white matter of the spinal cord, and it was surrounded by remarkable astroglial reaction with GFAP-positive, enlarged, hypertrophied astrocytes in the band of tissue 100-150 μM thick surrounding the leukomyelitis (Fig. 2I-J).

In rats treated for 1 week with subdural infusion of 4 mg dexamethasone, the cavity of the crush was directly connected to the subdural space (Fig. 3A) and contained many free, un-phagocytized red blood cells (Fig. 3B) and debris that were positive on the LFB stain (Fig. 3C) and considered damaged myelin. There were rare phagocytic cells positive on the PAS stain and rare cells labelled positive with CD68 antibody scattered throughout (Fig. 3D-E). In the tissue surrounding the cavity of the crush, the GFAP stain revealed a band of astrogliosis, approximately 100-150 μM wide (Fig. 3F), with apparently increased numbers of markedly hypertrophied astrocytes (Fig. 3G).

In both dexamethasone-treated and un-treated rats in areas of the spinal cord at a distance, caudal to and separate from the lesion cavity, there were foci of haemorrhage in the dorsal column (Fig. 4A) surrounded by phagocytic cells with brown, finely granular material in the cytoplasm interpreted as haemosiderin (Fig. 4B). Although haemorrhages were not accompanied by loss of myelin (Fig. 3C), many scattered cells had PAS-positive cytoplasm (Fig. 4D), and there was astrogliosis in the surrounding tissue (Fig. 4E).

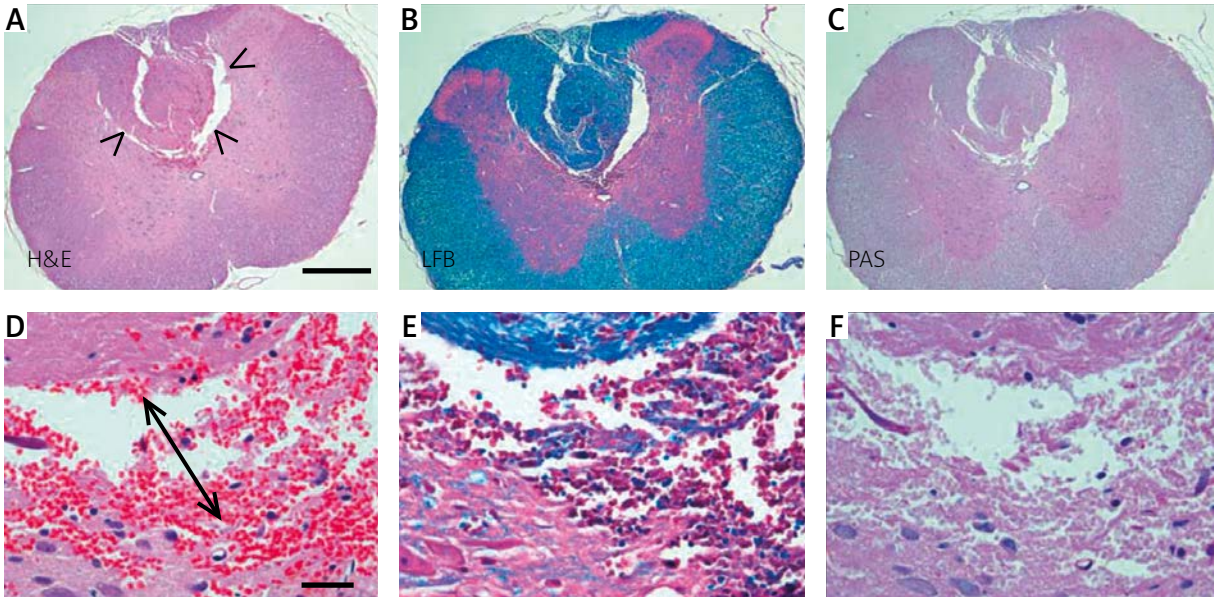

Fig. 1. Cross sections of the thoracic spinal cord from a rat with balloon crush injury perfused 2 h post-op. Large round area in the dorsal column appears separated from the surrounding tissue (arrowheads in **A**) and is surrounded by haemorrhages (**D**). Luxol fast blue (LFB) stain reveals tissue disruption around the dorsal column (**B, E**) but no evidence of myelin loss. Periodic acid-Schiff (PAS) stain reveals no active phagocytosis in the area of the disruption and haemorrhage (**C, F**). Bar 600 μm – **A-C**; 120 μm – **D-F**.

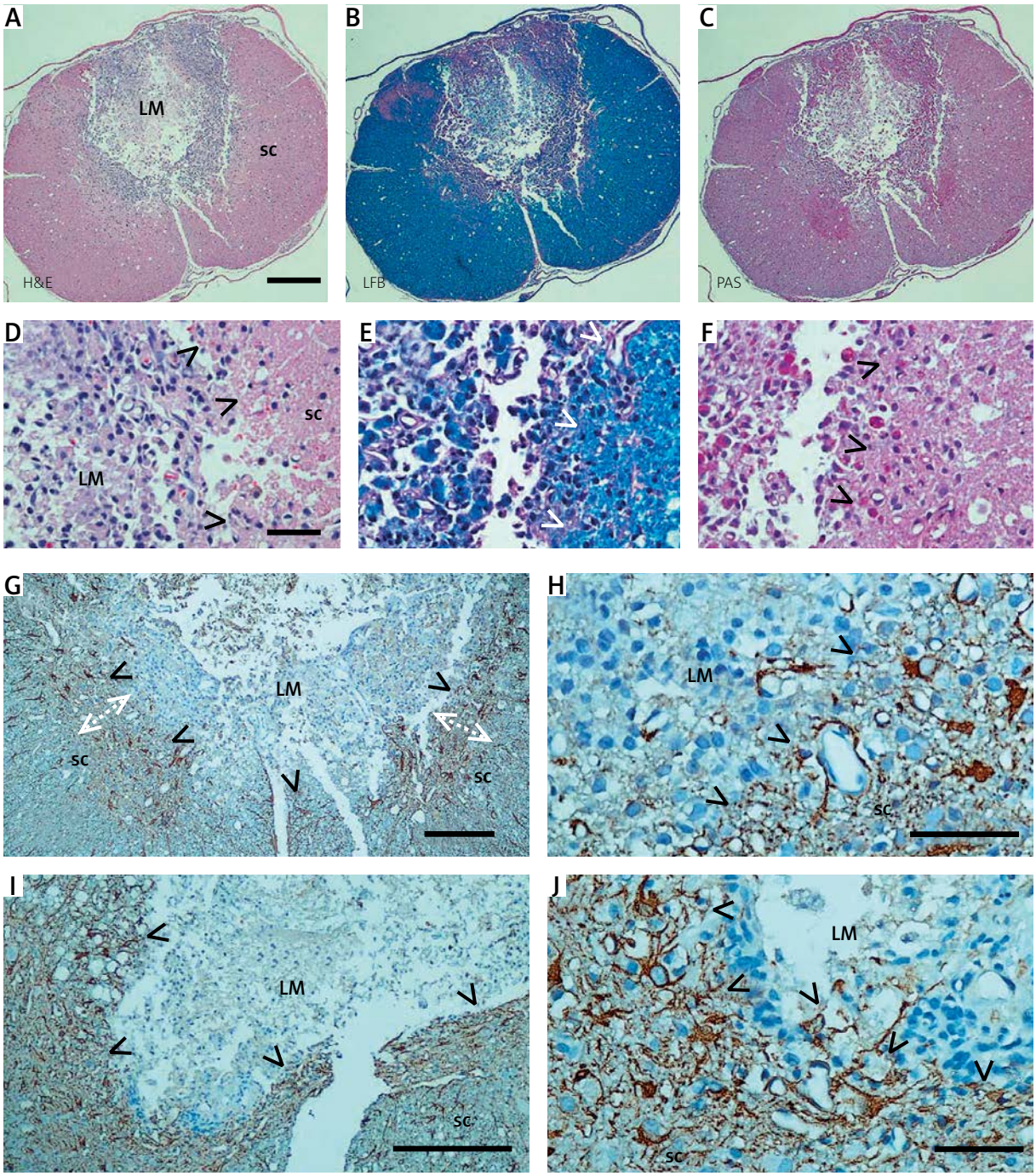

Fig. 2. Cross sections from the thoracic spinal cord 1 week after the balloon crush. The dorsal column is obliterated by leukomyelitis (LM) whose severe inflammatory infiltrate is delineated by arrowheads from the surrounding tissue of the spinal cord (sc) and is rich in macrophages that internalize LFB-positive myelin debris (**E**) and a large proportion of which are positive on PAS stain (**F**). A proportion of macrophages in the area of leukomyelitis are positive or weakly positive on anti-CD68 antibody staining (**G**), but there is strong positive staining of cells in the lumen of blood vessels in the adjacent tissue (**H**) that are interpreted as monocytes. Band-like astrogliosis is evidenced by anti-GFAP antibody (**I-J**) in the tissue surrounding the cavity of the LM. Bars, **A-C** – 600 μM; **D-H, J** – 60 μM; **I** – 200 μM.

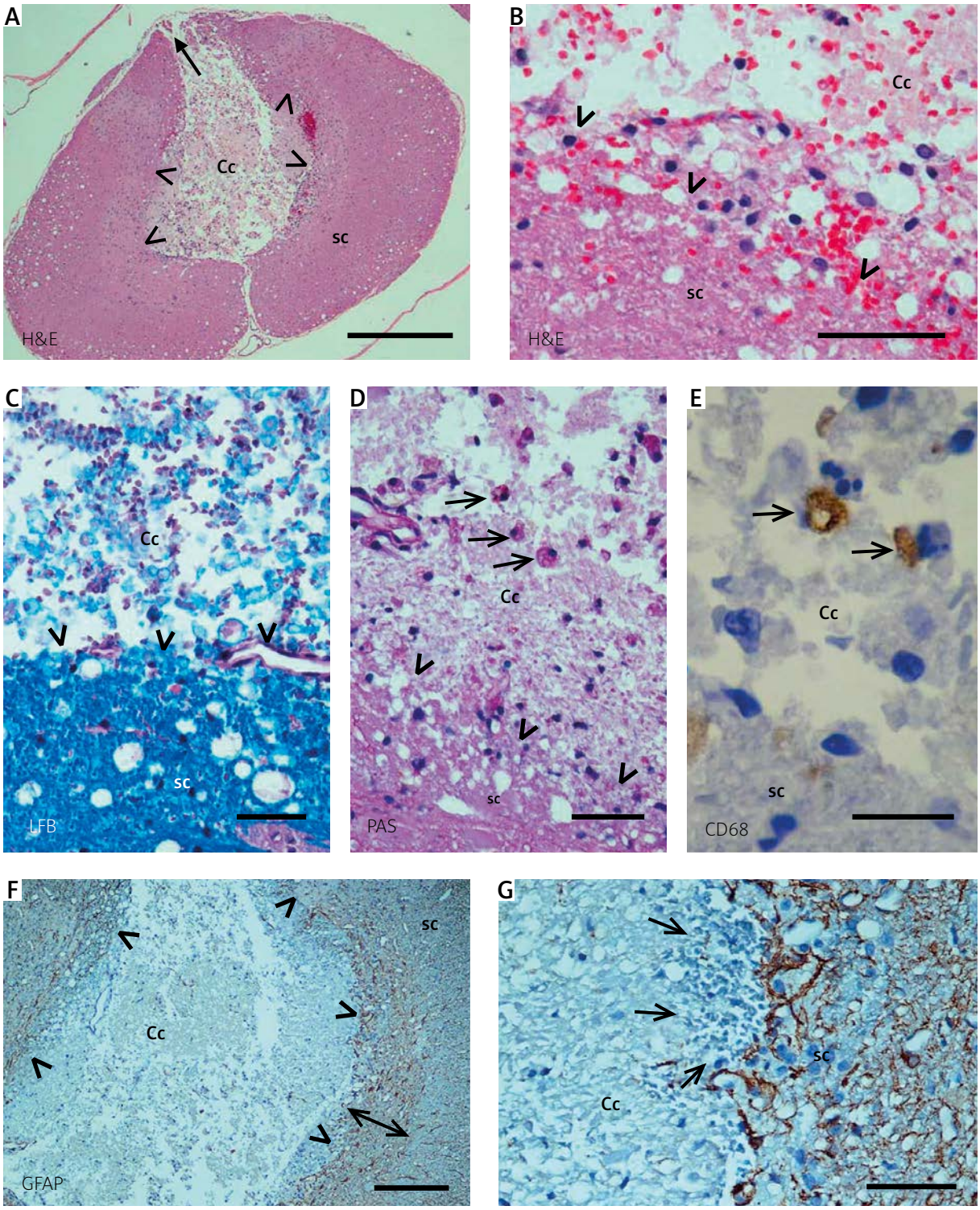

Fig. 3. The thoracic spinal cord 1 week after the crush, with 4 mg dexamethasone infused throughout the post-op period subdurally in the vicinity of the crush lesion. The dorsal column is obliterated by the crush cavity (Cc) delineated by arrowheads, which apparently is connected with the subdural space (arrow in **A**) and contains scattered haemorrhages and proteinaceous material that stains positively with eosin on the H&E stain (**A, B**), and on the LFB stain (**C**), indicating widespread presence of damaged myelin that is not internalized by phagocytes. Scattered throughout there are rare individual PAS-positive cells (arrows in **D**) interpreted as macrophages. A proportion of cells scattered in the crush cavity stain positively with anti-CD68 antibody (**E**). The tissue of the spinal cord surrounding the crush contains a band of astrogliosis evidenced by anti-GFAP antibody (double headed arrow in **F, G**). Bars, **A** – 600 μM; **B-E, G** – 60 μM; **F** – 200 μM.

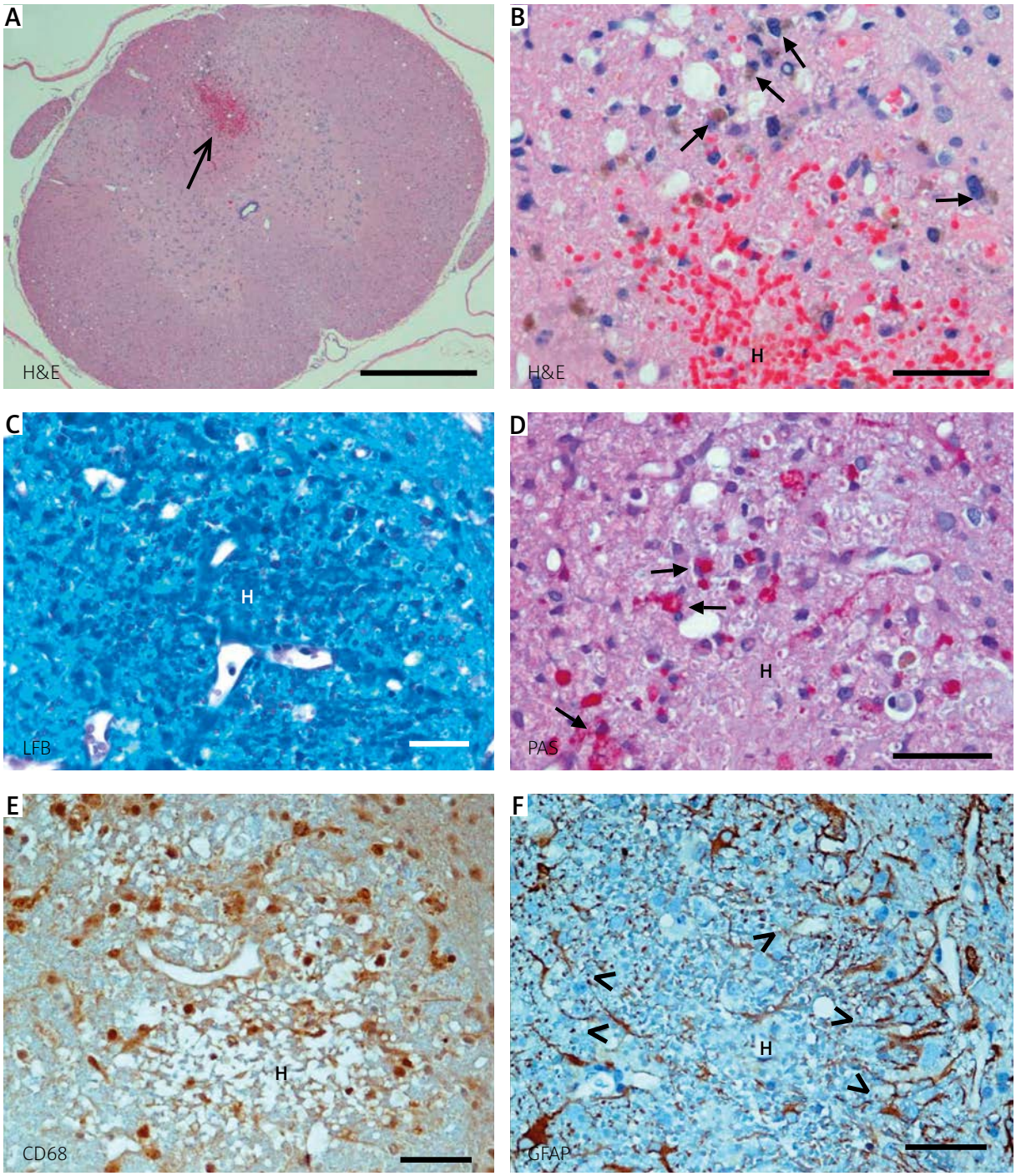

Fig. 4. In an untreated rat surviving the balloon crush for 1 week, the thoracic spinal cord at a distance from the crush lesion contains a large area of haemorrhage in the dorsal column, arrow in **A**. The haemorrhage is surrounded by scattered cells with elongated, sometimes subcleaved nucleus and finely granular brown material in the cytoplasm (small arrows in **B**). The phagocytic cells are interpreted as macrophages or microglia and the brown material as hemosiderin. The haemorrhage is not accompanied by loss of myelin (**C**). There are scattered cells with cytoplasm positive for PAS stain (**D**) that infiltrate the hemorrhagic area (**H**) that is delineated by arrowheads and surrounded by astrogliosis in **E**. Bars, **A** – 600 μM; **B-E** – 60 μM.

Histological analysis of extraneural tissues in rats treated with dexamethasone revealed remarkable organ pathology including splenic lymphoid atrophy, hepatic degeneration, kidney calcinosis, atrophying myopathy, colitis, degenerative changes in the islets of Langerhans in the pancreas and hemorrhagic cystitis. Analysis of extraneural tissues in the un-treated rats was not remarkable.

Discussion

In this study we successfully inhibited a severe phagocyte-rich inflammatory reaction to a spinal cord injury. Leukomyelitis, inflammation of the white matter in the spinal cord, was initiated by massive damage to the white matter in the dorsal column by means of crushing by an inflated catheter balloon placed epidurally. Subdural infusion of dexamethasone, a powerfully anti-inflammatory, stable, synthetic analogue of glucocorticoids, allowed for circumvention of the blood-brain barrier and apparently for achieving a sufficiently high concentration of this drug in the cerebrospinal fluid in proximity of the crush lesion to prevent severe, phagocyte-rich inflammation. Since the crush cavity was directly connected with the subdural space, it is considered that dexamethasone diffused from the subdural space into the crush cavity and thus inhibited massive infiltration by macrophages, therefore effectively arresting destruction of the neural tissue surrounding the cavity of the crush by the inflammatory process of leukomyelitis.

Although methylprednisolone has previously been used to treat spinal cord injury [6,7], this drug is unstable in an aqueous solution beyond 24 hours, and in this study we used a more stable and 7 times more powerful [20] glucocorticoid analogue, dexamethasone. Anti-inflammatory activities of dexamethasone are powerful and multifactorial [20]. *In vitro*, dexamethasone can suppress phagocytosis by activation of murine peritoneal macrophages [4,5], which parallels reduction in the lysosomal secretion [22], with the reduced secretion of the lysosomal elastase [14], arachidonic acid [5], prostaglandins [10], thromboxane B2 and leukotriene B4 [21]. Dexamethasone inhibited the proliferation of macrophages after their activation by oxidized low-density lipoprotein, which coincided with the reduction in the levels of the granulocyte/macrophage colony stimulating factor in one study [52], and inhibited the differentiation of macrophages into multinucleated osteoclasts, bone-lysing cells, in another [46]. Other *in vitro* studies determined that a lipopolysaccharide-activated macrophage ability to kill mastocytoma tumours was inhibited by dexamethasone in parallel with the reduced glucose uptake by treated macrophages [44], the latter observation having been confirmed in another study [51]. Dexamethasone inhibits the toxicity of macrophages by reducing their nitric oxide production [36], and by related inhibition of inducible nitric oxide synthase [31]. In an *in vivo* study using a balloon injury of femoral arteries in the rabbit, daily administration of intramuscular 1 mg/kg b.w. dexamethasone resulted in a remarkable reduction of the macrophage accumulation in the wall of the damaged arteries coincident with the reduced expression of monocyte chemoattractant protein-1 [47]. This treatment did not, however, affect the levels of circulating monocytes, the adhesion of monocytes to the vascular endothelium or their ability to migrate [47], indicating that although anti-inflammatory activities of dexamethasone are powerful and multifactorial, there are a number of mechanisms of inflammation that this drug does not affect.

In our model of leukomyelitis, dexamethasone inhibited accumulation of macrophages in the cavity of the crush by mechanisms we did not investigate. In rats not treated with dexamethasone we observed widespread phagocytic activity of macrophages with the internalization of LFB-positive myelin debris. Free, LFB-positive, myelin material was not observed in the lesion cavity in the untreated rats. In contrast, large amounts of LFB-positive material remained free in the cavity of injury in the dexamethasone-treated rats, presumably because it was not removed by macrophage phagocytosis. Given the severity of the inflammatory response following the massive myelin damage in our model of the spinal cord injury and complete internalization of myelin debris by macrophages, the notion of severe pro-inflammatory activity of damaged myelin appears appropriate. Therefore, inhibiting its internalization by macrophage phagocytosis in dexamethasone-treated rats allowed us to postpone the onset of leukomyelitis for 1 week but not to eliminate it. Clearly, potent pro-inflammatory activity of non-phagocytized myelin debris in the crush lesion will need to be addressed in future studies where an effective but non-toxic anti-inflammatory treatment is administered for a longer period of time to SCI

rats, allowing perhaps for elimination of damaged myelin by mechanisms not requiring phagocytosis with the associated tissue destruction.

Although the mouse anti-human CD68 antigen antibody used in this study labelled well intravascular monocytes in the neural tissue surrounding the cavity of injury, only a proportion of mononuclear cells in the cavity of injury were labelled. This antibody was selected due to its reliable labelling of macrophages in formalin-fixed and paraffin-embedded tissues [16]. Since a virtually uniform population of cells internalizing the LFB-positive material had a round to oval nucleus, and abundant, microvacuolated cytoplasm that often stained positive on the PAS reaction, we consider them macrophages and suggest that the patchy labelling with the anti-CD68 antibody may be indicative of dynamic changes in the surface epitopes of macrophages potently activated by damaged myelin.

The evidence of reactive astrogliosis in the spinal cord tissue surrounding the cavity of leukomyelitis is consistent with astrogliosis around stroke lesions [2,38]. Although the role of astrogliosis in progression of leukomyelitis is unknown, old lesions in the spinal cord, also known as syringomyelia, that are filled with clear cerebrospinal fluid and do not contain inflammatory cells, are invariably surrounded by a wall of hypertrophied astrocytic processes [26,35]. Interestingly, the high dose of dexamethasone used in this study did not appear to have an inhibitory effect on astrogliosis despite being potently inhibitory to phagocytosis.

Evidence of acute haemorrhages in areas isolated from the site of the injury is indicative of fragility of blood vessels of the spinal cord in post-traumatic rats. Although the precise mechanism of acute haemorrhages is unknown, it is important to emphasize that the movement of the rats was not restricted post-operatively and the potential for movement of the spinal cord remained. This observation may serve as supportive evidence for the need to immobilize the spine of the traumatized patients, apparently to prevent additional haemorrhages after the initial spinal cord injury.

Acknowledgements

We wish to thank Dr. H. Szechtman and M. Tucci for their help with the open field studies. This study was funded by the Medical University of Lublin, Poland.

Disclosure

The authors report no conflict of interest.

References

1. Anderson DK, Means ED, Waters TR, Green TS. Microvascular perfusion and metabolism in injured spinal cord after methylprednisolone treatment. J Neurosurg 1982; 56: 106-113.
2. Bailey EL, Smith C, Sudlow CLM, Wardlaw JM. Pathology of lacunar ischemic stroke in humans – a systematic review. Brain Pathol 2012; 22: 583-591.
3. Bao F, Dekaban GA, Weaver LC. Anti-CD11d antibody treatment reduces free radical formation and cell death in the injured spinal cord of rats. J Neurochem 2005; 94: 1361-1373.
4. Becker J, Grasso RJ. Suppression of phagocytosis by dexamethasone in macrophage cultures: inability of arachidonic acid, indomethacin, and nordihydroguaiaretic acid to reverse the inhibitory response mediated by a steroid-inducible factor. Int J Immunopharmacol 1985; 7: 839-847.
5. Becker JL, Grasso RJ, Davis JS. Dexamethasone action inhibits the release of arachidonic acid from phosphatidylcholine during the suppression of yeast phagocytosis in macrophage cultures. Biochem Biophys Res Commun 1988; 153: 583-590.
6. Bracken MB, Shepard MJ, Collins WF, Holford TR, Young W, Baskin DS, Eisenberg HN, Flamm E, Leo-Summers L, Maroon J, Marshall LF, Perot PL, Piepmeier J, Sonntag VKH, Wagner FC, Wilberger JE, Winn HR. A randomized, controlled trial of methylprednisolone or naloxone in the treatment of acute spinal-cord injury. N Eng J Med 1990; 322: 1405-1411.
7. Bracken MB. Steroids for acute spinal cord injury (Review). Cochrane Database Syst Rev 2012; 1: 1-51.
8. Braughler JM, Hall ED. Correlation of methylprednisolone levels in cat spinal cord with its effects on $(Na^+ + K^+)$-ATPase, lipid peroxidation, and alpha motor neuron function. J Neurosurg 1982; 56: 838-844.
9. Braughler JM, Hall ED. Effects of multi-dose methylprednisolone sodium succinate on injured cat spinal cord neurofilament degradation and energy metabolism. J Neurosurg 1984; 61: 290-295.
10. Brune K, Kalin H, Rainsford KD, Wagner K. Dexamethasone inhibits the release of prostaglandins and the formation of autophagic vacuoles from stimulated macrophages. Adv Prostaglandin Thromboxane Res 1980; 8: 1679-1684.
11. Carlson SL, Parrish ME, Springer JE, Doty K, Dossett L. Acute inflammatory response in spinal cord following impact injury. Exp Neurol 1998; 151: 77-88.
12. Chang HT. Subacute spinal cord contusion: few lymphocytes and many macrophages. Spinal Cord 2007; 45: 174-182.
13. Chen H-C, Fong T-H, Lee A-W, Chi W-T. Autophagy is activated in injured neurons and inhibited by methylprednisolone after experimental spinal cord injury. Spine 2012; 37: 470-475.
14. Dahlgren ME, Davies P, Bonney RJ. Phorbol myristate acetate induces the secretion of an elastase by populations of resident and elicited mouse peritoneal macrophages. Biochim Biophys Acta 1980; 630: 338-351.

15. Emmez H, Borcek AO, Kaymaz M, Kaymaz F, Durdag E, Civi S, Gulbahar O, Aykol S, Pasaoglu A. Neuroprotective effects of gabapentin in experimental spinal cord injury. World Neurosurg 2010; 73: 729-734.
16. Falini B, Flenghi L, Pileri S, Gambacorta M, Bigerna B, Durkop H, Eitelbach F, Thiele J, Pacini R, Cavaliere A, Martelli M, Cardarelli N, Sabattini E, Poggi S, Stein H. PG-M1: A new monoclonal antibody directed against a fixative-resistant epitope on the macrophage-restricted form of the CD68 molecule. Am J Pathol 1993; 142: 1359-1372.
17. Felleiter P, Muller N, Schumann F, Felix O, Lierz P. Changes in the use of methylprednisolone protocol for traumatic spinal cord injury in Switzerland. Spine 2012; 37: 953-956.
18. Fitch MT, Doller C, Combs CK, Landreth GE, Silver J. Cellular and molecular mechanisms of glial scarring and progressive cavitation: in vivo and in vitro analysis of inflammation-induced secondary injury after CNS trauma. J Neurosci 1999; 19: 8182-8198.
19. Fleming JC, Norenberg MD, Ramsay DA, Dekaban GA, Marcillo AE, Saenz AD, Pasquale-Styles M, Dietrich DD, Weaver LC. The cellular inflammatory response in human spinal cords after injury. Brain 2006; 129: 3249-3269.
20. Fraser CM, Mays A. Steroids. In: The Merck Veterinary Manual. 6th ed. Fraser CM, Mays A (eds.). Merck & CO., Inc., Rahway 1986; pp. 1592-1596.
21. Fuller RW, Kelsey CR, Cole PJ, Dollery CT, McDermott J. Dexamethasone inhibits the production of thromboxane B2 and leukotriene B4 by human alveolar and peritoneal macrophages. Clin Sci 1984; 67: 653-656.
22. Gewert K, Tapper H, Naucler C, Sundler R. Dexamethasone downregulates lysosomal secretion in mouse macrophages: involvement of signalling through protein kinase C. J Inflamm 1996; 47: 115-125.
23. Gul S, Hanci V, Bahadir B, Acikgoz S, Baktas S, Ankarali H, Kalayci M, Acikgoz B. The effectiveness of dexmedetomidine in experimental spinal cord injury compared to methylprednisolone in rats. J Clin Neurosci 2010; 17: 490-494.
24. Ha K-Y, Carragee E, Cheng Y, Kwon S-E, Kim Y-H. Pregabalin as a neuroprotector after spinal cord injury in rats: biochemical analysis and effect on glial cells. J Korean Med Sci 2011; 26: 404-411.
25. Hanci V, Kerimoglu A, Koca K, Baskesen A, Kilic K, Tastekin D. The biochemical effectiveness of N-acetylcysteine in experimental spinal cord injury in rats. Turkish J Trauma Emerg Surg 2010; 16: 15-21.
26. Horenstein S. Intramedullary cyst formation with progressive gliosis (traumatic syringomyelia) following spinal cord injury. Trans Am Neurol Assoc 1970; 95: 263-266.
27. Hughes JT. Disorders of the spine and spinal cord. In: Greenfield's Neuropathology. 5th ed. Adams JH, Duchen LW (eds.). Oxford University Press, New York 1992; pp. 1083-1115.
28. Kavakli HS, Koca C, Alici O. Antioxidant effects of curcumin in spinal cord injury in rats. Turk J Trauma Surg 2011; 17: 14-18.
29. Kigerl KA, McGaughy VM, Popovich PG. Comparative analysis of lesion development and intraspinal inflammation in four strains of mice following spinal contusion injury. J Comp Neurol 2006; 494: 578-594.
30. Kigerl KA, Gensel JC, Ankeny DP, Alexander JK, Donnelly DJ, Popovich PG. Identification of two distinct macrophage subsets with divergent effects causing either neurotoxicity or neuroregeneration in the injured mouse spinal cord. J Neurosci 2009; 29: 13435-13444.
31. Korhonen R, Lahti A, Hamalainen M, Kankaanranta H, Moilanen E. Dexamethasone inhibits inducible nitric-oxide synthase expression and nitric oxide production by destabilizing mRNA in lipopolysaccharide-treated macrophages. Mol Pharmacol 2002; 62: 698-704.
32. Kose EA, Bakar B, Ayva SK, Kilinc K, Apan A. Neuroprotective effects of racemic ketamine and (S)-ketamine on spinal cord injury in rat. Injury Int J Care Inj 2012; 43: 1124-1130.
33. Kwiecien JM. Cellular mechanisms of white matter regeneration in an adult dysmyelinated rat model. Folia Neuropathol 2013; 51: 189-202.
34. Kwiecien JM, Blanco M, Fox JG, Delaney KH, Fletch AL. Neuropathology of bouncer Long Evans, a novel dysmyelinated rat. Comp Med 2000; 50: 503-510.
35. Levine DN. The pathogenesis of syringomyelia associated with lesions at the foramen magnum: a critical review of existing theories and proposal of a new hypothesis. J Neurol Sci 2004; 220: 3-21.
36. Li Y, Ito N, Suzuki T, Stechschulte DJ, Dileepan KN. Dexamethasone inhibits nitric oxide-mediated toxicity via effects on both macrophages and target cells. Immunopharmacol 1995; 30: 177-186.
37. Lin H-S, Ji Z-S, Zheng L-H, Guo G-Q, Chen B, Wu H, Zhang G-W. Effect of methylprednisolone on the activities of caspase-3, -6, -8, and -9 in rabbits with acute spinal cord injury. Exp Ther Med 2012; 4: 49-54.
38. Mancardi GL, Romagnoli P, Tassinari T, Gandolfo C, Primavera JM, Loeb C. Lacunae and cribriform cavities of the brain. Eur Neurol 1988; 28: 11-17.
39. Mantovani A, Sica A, Sozzani S, Allavena P, Vecchi A, Locati M. The chemokine system in diverse forms of macrophage activation and polarization. Trends Immunol 2004; 25: 677-686.
40. Markandaja M, Sten DM, Menaker J. Acute treatment options for spinal cord injury. Curr Treatment Options Neurol 2012; 14: 175-187.
41. Meng B, Zhang Q, Huang C, Zhanh HT, Tang T, Yang HL. Effects of a single dose of methylprednisolone versus three doses of rosiglitazone on nerve growth factor levels after spinal cord injury. J Int Med Res 2011; S39: 805-814.
42. Ning N, Dang X, Bai C, Zhang C, Wang K. Panax notoginsenoside produces neuroprotective effects in rat model of acute spinal cord ischemia-reperfusion injury. J Ethnopharmacol 2012; 139: 504-512.
43. Park S-J, Oh I-S, Kwon J-Y, Ha K-Y. The effect of irradiation and methylprednisolone in spinal cord injured rats. Spine 2011; 36: 434-440.
44. Perret G, Lemaire G. Dexamethasone inhibits antitumor potential of activated macrophages by a receptor mediated action. Biochem Biophys Res Commun 1986; 136: 130-136.
45. Pettiford JN, Bikhchandani J, Ostlie BJ, St. Peter SD, Sharp RJ, Juang D. A review: the role of high dose methylprednisolone in

spinal cord trauma in children. Pediatr Surg Int 2012; 28: 287-294.
46. Pharoah MJ, Heersche JMN. Dexamethasone inhibits formation of osteoclast-like cells in bone marrow cultures. J Dent Res 1986; 65: 1006-1009.
47. Poon M, Gertz SD, Fallon JT, Wiegman P, Berman JW, Sarembock IJ, Taubman MB. Dexamethasone inhibits macrophage accumulation after balloon arterial injury in cholesterol fed rabbits. Atherosclerosis 2001; 155: 371-380.
48. Popovich PG, Guan Z, Wei P, Huitinga I, van Rooijen N, Stokes BT. Depletion of hematogenous macrophages promotes partial hindlimb recovery and neuroanatomical repair after experimental spinal cord injury. Exp Neurol 1999; 158: 351-365.
49. Popovich PG, Hickey WF. Bone marrow chimeric rats reveal the unique distribution of resident and recruited macrophages in the contused rat spinal cord. J Neuropathol Exp Neurol 2001; 60: 676-685.
50. Popovich PG, Wei P, Stokes BT. Cellular inflammatory response after spinal cord injury in Sprague-Dawley and Lewis rats. J Comp Neurol 1997; 377: 443-464.
51. Rist RJ, Naftalin RJ. Dexamethasone inhibits the hexose monophosphate shunt in activated rat peritoneal macrophages by reducing hexokinase-dependent sugar uptake. Biochem J 1991; 278: 129-135.
52. Sakai M, Biwa T, Matsumura T, Takemura, T, Matsuda H, Anami Y, Sasahara T, Kobori S, Shichiri M. Glucocorticoid inhibits oxidized LDL-induced macrophage growth by suppressing the expression of granulocyte/macrophage colony-stimulating factor. Artheroscler Thromb Vasc Biol 1999; 19: 1726-1733.
53. Sanli AM, Serbes G, Caliskan M, Kaptanoglu E, Sargon MF, Kilinc K, Besalti O, Sekerci Z. Effect of granulocyte-colony stimulating factor on spinal cord tissue after experimental contusion injury. J Clin Neurosci 2010; 17: 1548-1552.
54. Sanli AM, Serbes G, Sargon MF, Caliskan M, Kilinc K, Bulut H, Sekerci Z. Mathothrexate attenuates early neutrophil infiltration and the associated lipid peroxidation in the injured spinal cord but does not induce neurotoxicity in the injured spinal cord in rats. Acta Neurochirurg 2012; 154: 1045-1054.
55. Sanli AM, Turkoglu E, Serbes G, Sargon MF, Besalti O, Kilinc K, Irak A, Sekerci Z. Effect of curcumin on lipid peroxidation, early ultrastructural findings and neurological recovery after experimental spinal cord contusion injury in rats. Turk Neurosurg 2012; 22: 189-195.
56. Satake K, Matsuyama Y, Kamyia M, Kawakami H, Iwata H, Adachi K, Kiuchi K. Nitric oxide via macrophage iNOS induces apoptosis following traumatic spinal cord injury. Mol Brain Res 2000; 85: 114-122.
57. Schnell L, Fearn S, Klassen H, Schwab ME, Perry VH. Acute inflammatory responses to inflammatory lesions in the CNS: differences between brain and spinal cord. Eur J Neurosci 1999; 11: 3648-3658.
58. Schwab JM, Brechtel K, Mueller CA, Failli V, Tuli SK, Schluesener HJ. Experimental strategies to promote spinal cord regeneration – an integrative perspective. Prog Neurobiol 2006; 78: 91-116.
59. Slausson DO, Cooper BJ. Pathology – the study of disease. W: Mechanisms of Disease: A Textbook of Comparative General Pathology. Salusson DO, Cooper BJ (eds.). Williams & Wilkins, Baltimore 1990; pp. 1-18.
60. Soriano SG, Amaravadi LS, Wang YF, Zhou H, Yu GX, Tonra JR, Fairchild-Huntress V, Fang Q, Dunmore JH, Huszhar D, Pan Y. Mice deficient in fractalkine are less susceptible to cerebral ischemia-reperfusion injury. J Neuroimmunol 2002; 125: 59-65.
61. Vanicky I, Urdzikova L, Saganova L, Cizkova D, Galik J. A simple and reproducible model of spinal cord injury induced by epidural balloon inflation in the rat. J Neurotrauma 2001; 18: 1399-1407.
62. Vanicky I, Urdzikova L, Saganova K, Marsala M. Intrathecal methylprednisolone does not improve outcome after severe spinal cord injury in the rat. Neurosci Res Commun 2002; 31: 183-191.
63. Xiong M, Chen S, Yu H, Liu Z, Zeng Y, Li F. Neuroprotection of erythropoietin and methylprednisolone against spinal cord ischemia-reperfusion injury. J Huazhong Univ Sci Technol 2011; 31: 652-656.
64. Yilmaz ER, Kertmen H, Dolgun H, Gurer B, Sanli AM, Kanat MA, Arikok AT, Bahsi SY, Erguder BE, Sekerci Z. Effects of darbepoietin-alpha in spinal cord ischemia-reperfusion injury in the rabbit. Acta Neurochir 2012; 154: 1037-1044.

Original article

Folia Neuropathologica

Prognostic significance of the markers IDH1 and YKL40 related to the subventricular zone

Kelvin Manuel Piña Batista[1], Ivan Fernandez Vega[2], Sayoa Alvarez de Eulate-Beramendi[1], Julio Cesar Gutierrez Morales[1], Almaz Kurbanov[3], Dorisme Asnel[4], Angela Meilan[5], Aurora Astudillo[6]

[1]Department of Neurosurgery, Hospital Universitario Central de Asturias, [2]Department of Neuropathology, Hospital Universitario de Araba, [3]Goodyear Research Institute, Mayfield Clinic, [4]Department of Surgery, Hospital Universitario Central de Asturias, [5]Department of Neuroradiology, Hospital Universitario Central de Asturias, [6]Department of Neuropathology, Hospital Universitario Central de Asturias

Folia Neuropathol 2015; 53 (1): 52-59 DOI: 10.5114/fn.2015.49974

Abstract

Glioblastoma multiforme (GBM), a highly aggressive brain cancer characterized by uncontrolled proliferation, resistance to cell death, angiogenesis, and vascular edema, remains one of the deadliest types of cancer. The subventricular zone (SVZ) harbors cells with great proliferative potential, and the microenvironment within the SVZ is permissive to growth and proliferation. This neurogenic niche is suspected to be a vulnerable site for the origin of subtypes of GBM. The aim of our study was to determine the immunohistochemical expression of mIDH1 and YKL40 in relationship to the SVZ of GBMs. YKL40, also known as chitinase-like protein 1, is included as a mesenchymal marker and associated with a poor prognosis. The protein is a secreted inflammatory molecule with no chitinolytic activity. However, the mutation of IDH1 (mIDH1) has been found in the cytoplasm and peroxisomes of 70-80% of secondary GBMs. In our study we found that YKL40-positive GBM is significantly linked to SVZ types IV and V ($p < 0.0001$). Our results show the diversity among GBMs related to the SVZ, which should be considered in the design of future targeted therapies. There was a significant impact of patient age, mIDH1 positivity, SVZ type III, and chemoradiotherapy on overall survival.

Key words: *glioblastoma, isocitrate dehydrogenase 1 mutation, YKL40 expression.*

Introduction

Glioblastoma multiforme (GBM), a highly aggressive brain cancer characterized by uncontrolled proliferation, resistance to cell death, angiogenesis, and vascular edema, remains one of the deadliest types of cancer [2,17,21]. The current standard of care involves aggressive surgery, radiation and chemotherapy, yet provides only a modest survival benefit [16, 27,37].

Based on cancer stem cell theory, and images of GBMs, recently there has been advanced a relevant classification related to the subventricular zone (SVZ) and its survival impact [18,22,24]. Since the SVZ harbors cells with great proliferative potential and the microenvironment within the SVZ is permis-

Communicating author:
Kelvin Manuel Piña Batista, MD, PhD, Department of Neurosurgery, Hospital Universitario Central de Asturias, e-mail: pineappledr@gmail.com

sive to growth and proliferation, this neurogenic niche is suspected to be a vulnerable site for the origin of subtypes of GBM [13]. Recently, there has been a consensus about the subpopulation of cancer cells with stem cell characteristics, including self-renewal and multipotentiality; these cancer stem cells can propagate tumors *in vivo* [8,12]. Recent evidence suggests that tumor location plays an important role in prognosis and is likely related to the genetic profile of tumor cells of origin [18,30]. Furthermore, some authors have constructed prognostic models and analyzed probabilistic radiographic atlases of GBM phenotypes [11,13].

The GBM heterogeneity has motivated several studies to evaluate factors that predict prolonged survival for patients with GBM [4,18,20,24,38]. Such heterogeneity could be related, according to some authors, to the stem cell-like characteristics [24]. Lim *et al*. proposed a classification scheme that divides the GBMs into four groups by the spatial relationship of the contrast-enhancing lesion with the subventricular zone and cortex: type I – tumor in which the contrast-enhancing lesion contacts both the SVZ and the cortex; type II – tumor contacts the SVZ but not the cortex; type III – tumor contacts the cortex but not the SVZ; and type IV – tumor contacts neither the SVZ nor the cortex. Regarding the multifocal and/or multicentric GBMs there are many theories showing a close association with group I given the findings consistent with high migratory and invasiveness of cells, according to Willis' theory [24,33].

Based on recent studies [39], YKL40, also known as chitinase-like protein 1, is included as a mesenchymal marker and associated with a poor prognosis. The protein is a secreted inflammatory molecule with no chitinolytic activity [15] YKL40 has been postulated as a potential serum marker in glioblastoma [4,19] since it was found to have elevated levels in the serum of patients with GBM. However, the mutation of IDH1 (mIDH1) has been found in the cytoplasm and peroxisomes of 70-80% of secondary GBMs. mIDH1 is a selective marker for secondary glioblastoma supplementing clinical judgment to distinguish it from primary glioblastoma. There are few reports related to the mutated IDH1 expression and its subventricular zone relationship [11]. The aim of our study was to determine the immunohistochemical expression of mIDH1 and YKL40 in relationship to the SVZ of GBMs.

Material and methods

A retrospective study was performed on 204 GBMs operated on at the Neurosurgical Unit of Asturias Hospital, Spain, between December 2005 and September 2011. We divided the GBMs into five groups. The first four groups were selected accordingly to the Lim [24] classification. We then selected multifocal or multicentric presentation of GBMs as a fifth group.

Detailed data regarding clinical presentation, imaging features, surgical procedure, pathological analysis, oncological treatment, progression-free survival (PFS), and overall survival (OS) outcome were recorded. The extent of resection was determined by early postoperative MRI (within 48 hours). Subtotal and total resection were defined as those tumors with residual and no residual enhancement, respectively, achieved by comparing pre- and postoperative MRI. Extent of resection was classified as either total (> 95%), subtotal (< 95%) or biopsy by a neuroradiologist blinded to patient outcomes. Patients were informed of the investigational nature of this study and written informed consent was obtained from each patient in accordance with institutional guidelines. Patients with a Karnofsky Performance Scale (KPS) score ≥ 70 and age < 60 were included to receive conventional radiotherapy and chemotherapy after surgical resection: 1.8-2.0 Gy per day, over a period of 6 weeks, for a total dose of 60 Gy and temozolomide therapy at a dose of 75 mg/m^2 per day, seven days a week for 42 consecutive days during radiotherapy (as used in the EORTC study by Stupp *et al*.) [3,23,36].

The pathology was determined by a senior neuropathologist in all instances, and the grading criteria were based on the World Health Organization (WHO) classification system.

All statistical analyses were performed with SPSS Statistics version 20 (IBM) with a significance level of $p = 0.05$. Fisher's exact test was used for evaluation of the association between YKL40 and mIDH1 (with positive and negative expression) and covariates. Survival analysis was carried out with the Kaplan-Meier method and a log rank test. For multivariate analysis of OS and PFS, a Cox proportional hazards model was performed using age (< 65 vs. ≥ 65), gender, initial KPS score (< 70 vs. ≥ 70), hemisphere, subventricular relationship, extent of resection, and first line therapy as covariates. All tests were two-sided, and a p value of < 0.05 was con-

Table I. Patient characteristics

Factor	All patients (N = 204), n (%)
Median age at diagnosis (years) ± SD	63 ± 10.86
Range	26-85
Sex	
Male	115 (56.4)
Female	89 (43.6)
Karnofsky Performance Scale score	
< 70	30 (14.7)
≥ 70	174 (85.3)
Hemisphere	
Right	115 (56.4)
Left	89 (43.6)
Subventricular relationship	
Group I	18 (8.8)
Group II	35 (17.2)
Group III	75 (36.8)
Group IV	42 (29.6)
Group V	34 (16.7)
Surgery	
Gross total resection	44 (21.6)
Subtotal resection	119 (58.3)
Biopsy	41 (20.1)
First-line therapy	
Radiotherapy	36 (17.6)
Chemotherapy	1 (0.5)
Radiotherapy and chemotherapy	123 (60.3)
Therapeutic absention	44 (21.6)

sidered significant. The confidence intervals were calculated at the 95% level.

Results

The population of our study consisted of a total of 204 patients harboring GBMs. The baseline clinical data are summarized in Table I. Among the patients in the study, the median age was 63 ± 10.86 years. Most patients were male (115). The median initial KPS score was 80. Overall, for surgical resection, 44 patients underwent gross total resection (GTR), 119 patients underwent subtotal resection (STR), and 41 patients underwent biopsy. Although statistically significant ($p < 0.05$), there was not a greater extent of resection or more radiotherapy combined with chemotherapy, among mIDH1-positive GBMs.

In 94 patients, YKL-positive cells were identified. YKL40 expression was found predominately in the cytoplasm. YKL40 was strongly stained in all positive samples. One hundred and ten were YKL40 negative. In 42 patients the mIDH1 was positive. One hundred sixty-two were IDH1 negative.

The median OS was 34.64 weeks ± 45.5 and the median PFS was 15.35 ± 26.93 weeks. Kaplan-Meier estimates for OS by subventricular relationship are shown in Figures 2 and 3. The median OS (more than 54 weeks) after pathological diagnosis was higher in patients with mIDH1-positive GBMs (55.4%) than in those with YKL40-positive GBMs (23.2%) ($p > 0.001$ and $p > 0.05$, respectively). Long-term survival (LTS) was identified in 4 (66.7%) IDH1-positive GBMs. Long-term survival was identified in 1 (16.7%) YKL40-positive GBM (Table II). The median PFS among those with mIDH1-positive GBMs was higher than those with YKL40-positive GBMs (1 and 0, respectively).

Tumor location

All tumors were supratentorial in location. We did not find statistically significant differences between the right and left hemisphere linked to YKL40 and mIDH1 immunoexpression. Of 204 patients, 12 YKL40-positive GBMs and 3 mIDH1-positive GBMs had type I tumors; 16 YKL40-positive GBMs and 2 mIDH1-positive GBMs had type II tumors; 17 YKL40-positive GBMs and 33 mIDH1-positive GBMs had type III tumors; 29 YKL40-positive GBMs and 2 mIDH1-positive GBMs had type IV tumors, and 20 YKL40-positive GBMs and 2 mIDH1-positive GBMs had type V tumors.

Multivariate analysis

A multivariate proportional hazards model analysis, based on the forward stepwise selection technique, was used. The covariates significantly associated with improved OS were: younger age at diagnosis (hazard ratio [HR] = 1.44; 95% CI: 1.03-2.01, $p = 0.031$), type III and type I GBMs (HR = 0.46; 95% CI: 0.25-0.84, $p = 0.013$), and chemoradiothera-

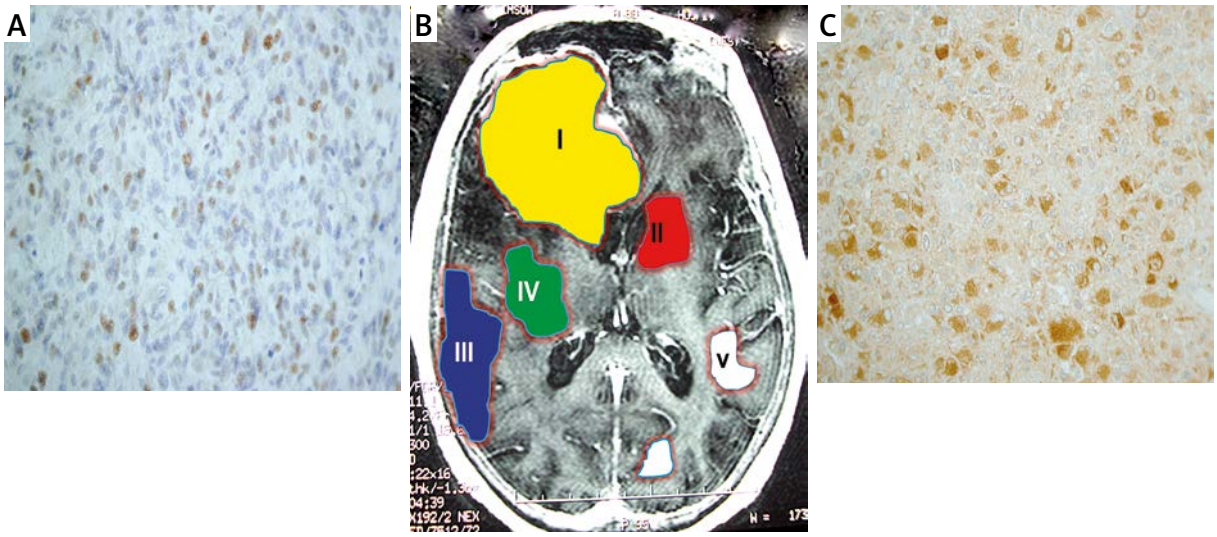

Fig. 1. Magnetic resonance imaging (**B**) and photomicrographs (**A** and **C**) of glioblastoma multiformes (GBM) in the present study. **A)** Immunohistochemical staining of mIDH1 showing classic histological features of GBM. mIDH1 has been found linked to group 3 in a large proportion of cases. **B)** Classification of GBM into groups I-IV [18,24], based on MRI, and the multifocal (V) group considered in our series. **C)** Immunohistochemical staining of YKL40.

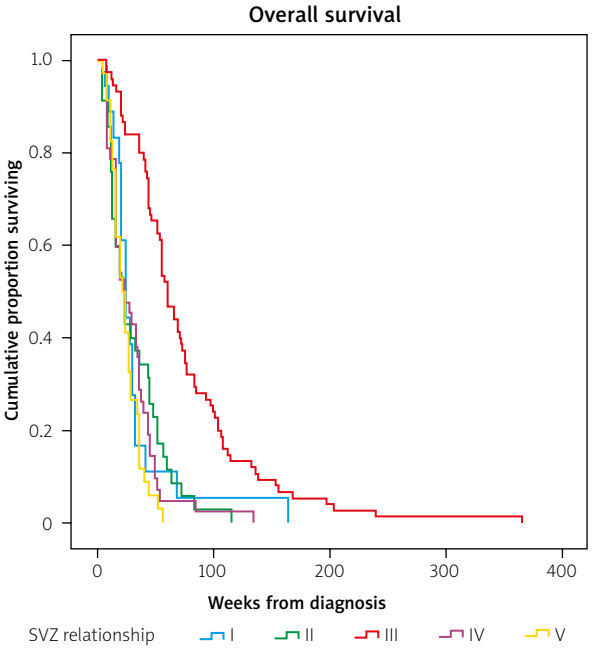

Fig. 2. Kaplan-Meier survival curves of overall survival categorized according to the subventricular zone relationship (log rank $p = 0.00$).

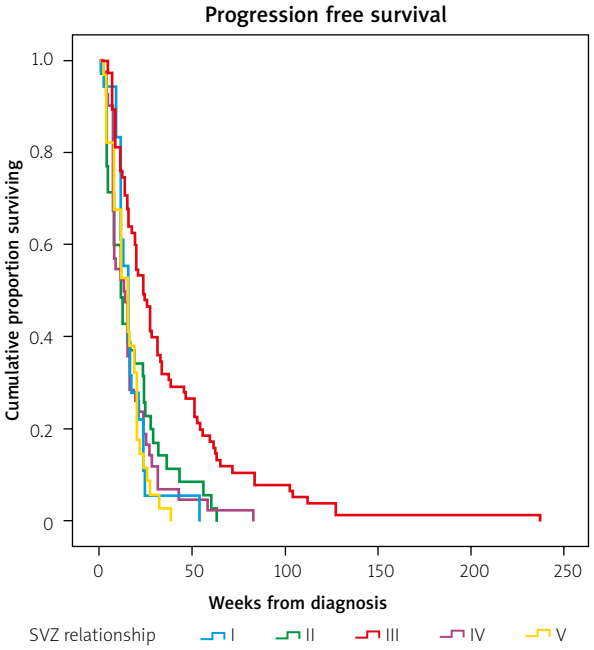

Fig. 3. Kaplan-Meier survival curves of progression-free survival categorized according to the subventricular zone relationship (log rank $p = 0.00$).

py (HR = 0.20; 95% CI: 0.12-0.33, $p = 0.000$) were the most independent factors linked to OS. The results of this model are given in Table III. In regards to PFS, good performance status (KPS) (HR = 0.48; 95% CI: 0.31-0.75, $p = 0.001$), mIDH1 (HR = 0.60; 95% CI: 0.40-0.90, $p = 0.015$), and chemoradiotherapy (HR = 0.33; 95% CI: 0.21-0.52, $p = 0.000$). Significantly more mIDH1- positive GBMs showed a relation with type III ($n = 33$; 44%) compared to YKL40-positive GBMs ($n = 17$; 22.7%).

Table II. Patient characteristic of the study population compared to YKL40 and mIDH1

Factor	YKL40+	YKL40–	Mutated IDH1+	Mutated IDH1–	*p* value YKL40/mIDH1
Age					< 0.0001
< 65	45 (38.1)	73 (61.9)	37 (31.4)	81 (68.6)	
≥ 65	49 (57)	37 (43)	5 (5.8)	81 (94.2)	
Sex					0.26/0.22
Male	57 (49.6)	58 (50.4)	20 (17.4)	95 (82.6)	
Female	37 (41.6)	52 (58.4)	22 (24.7)	67 (75.3)	
Karnofsky Performance Scale score					1.00/0.14
< 70	14 (46.7)	16 (53.3)	3 (10)	27 (90)	
≥ 70	80 (46)	94 (54)	39 (22.4)	135 (77.6)	
Hemisphere					0.11/0.60
Right	47 (40.9)	68 (59.1)	22 (19.1)	93 (80.9)	
Left	47 (52.8)	42 (47.2)	20 (22.5)	69 (77.5)	
Subventricular relationship					< 0.0001/< 0.0001
Group I	12 (66.7)	6 (33.3)	3 (16.7)	15 (83.3)	
Group II	16 (45.7)	19 (54.3)	2 (5.7)	33 (94.3)	
Group III	17 (22.7)	58 (77.3)	33 (44)	42 (56)	
Group IV	29 (69)	13 (31)	2 (4.8)	40 (95.2)	
Group V	20 (58.8)	14 (41.2)	2 (5.9)	32 (94.1)	
First-line therapy					0.005/< 0.0001
Radiotherapy	21 (58.3)	15 (41.7)	1 (2.8)	35 (97.2)	
Chemotherapy	0 (0)	1 (100)	0 (0)	1 (100)	
Radiotherapy and chemotherapy	45 (36.6)	78 (63.4)	40 (32.5)	83 (67.5)	
Therapeutic absention	28 (63.6)	16 (36.4)	1 (2.3)	43 (97.7)	
Surgery					0.003/0.03
Gross total resection	13 (29.5)	31 (70.5)	12 (27.3)	32 (72.7)	
Subtotal resection	54 (45.4)	65 (54.6)	27 (22.7)	92 (77.3)	
Biopsy	27 (65.9)	14 (34.1)	3 (7.3)	38 (92.7)	
Overall survival (weeks)					0.097/0.001
≤ 54	81 (55.1)	66 (44.9)	11 (7.5)	136 (92.5)	
> 162	1 (16.7)	5 (83.3)	4 (66.7)	2 (33.3)	
Progression-free survival (weeks)					1.000/0.174
≤ 54	90 (49.2)	93 (50.8)	31 (16.9)	152 (83.1)	
> 162	0 (0)	1 (100)	1 (100)	0 (0)	

Discussion

Patients diagnosed with GBM have a dismal prognosis [5]. Even though median survival is poor, individual survival is heterogeneous, with some patients surviving for several years [5,9,34]. Age at diagnosis, KPS score, and extent of resection have been the most well-documented predictors of survival. Age has consistently been shown to be one of the most powerful prognostic factors for survival in patients with GBM, with younger patients living much longer than older patients. Furthermore, the poor tolerance of older patients to aggressive toxic systemic chemotherapy often results in either treatment-related complications and/or suboptimal tumor treatment [10,28,31]. In the present study, we found a particularly strong tendency among young adults to harbor mIDH1-positive GBMs. Furthermore, Cox's regression model showed that younger patients were associated with better OS, consistent with previous published series [2,6,7,26]. Nevertheless, extent of resection remains a topic of debate, particularly for incomplete resections. The most comprehensive work to date on the value of extent of resection suggests that ≥ 98% is necessary to impact survival in patients with GBM [31,40]. In our study the extent of resection was not a prognostic factor in the Cox's regression model and in the characteristics linked to YKL40 and mIDH1 expression, judging by postoperative enhancing MRI rather than by the neurosurgeon himself may be the reason.

In the present study we found that YKL40-positive immunoexpression, reflecting the mesenchymal GBM subgroup [9,15,39], was not significant in the OS and PFS Cox's proportional hazards model. Interestingly, our data showed more YKL40-positive expression among subventricular contacting GBMs than mIDH1-positive GBMs. The expression of mIDH1 is associated with prolonged OS and PFS in a Cox's regression model, consistent with other population-based studies of GBMs [14,29,32,35,41]. The gross total resection and the radiotherapy combined with chemotherapy associations were not of prognostic value for either OS or PFS.

Recent evidence suggests that GBMs with both SVZ and cortical involvement and SVZ contact alone result

Table III. Multivariate analysis of factors associated with overall survival (OS) and progression-free survival (PFS) Cox's proportional hazards model with a forward stepwise approach

Factor	OS		PFS	
	p	HR (95% CI)	*p*	HR (95% CI)
Age (< 65 vs. ≥ 65)	0.031	1.44 (1.03-2.01)	0.265	1.18 (0.87-1.60)
Karnofsky Performance Scale score (< 70 vs. ≥ 70)	0.207	1.32 (0.85-2.04)	0.001	0.48 (0.31-0.75)
Gross total resection	0.390		0.248	
Subtotal resection	0.211	1.27 (0.87-1.86)	0.142	1.31 (0.91-1.89)
Biopsy	0.262	1.36 (0.79-2.32)	0.889	0.96 (0.54-1.69)
YKL40 (no vs. yes)	0.999	1.00 (0.71-1.40)		
Mutated IDH1 (no vs. yes)	0.028	0.62 (0.41-0.95)	0.015	0.60 (0.40-0.90)
Group I	0.011			
Group II	0.607	0.84 (0.45-1.59)		
Group III	0.013	0.46 (0.25-0.84)		
Group IV	0.886	1.04 (0.57-1.90)		
Group V	0.858	0.94 (0.49-1.79)		
Radiotherapy	0.000		0.000	
Chemotherapy	0.005	0.46 (0.27-0.79)	0.640	1.63 (0.21-12.66)
Radiotherapy and chemotherapy	0.000	0.20 (0.12-0.33)	0.000	0.33 (0.21-0.52)
Therapeutic absention	0.000	1.09 (0.53-0.17)	0.002	2.39 (1.38-4.14)

in shorter PFS and OS [13,18]. Interestingly, we found significantly more type III GBMs than the remaining groups among mIDH1-positive GBMs. mIDH1 positivity was more frequent in secondary GBMs than in primary GBMs (37 and 5, respectively). Of note, among YKL40-positive GBMs there were more type IV and V than type III GBMs. The main reasons for a less favorable outcome in GBM patients with SVZ involvement are not yet completely understood. Type IV and V were particularly linked to YKL40-positive GBMs. In our series we identified 34 (16.7%) type V GBMs. In the literature, the incidence of multiple lesions at the time of diagnosis ranged anywhere from 0.5 to 20% [14].

To the best of our knowledge, the immunoexpression of YKL40 has never been assessed in the GBMs associated with the subventricular zone. Since 2002 there have been published fewer papers addressing YKL40 and its expression in GBM, even though it seems related to radiotherapy resistance [15] and mesenchymal subtype, and inversely associated with EGFR. Additional studies concluded that patients with tumors adjacent to the SVZ were more likely to be multifocal at diagnosis and to have noncontiguous tumor recurrences [24]. YKL40 positivity contributes to progression of GBM through invasion, anchorage-independent growth and drug resistance [23].

Conclusions

According to the findings in the present study and the review of the literature, GBM is a highly aggressive tumor. Despite modest improvement in the OS of patients with GBM in the last decade, the outcome remains poor. Therefore, the need for more effective novel treatments in this neoplasm is urgently welcomed.

We demonstrate for the first time that YKL40 GBMs are significantly linked to SVZ types IV and V ($p < 0.0001$). However, it will be necessary to gain more information about its mechanisms of action in order to move forward with the use of YKL40 for potential application in glioma therapy. Our results show the diversity among GBMs related to the SVZ, which should be considered in the design of future targeted therapies. Age less than 65 years, mIDH1 positivity, type III GBMs, and temozolomide therapy are factors that independently predicted a prolonged OS. These results, however, may be limited by an inherent bias in patient selection, which may favor patients with more superficial tumors. We attempted to minimize the limitations by using strict inclusion criteria and Cox's proportional hazard model analysis. Therefore, despite this potential source of bias, these findings may help to guide treatment paradigms, prognosticate survival, and provide more information for GBM patients through the identification of these prognostic factors.

Disclosure

Authors report no conflict of interest.

References

1. Agnihotri S, Burrell KE, Wolf A, Jalali S, Hawkins C, Rutka JT, Zadeh G. Glioblastoma: a brief review of history, molecular genetics, animal models and novel therapeutic strategies. Arch Immunol Ther Exp 2013; 61: 25-41.
2. Batchelor TT, Betensky RA, Esposito JM, Pham L-DD, Dorfman MV, Piscatelli N, Jhung S, Rhee D, Louis DN. Age-dependent prognostic effects of genetic alterations in glioblastoma. Clin Cancer Res 2004; 10: 228-233.
3. Behm T, Horowski A, Schneider S, Bock HC, Mielke D, Rohde V, Stockhammer F. Concomitant and adjuvant temozolomide of newly diagnosed glioblastoma in elderly patients. Clin Neurol Neurosurg 2013; 115: 2142-2146.
4. Bernardi D, Padoan A, Ballin A, Sartori M, Manara R, Scienza R, et al. Serum YKL-40 following resection for cerebral glioblastoma. J Neurooncol 2011; 107: 299-305.
5. Bleeker FE, Molenaar RJ, Leenstra S. Recent advances in the molecular understanding of glioblastoma. J Neurooncol 2012; 108: 11-27.
6. Bozdag S, Li A, Riddick G, Kotliarov Y, Baysan M, Iwamoto FM, Cam MC, Kotliarova S, Fine HA. Age-specific signatures of glioblastoma at the genomic, genetic, and epigenetic levels. PLoS One 2013; 8: e62982.
7. Burger PC, Green SB. Patient age, histologic features, and length of survival in patients with glioblastoma multiforme. Cancer 1987; 59: 1617-1625.
8. Chaichana KL, Martinez-Gutierrez JC, De la Garza-Ramos R, Weingart JD, Olivi A, Gallia GL, Lim M, Brem H, Quinones-Hinojosa A. Factors associated with survival for patients with glioblastoma with poor pre-operative functional status. J Clin Neurosci 2013; 20: 818-823.
9. Colman H, Zhang L, Sulman EP, Mcdonald JM, Shooshtari L, Rivera A, Popoff S, Nutt CL, Louis DN, Cairncross JG, Gilbert MR, Phillips HS, Mehta MP, Chakravarti A, Pelloski CE, Bhat K, Feuerstein BG, Jenkins RB, Aldape K. A multigene predictor of outcome in glioblastoma. Neurooncol 2010; 12: 49-57.
10. Devaux B, O Fallon JR, Kelly PJ. Resection, biopsy, and survival in malignant glial neoplasms. J neurosurg 1993; 78: 767-775.
11. Ellingson BM, Lai A, Harris RJ, Selfridge J, Yong WH, Das K, Pope WB, Nghiemphu PL, Vinters HV, Liau LM, Mischel PS, Cloughsy TF. Probabilistic radiographic atlas of glioblastoma phenotypes. Am J Neuroradiol 2013; 34: 533-540.
12. Galli R, Binda E, Orfanelli U, Cipelletti B, Gritti A, De Vitis S, Fiocco R, Dimeco F, Vescovi A. Isolation and characterization of tumorigenic, stem-like neural precursors from human glioblastoma. Cancer Res 2004; 64: 7011-7021.
13. Haskins WE, Zablotsky BL, Foret MR, Ihrie RA, Alvarez-Buylla A, Eisenman RN, Berger MS, Lin CH. Molecular characteristics in

MRI-classified group 1 glioblastoma multiforme. Front Oncol 2013; 3: e183.
14. Hassaneen W, Levine NB, Suki D, Salaskar AL, de Moura Lima A, McCutcheon IE, Prabhu SS, Lang FF, DeMonte F, Rao G, Weinberg JS, Wildrick DM, Aldape KD, Sawaya R. Multiple craniotomies in the management of multifocal and multicentric glioblastoma. J Neurosurg 2011; 114: 576-584.
15. Horbinski C, Wang G, Wiley CA. YKL-40 is directly produced by tumor cells and is inversely linked to EGFR in glioblastomas. Int J Clin Exp Pathol 2010; 3: 226-237.
16. Iacob G, Dinca EB. Current data and strategy in glioblastoma multiforme. J Med Life 2009; 2: 386-393.
17. Iwamoto FM, Hottinger AF, Karimi S, Riedel E, Dantis J, Jahdi M, Panageas KS, Lassman AB, Abrey LE, Fleisher M, DeAngelis LM, Holland EC, Hormigo A. Serum YKL-40 is a marker of prognosis and disease status in high-grade gliomas. Neurooncol 2011; 13: 1244-1251.
18. Jafri NF, Clarke JL, Weinberg V, Barani IJ, Cha S. Relationship of glioblatoma multiforme to the subventricular zone is associated with survival. Neurooncol 2013; 15: 91-96.
19. Johansen JS, Cintin C, Jorgensen M, Kamby C, Price PA. Serum YKL-40: a new potentialmarker of prognosis and location of metastases of patients with recurrent breast cancer. Eur J Cancer 1995; 31: 1437-1442.
20. Kappadakunnel M, Eskin A, Dong J, Nelson SF, Mischel PS, Liau LM, Ngheimphu P, Lai A, Cloughesy TF, Goldin J, Pope WB. Stem cell associated gene expression in glioblastoma multiforme: relationship to survival and the subventricular zone. J Neurooncology 2009; 96: 359-367.
21. Karsy M, Gelbman M, Paarth S, Balumbu O, Moy F, Arslan E. Established and emerging variants of glioblastoma multiforme: review of morphological and molecular features. Folia Neuropathol 2012; 50: 301-321.
22. Kimura M, Lee Y, Miller R, Castillo M. Glioblastoma multiforme: relationship to subventricular zone and recurrence. Neuroradiol J 2013; 26: 542-547.
23. Ku BM, Lee YK, Ryu J, Jeong JY, Choi J, Eun KM, Shin HY, Kim DG, Hwang EM, Yoo JC, Park JY, Roh GS, Kim HJ, Cho GJ, Choi WS, Paek SH, Kang SS. CHI3L1 (YKL-40) is expressed in human gliomas and regulates the invasion, growth and survival of glioma cells. Int J Cancer 2011; 128: 1316-1326.
24. Lim DA, Cha S, Mayo MC, Chen MH, Keles E, Vandenberg S, Berger MS. Relationship of glioblastoma multiforme to neural stem cell regions predicts invasive and multifocal tumor phenotype. Neurooncol 2007; 9: 424-429.
25. Maher EA, Furnari FB, Bachoo RM, Rowitch DH, Louis DN, Cavanee WK, DePinho RA. Malignant glioma: genetics and biology of a grave matter. Genes Dev 2001; 15: 1311-1333.
26. Michaelsen SR, Christensen IJ, Grunnet K, Stockhausen MT, Broholm H, Kosteljanetz M, Poulsen HS. Clinical variables serve as prognostic factors in a model for survival from glioblastoma multiforme: an observational study of a cohort of consecutive non-selected patients from a single institution. BMC Cancer 2013; 13: e402.
27. Olsen JJ, Nayak L, Ormond R, Wen PY, Kalkanis S. The role of cytotoxic chemotherapy in the management of progressive glioblastoma. J Neurooncol 2014; 118: 501-555.
28. Osorio JA, Aghi MK. Optimizing glioblastoma resection: intraoperative mapping and beyond. CNS Oncol 2014; 3: 359-366.
29. Popov S, Jury A, Laxton R, Doey L, Kandasamy N, Al-Sarraj S, Jürgensmeier JM, Jones C. IDH1-Associated. Primary glioblastoma in young adults displays differential patterns of tumour and vascular morphology. PLoS One 2013; 8: e56328.
30. Sanai N, Alvarez-buylla A, Berger MS. Neural stem cells and the origin of gliomas. N Engl J Med 2005; 353: 811-822.
31. Sanai N, Polley M-Y, McDermott MW, Parsa AT, Berger MS. An extent of resection threshold for newly diagnosed glioblastomas. J Neurosurg 2011; 115: 3-8.
32. Sang Yun H, So Young K, In-Gu D, Yeon-Lim S. Glioblastoma with oligodendroglial component represents a subgroup of glioblastoma with high prevalence of IDH1 mutation and association with younger age. J Neurooncol 2013; 112: 439-448.
33. Shakur SF, Bit-Ivan E, Watkin WG, Merrell RT, Farhat HI. Multifocal and multicentric glioblastoma with leptomeningeal gliomatosis: a case report and review of the literature. Case Rep Med 2013; 2013: 132679.
34. Smoll NR, Schaller K, Gautschi OP. Long-term survival in patients with glioblastoma multiforme (GBM). J Clin Neurosci 2013; 20: 670-675.
35. SongTao Q, Lei Y, Si G, YanQing D, HuiXia H, XueLin Z, LanXiao W, Fei Y. IDH mutations predict longer survival and response to temozolomide in secondary glioblastoma. Cancer Sci 2011; 103: 269-273.
36. Stupp R, Mason WP, van den Bent MJ, Weller M, Fisher B, Taphoorn MJ, Belanger K, Brandes AA, Marosi C, Bogdahn U, Curschmann J, Janzer RC, Ludwin SK, Gorlia T, Allgeier A, Lacombe D, Cairncross JG, Eisenhauer E, Mirimanoff RO; European Organisation for Research and Treatment of Cancer Brain Tumor and Radiotherapy Groups; National Cancer Institute of Canada Clinical Trials Group. Radiotherapy plus Concomitant and Adjuvant Temozolomide for Glioblastoma. N Engl J Med 2005; 352: 987-996.
37. Stupp R. ESMO minimum clinical recommendations for diagnosis, treatment and follow-up of malignant glioma. Ann Oncol 2005; 16 (Suppl 1): i64-65.
38. Tabouret E, Barrie M, Thiebaut A, Matta M, Boucard C, Autran D, Loundou A, Chinot O. Limited impact of prognostic factors in patients with recurrent glioblastoma multiforme treated with a bevacizumab-based regimen. J Neurooncol 2013; 114: 191-198.
39. Verhaak RG, Hoadley KA, Purdom E, Wang V, Qi Y, Wilkerson MD, Miller CR, Ding L, Golub T, Mesirov JP, Alexe G, Lawrence M, O´Kelly M, Tamayo P, Weir BA, Gabriel S, Winckler W, Gupta S, Jakkula L, Feiler HS, Hodgson JG, James CD, Sarkaria JN, Brennan C, Kahn A, Spellman PT, Wilson RK, Speed TP, Gray JW, Meyerson M, Getz G, Perou CM, Hayes DN. Integrated genomic analysis identifies clinically relevant subtypes of glioblastoma characterized by abnormalities in PDGFRA, IDH1, EGFR, and NF1. Cancer Cell 2010; 17: 98-110.
40. Woodworth GF, Garzon-Muvdi T, Ye X, Blakeley JO, Weingart JD, Burger PC. Histopathological correlates with survival in reoperated glioblastomas. J Neurooncol 2013; 113: 485-493.
41. Zou P, Xu H, Chen P, Yan Q, Zhao L, Zhao P, Gu A. IDH1/IDH2 Mutations define the prognosis and molecular profiles of patients with gliomas: A meta-analysis. PLoS One 2013; 8: e68782.

Original paper

Folia Neuropathologica

Hydrocephalus induced via intraventricular kaolin injection in adult rats

Zhang Shaolin[1,2], Wang Zhanxiang[1], Xu Hao[1], Zhang Feifei[1], Huang Caiquan[1], Chen Donghan[1], Bao Jianfeng[3], Liu Feng[1], Shen Shanghang[1]

[1]Department of Neurosurgery, The First Affiliated Hospital of Xiamen University, Xiamen 361003, China, [2]Department of Neurosurgery, The First Hospital of Nanping, Nanping, Fujian 353000, China, [3]Fujian Provincial Key Laboratory of Plasma and Magnetic Resonance, State Key Laboratory of Physical Chemistry of Solid Surfaces, Xiamen University, Xiamen 361003, China

Folia Neuropathol 2015; 53 (1): 60-68 DOI: 10.5114/fn.2015.49975

Abstract

Hydrocephalus is a common neurological disease in humans, but a uniform and particularly effective hydrocephalic animal model amenable to proper appraisal and deep study has not yet been established. In this study, we attempted to construct a high-efficiency model of hydrocephalus via intraventricular kaolin injection. Adult male Sprague-Dawley rats were randomly divided into 2 groups: the control group (n = 15) and the experimental group (n = 30). Kaolin was injected into the lateral ventricle of experimental animals. Control rats underwent the same procedure but received sterile saline injection instead of kaolin. All animals with kaolin injection into the lateral ventricle developed hydrocephalus according to magnetic resonance imaging (MRI) results (success rate up to 100%). Also, the Morris water maze (MWM) test demonstrated disturbed spatial learning and memory. Furthermore, there were significant differences between groups with respect to the histological changes in the periventricular tissue. Our results indicate that experimental hydrocephalus induced by lateral ventricle injection of kaolin in adult rats is feasible and may be widely used.

Key words: *kaolin, hydrocephalus, animal model, MRI, Morris water maze.*

Introduction

Hydrocephalus is a common neurosurgical disease that is often the result of intracranial hemorrhage, tumor, intracranial infection and brain injury. Abnormalities of cerebrospinal fluid (CSF) secretion, circulation and absorption cause excessive accumulation of CSF in the ventricular system and expansion of the ventricular system, which may cause damage of surrounding brain tissue and persistent neurological deficits, leading to the development of hydrocephalus.

The sustained enlargement of cerebral ventricles can result in compression and distortion of brain tissue. Compression and distortion of brain tissue give rise to deleterious effects, such as inflammatory responses, gliosis, fiber stretching, damage to neurons and cellular pathways, destruction of periventricular axons, demyelination, reduced cerebral blood flow and oxygen levels, and altered clearance

Communicating author:
Wang Zhanxiang, Department of Neurosurgery, The First Affiliated Hospital of Xiamen University, No. 55 ZhenHai Road, Xiamen 361003, China, phone: +86 5922139815, fax: +86 5922139315, e-mail: wangzx1166@163.com

of proteins and toxins [8-10,22,25,33], that may be associated with neurological deficits in hydrocephalus patients, including low intelligent quotient (IQ) scores, learning disabilities, memory loss, mental retardation, impaired gait, and urinary incontinence [12,13]. These deleterious effects of hydrocephalus on the brain depend on the magnitude and duration of ventriculomegaly and degree of compression of brain tissue, which are also modified by the age of onset [9].

Many animal models of hydrocephalus have been established, but most models mimic "obstructive" hydrocephalus by blocking CSF flow at the 4th ventricle outlets [21,26,27,29,34]. Communicating hydrocephalus has been difficult to model in rodents because the subarachnoid spaces are extremely small and difficult to access. Transgenic models [15], growth factors such as TGF-β1 and FGF-2 [24,30], neurotoxins [14], and viral [6] and bacterial inoculations [32] have also been used to produce communicating hydrocephalus. However, these methods have not been widely applied because of complexity, costliness, low success rate and high acute mortality, etc.

Although hydrocephalus can be experimentally induced through a variety of techniques [1,15,29,30], the most widely used method of experimental hydrocephalus involves induction by injection of kaolin into the cistern magna in neonatal, juvenile and adult rodents [16,21]. Ventricular enlargement occurs as a result of the inflammatory scarring, which causes an obstruction of the CSF pathways near the 4th ventricle outlets [16,21,23]. This method is long-term and widely used; however, there are also many deficiencies (such as high acute mortality rates, low success rate, difficulty to form a communicating hydrocephalus and uncontrollable hydrocephalic severity) [2,4,21,29].

It is well known that communicating hydrocephalus, clinically, is more universal than obstructive hydrocephalus. For a long time, the lack of appropriate animal models of communicating hydrocephalus has clearly restricted investigative progress of this disease. Recently, communicating hydrocephalus with suspension of 25% kaolin injections into the basal cisterns or the cortical subarachnoid space of adult rats has been reported [18,23]. So, theoretically, if low concentration kaolin injections into the lateral ventricle may induce hydrocephalus, it should be communicating hydrocephalus.

Thus, we attempted to explore and develop a uniform, particularly effective and low mortality animal model of hydrocephalus.

Material and methods

Animals

Adult male Sprague-Dawley rats (240-260 g) were purchased from the Slac Laboratory Animal Co. Ltd. (Shanghai, China). The animals were kept in a temperature- and humidity-controlled room, allowed food and water freely, and housed in the same animal care facility during a 12-h light/dark cycle throughout the protocol. The rats were randomly divided into 2 groups: the experimental group (n = 30) with kaolin injection; and the control group (n = 15) with saline injection. All animal care and experimental procedures were licensed and carried out by the Local Institutional Animal Care and Use Committee according to the Institutional Animal Care and Use Committee guidelines.

Surgical induction

Rats were anesthetized by intraperitoneal injection of 10% chloral hydrate (0.4 ml/100 g), and were placed in a stereotaxic frame. The scalp was sterilized and incised, and the bregma was exposed. The injection coordinates, which were measured from the bregma to the lateral cerebral ventricles, were 0.8 mm posterior, 1.6 mm lateral and 3.7 mm deep. A 50 µl syringe with 30-gauge needle was inserted into the lateral ventricle (depth: 3.7 mm), and a 30 µl sterile suspension of 3% kaolin (ultrasonic emulsification about 15 minutes) in saline was injected slowly into the lateral ventricle at a rate of approximately 10 µl/min. The skin incision was sutured, and the animal was replaced to its cage and was monitored daily for the duration of the experiment. Control group rats underwent the same procedure but received sterile saline injection instead of kaolin.

Morris water maze test

Ten days later, spatial learning and memory was examined with the Morris water maze (MWM) test. The water maze consisted of a black pool (1.5 m in diameter, 50 cm high, bottom 45 cm above floor level) filled with water (made opaque with ink) and a black platform (10 cm in diameter, 30 cm high)

submerged 2 cm below the water surface. The quadrant in which the platform was placed and the remaining quadrants, clockwise from the former, were designated "1", "2", "3" and "4", respectively. The water was maintained at 21 ± 1°C, and the platform was placed in the "1" quadrant of the four virtual quadrants 30 cm away from the sidewall. The movements of rats were recorded with a video camera connected to a computer. Data were analyzed using a tracking program (DigBehv-MWM, Shanghai Jiliang Software Technology Co. Ltd., Shanghai, China). The experimental room (2.4 × 2.4 × 3.2 m) contained cues: a pole, maze, door, computer, air conditioning, and researcher. A quiet and constant environment (including temperature and humidity) of the laboratory was maintained during the experiment.

For maze performance, a 5-day protocol was used (day 1: visual cue trial; days 2-4: 3 trials per day, hidden platform; day 5: probe trial with platform removed). On the cue and training days, each rat was placed at one of the other three starting points, which were used in a random order so that each position could be used once. A 1 h interval was imposed before the beginning of the next trial. If the rat did not find the hidden platform within 60 seconds, it would be guided to find the platform and remain for 15 seconds. The platform location was immovable during the cue and learning period. The time that rats spent in finding the submerged platform (escape latency) was recorded in each trial. On the probe day, the platform was removed from the pool and each rat was given one 60-second trial in which the starting point was quadrant 3 located in the most distant position to the former platform. The number of times of crossing the former platform position and the swimming time in each quadrant of the pool without the platform were recorded and analyzed as the score. All the experiments were performed at 08:00 AM.

Magnetic resonance imaging and assessment of ventricular size

All MRI experiments were performed on a Varian 7.0 T small animal scanner with a 63/95-mm-quad birdcage coil. The imaging parameters were as follows: T2-weighted spin-echo imaging; three orientations (coronal, axial, sagittal); section thickness: 1 mm; number of slices were enough to cover the ventricle system area; TR: 5000 ms; TE: 50 ms; field-of-view: 5.0 × 5.0 cm; matrix size: 128 × 128; number of signals acquired: 1. The total imaging time was 17 min. Magnetic resonance imaging (MRI) was performed on all animals 15 days after the injection (after the MWM test).

The maximal width of the ventricles at the level of the foramen of Monro was taken as the cerebral ventricle diameter because these images had the widest ventricular space and were common in these MRI series. Ventricular volumes were measured from the coronal MRI scans of the saline control and hydrocephalic brains. The volumetric calculations of the ventricle were semiautomated by image analysis software (NIH Image) as follows: an appropriate intensity threshold was first chosen to exclude background tissue and to highlight the bright ventricles. This was followed by careful inspection of each image, and manual tracing was used to correct any areas of the ventricle that had been incorrectly deleted, or to delete non-ventricular regions that had been incorrectly included. This process resulted in a binary mask of ventricular pixels, which when multiplied by the volume of each pixel and summed over all slices produced the net ventricular volume in milliliters.

Sacrifice and histological analyses

On post-injection day 16 following MRI, rats were anesthetized with 10% chloral hydrate (0.4 ml/100 g i.p.) and perfused with 0.9% saline by left atrial perfusion. For histological analysis, the brains were removed from the skull, fixed in 10% formalin for 24 h at 4°C and then embedded in paraffin. The brain was sliced coronally into a thickness of 5 µm at the level of the lateral ventricle and then stained with hematoxylin and eosin (H&E).

Statistical analysis

All data were analyzed using GraphPad Prism (GraphPad, Inc., La Jolla, CA, USA) software to compare differences between groups. The data from the MWM were expressed as mean ± SEM and the ventricular volume was expressed as the median value (range). Statistical analysis of these MWM data was performed by two-way analysis of variance (ANOVA), and the ventricular volume was assessed by the Mann-Whitney *U* test. Statistical values of $p < 0.05$ were considered to be significant.

Results

Mortality, success rate, behavior and general changes

Rats were monitored and weighed daily. Two rats (hydrocephalic animals: 1 rat; controls: 1 rat) died from anesthesia or surgical trauma within 2 days after the operation. Forty-three rats (hydrocephalic animals: 29 rats; controls: 14 rats) participated in the entire course of the experiment. In the experimental group, 29 rats successfully developed moderate to severe hydrocephalus according to MRI examination (success rate up to 100%). Most rats of the hydrocephalus group exhibited coughing, irritability, emaciation, unsteady gait, increased urine, hunched back, hind legs weak and nasal and/or orbital secretions of blood and clear fluid after 1 post-operative day. These signs disappeared spontaneously within a few days. Weight growth of hydrocephalic animals was significantly slower than that of control animals.

Morris water maze test

Figure 1 shows the results of the MWM test. The hydrocephalus group tended to require more time to find the platform than the control group, and there was a significant difference between the two groups on the 3rd day and the 4th day ($p < 0.05$) (Fig. 1A). The control group spent a greater proportion of their swimming times in quadrant 1 that contained the hidden platform (27.86 ± 3.195 s), and there was a significant difference compared with the others ($p < 0.05$). In contrast, the mean swimming time of the hydrocephalus group in quadrant 1 was only 20.26 ± 3.166 s, and there was only a significant difference compared with quadrant 2 (Fig. 1B). The number of times of crossing the former platform position of hydrocephalic rats was higher than that of controls, but statistical significance was not reached (data not shown). All results reflected a decline of spatial learning and memory in hydrocephalic rats.

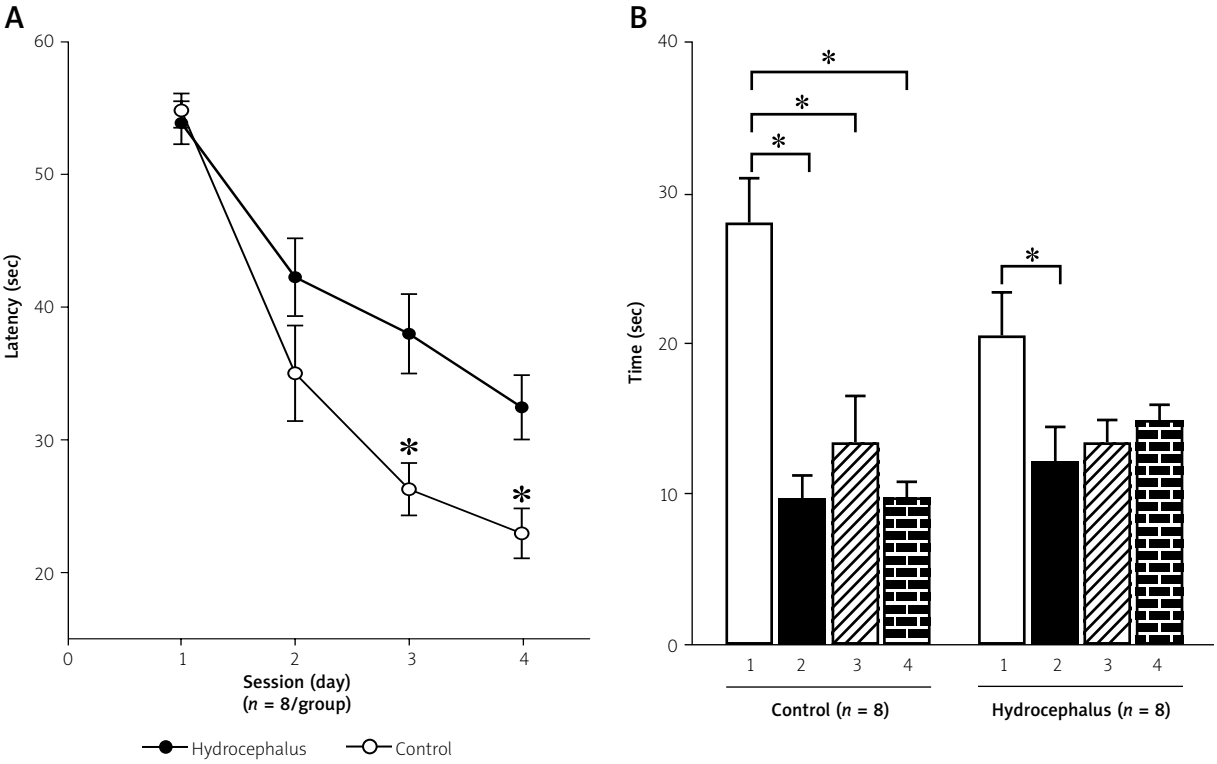

Fig. 1. A) Graph showing the mean escape latencies for finding the hidden platform. The mean escape latency in hydrocephalic rats was markedly longer compared with control rats, and there was a significant difference between the two groups on the 3rd and 4th day. **B)** Graph showing the swimming time in each quadrant of the pool without the platform. 1 is the quadrant in which the platform was initially placed, and 2, 3 and 4 are the remaining quadrants. The control rats spent a greater proportion of their swimming times in quadrant 1 (27.86 ± 3.195 s) than the hydrocephalus group (20.26 ± 3.166 s). *$p < 0.05$.

Magnetic resonance imaging and the enlarged ventricular system

Animals with saline injection into the lateral ventricle did not develop hydrocephalus; however, all rats with kaolin injection developed hydrocephalus. In these animals, MRI confirmed ventriculomegaly involving all ventricles (including the cerebral aqueduct, the third ventricle and the frontal horns and temporal horns of the lateral ventricle, etc.), and compression and thinning of the cortical tissue (Fig. 2A). Row 1 shows control rats at 16 days after saline injection. Row 2 shows hydrocephalic rats (16 days after kaolin injection). In comparison to the controls, there was obvious enlargement of all portions of the cerebral ventricles. General specimens show that control rats presented the normal configuration of the ventricular system, but experimental animals displayed significant expansion in the anterior horns and temporal horns of the lateral ventricle, midbrain aqueduct and fourth ventricle, and compression, thinning, fracture and distortion of the callosum and cortical tissue after kaolin injection (Fig. 2B). The lateral ventricles and the cerebral aqueduct were enlarged at the different sections and positions, and the fourth ventricle outlets remained open. Therefore, it corresponded to the classification of communicating hydrocephalus. The ventricular volume was detected in all the control rats (median value: 15.65 mm^3; range: 8.78-31.52 mm^3; $n = 14$), but in all the hydrocephalic rats (median value: 147.95 mm^3; range: 58.51-222.27 mm^3; $n = 29$). The ventricles were significantly dilated in the hydrocephalic rats compared to the controls ($p < 0.05$) (Fig. 3).

Histopathological findings

There was a significant difference between groups with respect to the histopathological changes in the vicinity of the lateral ventricle. Compared with the controls, the hydrocephalic animals showed advanced periventricular reactive astrogliosis with

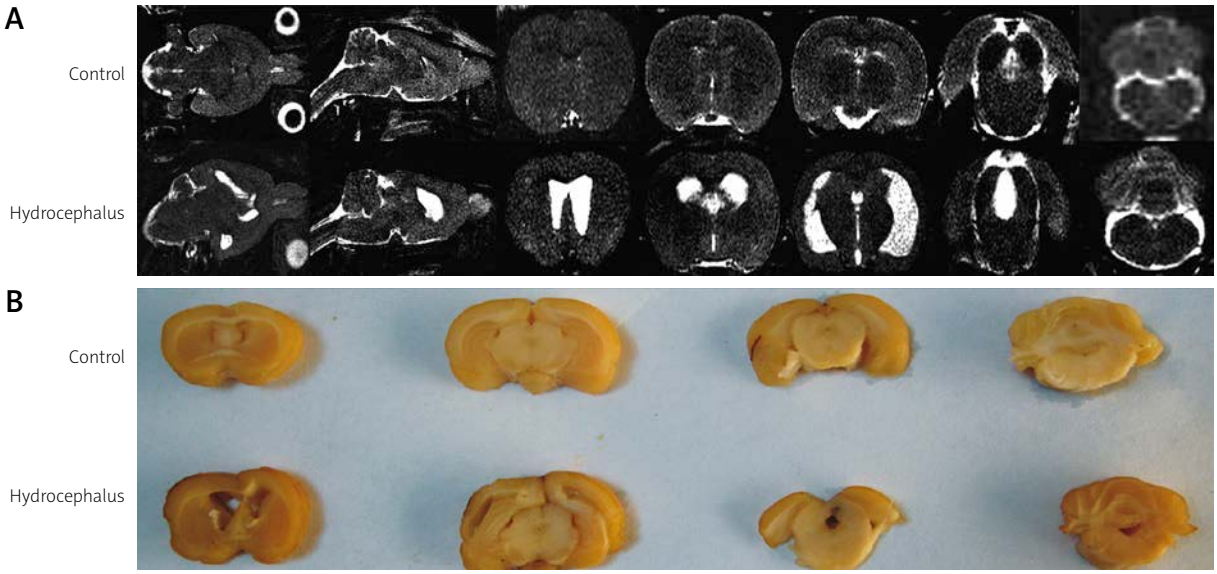

Fig. 2. A) Representative magnetic resonance imaging (T2-weighted) of rat brains in the horizontal plane (first column), in the mid-sagittal plane (second column) and at the coronal level of the lateral ventricle frontal horn (third column), optic chiasm (fourth column), lateral ventricle temporal horn (fifth column), cerebral aqueduct (sixth column) and basal cistern (seventh column). Row 1 shows control rats; the ventricles, cerebral aqueduct and cisterna magna are barely visible. Row 2 shows hydrocephalic rats at the 16th day after kaolin injection; the ventricles, cerebral aqueduct and cisterna magna show significant enlargement. **B)** General specimens of rat cerebral tissue with consecutive coronal sections. Row 1 – control group specimens showing no expansion of the ventricular system. Row 2 – experimental group represents significantly expanded lateral ventricle anterior horns (first column) and temporal horns (second column), midbrain aqueduct (third column) and fourth ventricle (fourth column), and compression, thinning, fracture and distortion of the corpus callosum and cortical tissue.

proliferation of hypertrophic astrocytes and disorder of organization structure; the ventricular wall was completely deprived of ependymal cells, which were lying loosely in the ventricular lumen (Fig. 4).

Discussion

The basic research on hydrocephalus has not experienced a breakthrough since the early 20th century. One of the main causes may be that we have not established a uniform and particularly effective animal model. Most studies have remained at the stage of animal model establishment. Regarding hydrocephalic animal model establishment, there are too many methods. This method of kaolin injection into the lateral ventricle to induce communicating hydrocephalus has a lot of advantages theoretically, but has not yet been widely applied. Therefore, we tried to construct and optimize the model of hydrocephalus after intraventricular kaolin injection for use in adult rats and provide a description of behavioral and histological changes.

Excluding unexpected death in the process of anesthesia or surgical trauma, all rats with kaolin injection into the lateral ventricle developed mod-

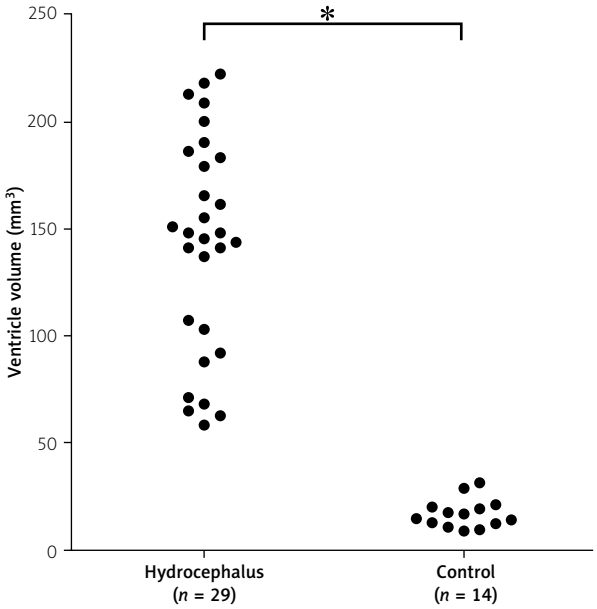

Fig. 3. Ventricular volumes were measured by NIH Image. Hydrocephalic rats exhibited significant ventricular dilation compared to controls (hydrocephalus – median value: 147.95 mm^3, range: 58.51-222.27 mm^3; controls – median value: 15.65 mm^3, range: 8.78-31.52 mm^3). The asterisk indicates $p < 0.05$ (Mann-Whitney *U* test).

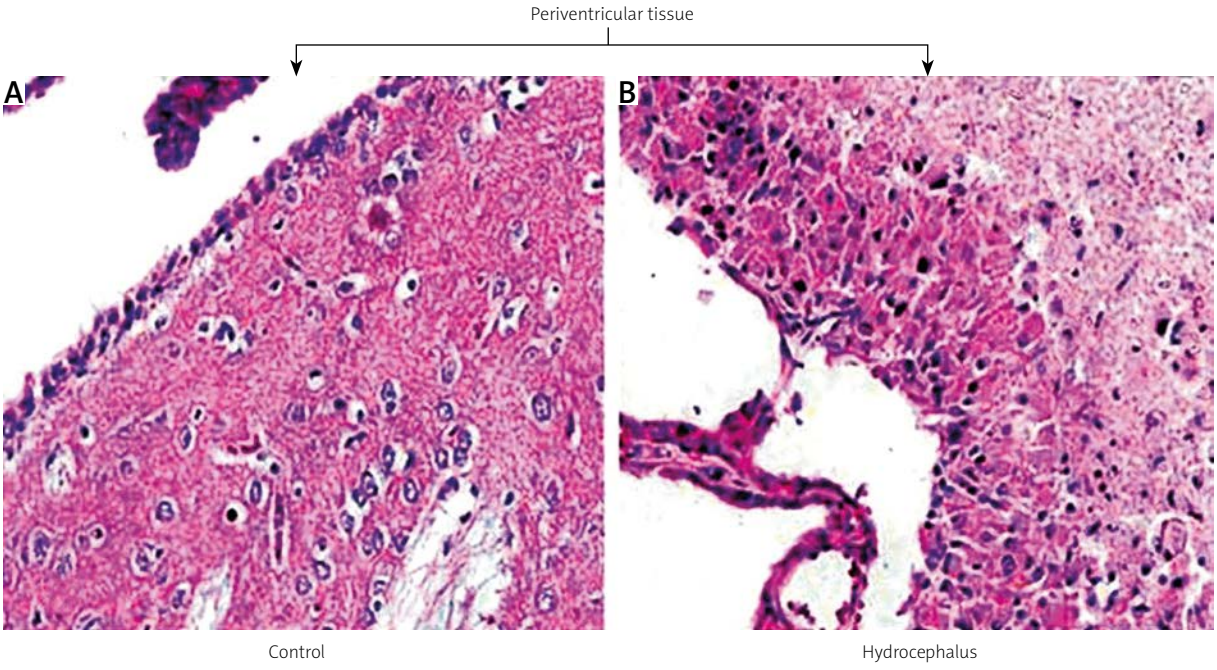

Fig. 4. Representative images of H&E staining of the lateral ventricle. Compared with the controls, the hydrocephalic animals showed advanced periventricular reactive astrogliosis with proliferation of hypertrophic astrocytes and disorder of organization structure; the ventricular wall was completely deprived of ependymal cells, which were lying loosely in the ventricular lumen (magnification, ×400).

erate to severe hydrocephalus according to MRI assay, and they could maintain long-term survival. However, using the technique of kaolin injection into the cistern magna of rodents, the acute mortality of animals was up to 10-50% [21,26,29]; and Bloch *et al*. reported that they had an about 20% acute mortality rate and 80% of the survivors died by 10 days [2]. The lower concentration kaolin suspensions after ultrasonic emulsification for about 15 minutes are less viscous, spread more easily through the CSF pathways and easily form a communicating hydrocephalus. Compared to kaolin injection into the cistern magna, the low concentration kaolin suspension injection into the lateral ventricle does not cause comprehensive adhesion of the cistern magna, facilitating CSF sample collection from the cistern magna, and does not lead to brain stem injury or a sharp rise of intracranial pressure, so the acute mortality rate is low. If we want to obtain more severely hydrocephalic animals and reduce animal death simultaneously, the method can be used again one week after injection. In addition, hydrocephalic animals exhibited a significant lag in weight gain, and severely hydrocephalic rats gradually lost weight. This phenomenon is in agreement with a previous report [21].

Magnetic resonance imaging and general specimens of rat cerebral tissue revealed that animals with severe hydrocephalus exhibited obvious expansion of ventricles, and thinning, distortion and compression of the cortical tissue and the corpus callosum. Hematoxylin and eosin (H&E) staining revealed that the hydrocephalic samples had high levels of glial cell hyperplasia, cell edema and liquefaction and organization structure disorder in the vicinity of the lateral ventricle. These changes in the hydrocephalus may directly cause deleterious effects and clinical symptoms such as dizziness, headache, gait disturbance, urinary incontinence and cognitive deficits/dementia that seriously threaten the patient's quality of life and the prognosis [5,7,9,20]. Impairments of gait and balance are the most common and the earliest symptoms of hydrocephalus. Patients may initially complain about dizziness, difficulty in walking on a slope or stairs, and difficulty in getting up from or sitting down on a chair; in the late stage of hydrocephalus, motor deficits are very common. Urinary incontinence in hydrocephalus results from detrusor hyperactivity owing to the partial or total absence of central inhibitory control. Patients initially suffer from increased urinary frequency; later developments are urge incontinence and, finally, permanent urinary incontinence. The cognitive deficits of hydrocephalus are mainly due to sub-cortical frontal dysfunction. The main clinical manifestations of cognitive deficits/dementia are as follows: psychomotor slowing, impaired attention and concentration, slowing and reduced precision of fine motor performance, changes of mood and personality, short-term memory impairment, indifference and bradyphrenia, etc. About one-third of children with hydrocephalus have been reported to have an IQ of < 70 and another third to have an IQ in the low normal range of 70-85 [19]. It has also been shown that children with congenital hydrocephalus have difficulties in learning and memory, problems that are not explained by low IQ scores alone. The decline of these above-mentioned functions is deemed "fronto-subcortical dementia" due to dysfunction of the frontal lobe and subcortical structures [3,31], and was partly observed in the course of our experiment, suggesting that the frontal cortex is severely affected in hydrocephalus [17]. In this study, disturbed spatial learning and memory were observed using the MWM test, which is consistent with the findings of previous studies [28].

The concentrations of kaolin reported in the literature were 25%, 20%, 10%, etc., and 25% kaolin was widely applied [11,18,21,29]. To determine the experimental concentration of kaolin, several different concentrations of kaolin (1%, 3%, 5%, 10%, 20%, 25%, 40% and 50%) were used in a small-sample experimental design in the preliminary experiment. The results showed that the high concentration kaolin suspensions were difficult to dissolve in saline, and tended to deposit more readily in the lateral ventricle in general specimens and spread with more difficultly through the CSF pathways, which may create a physical obstruction; moreover, they had a relatively low success rate and high acute mortality. However, the lower concentration kaolin suspensions, which can be dissolved and emulsified in saline by ultrasonic dissolution and did not jam the microsyringe, were less viscous and spread more easily through the CSF pathways, and had high success rates, low mortality rates and fewer complications. It seemed that the concentrations of 3% and 5% kaolin showed no significant difference in success rate. So we chose the 3% kaolin. In addition, we also attempted to use injection of autologous blood

from the caudal artery into the lateral ventricle to construct a model of hydrocephalus, but the success rate was very low.

Based on our experience, we conclude that this experimental hydrocephalus model, in which kaolin is injected into the lateral ventricle of adult rats, is viable because of its many advantages (including simplicity, cheapness, high success rate, low mortality, success in developing a communicating hydrocephalus and controllable hydrocephalic severity, etc.) and may be widely used. At the same time, we also provide a description of behavioral and histological changes, etc.

Conclusions

In summary, we have provided detailed information on the use of kaolin injection into the lateral ventricle to induce hydrocephalus in adult rats, and this model is similar to the clinical disease. In the next stage, we will explore further the biochemical changes in the cerebral tissue and CSF.

Acknowledgments

This study was partially supported by Xiamen University.

Disclosure

The authors report no conflict of interest.

References

1. Aquilina K, Hobbs C, Cherian S, Tucker A, Porter H, Whitelaw A, Thoresen M. A neonatal piglet model of intraventricular hemorrhage and posthemorrhagic ventricular dilation. J Neurosurg 2007; 107: 126-136.
2. Bloch O, Auguste KI, Manley GT, Verkman AS. Accelerated progression of kaolin-induced hydrocephalus in aquaporin-4-deficient mice. J Cereb Blood Flow Metab 2006; 26: 1527-1537.
3. Bonelli RM, Cummings JL. Frontal-subcortical circuitry and behavior. Dialogues Clin Neurosci 2007; 9: 141-151.
4. Chen X, Huang X, Li B, Zhao Z, Jiang L, Huang C, Lu Y. Changes in neural dendrites and synapses in rat somatosensory cortex following neonatal post-hemorrhagic hydrocephalus. Brain Res Bull 2010; 83: 44-48.
5. Dalen K, Bruaroy S, Wentzel-Larsen T, Laegreid LM. Intelligence in children with hydrocephalus, aged 4-15 years: a population-based, controlled study. Neuropediatrics 2008; 39: 146-150.
6. Davis LE. Communicating hydrocephalus in newborn hamsters and cats following vaccinia virus infection. J Neurosurg 1981; 54: 767-772.
7. Del Bigio MR. Neuropathological changes caused by hydrocephalus. Acta Neuropathol 1993; 85: 573-585.
8. Del Bigio MR. Pathophysiologic consequences of hydrocephalus. Neurosurg Clin N Am 2001; 12: 639-649.
9. Del Bigio MR. Cellular damage and prevention in childhood hydrocephalus. Brain Pathol 2004; 14: 317-324.
10. Del Bigio MR. Neuropathology and structural changes in hydrocephalus. Dev Disabil Res Rev 2010; 16: 16-22.
11. Deren KE, Packer M, Forsyth J, Milash B, Abdullah OM, Hsu EW, McAllister JP, 2nd. Reactive astrocytosis, microgliosis and inflammation in rats with neonatal hydrocephalus. Exp Neurol 2010; 226: 110-119.
12. Factora R, Luciano M. Normal pressure hydrocephalus: diagnosis and new approaches to treatment. Clin Geriatr Med 2006; 22: 645-657.
13. Fernell E, Hagberg B, Hagberg G, von Wendt L. Epidemiology of infantile hydrocephalus in Sweden. III. Origin in preterm infants. Acta Paediatr Scand 1987; 76: 418-423.
14. Fiori MG, Sharer LR, Lowndes HE. Communicating hydrocephalus in rodents treated with beta,beta'-iminodipropionitrile (IDPN). Acta Neuropathol 1985; 65: 209-216.
15. Hayashi N, Leifer DW, Cohen AR. Chronologic changes of cerebral ventricular size in a transgenic model of hydrocephalus. Pediatr Neurosurg 2000; 33: 182-187.
16. Hwang YS, Shim I, Chang JW. Anxiety responses and neurochemical changes in a kaolin-induced rat model of hydrocephalus. J Neurosurg Pediatr 2011; 7: 401-407.
17. Kiefer M, Unterberg A. The differential diagnosis and treatment of normal-pressure hydrocephalus. Dtsch Arztebl Int 2012; 109: 15-25; quiz 26.
18. Li J, McAllister JP, 2nd, Shen Y, Wagshul ME, Miller JM, Egnor MR, Johnston MG, Haacke EM, Walker ML. Communicating hydrocephalus in adult rats with kaolin obstruction of the basal cisterns or the cortical subarachnoid space. Exp Neurol 2008; 211: 351-361.
19. Lindquist B, Carlsson G, Persson EK, Uvebrant P. Learning disabilities in a population-based group of children with hydrocephalus. Acta Paediatr 2005; 94: 878-883.
20. Lindquist B, Persson EK, Uvebrant P, Carlsson G. Learning, memory and executive functions in children with hydrocephalus. Acta Paediatr 2008; 97: 596-601.
21. Lopes Lda S, Slobodian I, Del Bigio MR. Characterization of juvenile and young adult mice following induction of hydrocephalus with kaolin. Exp Neurol 2009; 219: 187-196.
22. McAllister JP, 2nd, Chovan P. Neonatal hydrocephalus. Mechanisms and consequences. Neurosurg Clin N Am 1998; 9: 73-93.
23. Nagra G, Wagshul ME, Rashid S, Li J, McAllister JP, 2nd, Johnston M. Elevated CSF outflow resistance associated with impaired lymphatic CSF absorption in a rat model of kaolin-induced communicating hydrocephalus. Cerebrospinal Fluid Res 2010; 7: 4.
24. Ohmiya M, Fukumitsu H, Nitta A, Nomoto H, Furukawa Y, Furukawa S. Administration of FGF-2 to embryonic mouse brain induces hydrocephalic brain morphology and aberrant differentiation of neurons in the postnatal cerebral cortex. J Neurosci Res 2001; 65: 228-235.

25. Owler BK, Pena A, Momjian S, Czosnyka Z, Czosnyka M, Harris NG, Smielewski P, Fryer T, Donvan T, Carpenter A, Pickard JD. Changes in cerebral blood flow during cerebrospinal fluid pressure manipulation in patients with normal pressure hydrocephalus: a methodological study. J Cereb Blood Flow Metab 2004; 24: 579-587.
26. Park YS, Park SW, Suk JS, Nam TK. Development of an acute obstructive hydrocephalus model in rats using N-butyl cyanoacrylate. Childs Nerv Syst 2011; 27: 903-910.
27. Shihab N, Davies E, Kenny PJ, Loderstedt S, Volk HA. Treatment of hydrocephalus with ventriculoperitoneal shunting in twelve dogs. Vet Surg 2011; 40: 477-484.
28. Shim I, Ha Y, Chung JY, Lee HJ, Yang KH, Chang JW. Association of learning and memory impairments with changes in the septohippocampal cholinergic system in rats with kaolin-induced hydrocephalus. Neurosurgery 2003; 53: 416-425.
29. Slobodian I, Krassioukov-Enns D, Del Bigio MR. Protein and synthetic polymer injection for induction of obstructive hydrocephalus in rats. Cerebrospinal Fluid Res 2007; 4: 9.
30. Tada T, Zhan H, Tanaka Y, Hongo K, Matsumoto K, Nakamura T. Intraventricular administration of hepatocyte growth factor treats mouse communicating hydrocephalus induced by transforming growth factor beta1. Neurobiol Dis 2006; 21: 576-586.
31. Tekin S, Cummings JL. Frontal-subcortical neuronal circuits and clinical neuropsychiatry: an update. J Psychosom Res 2002; 53: 647-654.
32. Wiesmann M, Koedel U, Bruckmann H, Pfister HW. Experimental bacterial meningitis in rats: demonstration of hydrocephalus and meningeal enhancement by magnetic resonance imaging. Neurol Res 2002; 24: 307-310.
33. Williams MA, McAllister JP, Walker ML, Kranz DA, Bergsneider M, Del Bigio MR, Fleming L, Frim DM, Gwinn K, Kestle JR, Luciano MG, Madsen JR, Oster-Granite ML, Spinella G. Priorities for hydrocephalus research: report from a National Institutes of Health-sponsored workshop. J Neurosurg 2007; 107: 345-357.
34. Zhao K, Sun H, Shan Y, Mao BY, Zhang H. Cerebrospinal fluid absorption disorder of arachnoid villi in a canine model of hydrocephalus. Neurol India 2010; 58: 371-376.

Original article

Folia Neuropathologica

Sertraline and curcumin prevent stress-induced morphological changes of dendrites and neurons in the medial prefrontal cortex of rats

Ali Noorafshan[1,2], Mohammad-Amin Abdollahifar[2], Saied Karbalay-Doust[1,2], Reza Asadi-Golshan[2], Ali Rashidian-Rashidabadi[2]

[1]Histomorphometry and Stereology Research Centre, Shiraz University of Medical Sciences, Shiraz, [2]Anatomy Department, School of Medicine, Shiraz University of Medical Sciences, Shiraz, Iran

Folia Neuropathol 2015; 53 (1): 69-79 DOI: 10.5114/fn.2015.49976

Abstract

Stress induces structural and behavioral impairments. The changes in dendrites and neurons are accompanied by impairments in the tasks mediated by the medial prefrontal cortex (mPFC). The present study was conducted to evaluate the structural changes of the dendrites and neurons of the mPFC after stress using stereological methods. In addition, the effects of a natural and a synthetic substance, i.e., curcumin and sertraline, were evaluated. The rats were divided into 7 groups: stress + distilled water, stress + olive oil, curcumin (100 mg/kg/day), sertraline (10 mg/kg/day), stress + curcumin, stress + sertraline, and control groups. The animals were submitted to chronic variable stress for 56 days. The results showed an average 15% reduction in the length of the dendrites per neuron in the mPFC after stress ($p < 0.004$). The total spine density was reduced by 50% in the stress (+ olive oil or + distilled water) groups in comparison with the control group ($p < 0.01$). The main reduction was seen in the thin and mushroom spines, while the stubby spines remained unchanged. Mean volume and surface area of the neurons were decreased by 14% and 10% on average in the stress (+ distilled water or + olive oil) rats in comparison to the control rats, respectively ($p < 0.01$). The data revealed that treatment of stressed rats with curcumin or sertraline can prevent the loss of spines and reduction of dendrite length, volume and surface area of the neurons. Sertraline and curcumin can prevent structural changes of the neurons and dendrites induced by stress in the mPFC of rats.

Key words: *stress, sertraline, curcumin, cortex, dendrite, neuron, stereology.*

Introduction

Chronic stress is perceived and the response is coordinated by the brain. It has been well documented that uncontrollable stress induced dendritic remodeling in several brain regions [37,39]. It has been reported that chronic stress for 21 days reduced the length as well as the number of dendrites and spines in the hippocampus [5]. The chronic stress-induced morphological changes may be correlated with the specialized functions of the prefrontal cortex (PFC) sub-regions in stress-related pathologies [30,31]. Alterations in spine shape (stubby, mushroom or thin shaped) and number have been reported in

Communicating author:

Saied Karbalay-Doust, Histomorphometry and Stereology Research Centre, Shiraz University of Medical Sciences, Zand Ave., Shiraz, Iran, Postal code: 71348-45794, phone/fax: +98-711-2304372, e-mail: karbalas@sums.ac.ir

neurodegenerative disorders, including depression [2,28]. Previous studies have shown morphological changes in the pyramidal neurons in the PFC following chronic stress [30,31]. Our previous study showed that stress affected behavioral tests, such as spatial learning and memory, anxiety, and anhedonia [23]. These behavioral changes might be accompanied by structural remodeling of the neurons including their dendrites. It has been reported that the changes in dendritic length and spine density are accompanied by impairments in the cognitive tasks selectively mediated by the mPFC [18]. These reports suggest that stress-induced remodeling in the mPFC may have distinct functional consequences. Previous studies have also demonstrated that chronic restraint stress changed the morphology of the neurons in the mPFC [32]. It has been reported that the prefrontal cortex shows alterations in the cerebral structures in depressed patients [19]. In addition, previous investigations have indicated reduced neuronal soma size in the prefrontal cortex [29,32]. In spite of these reports that reveal the possible chronic stress-induced morphological changes of neurons in the mPFC, no studies have been carried out on the neuron volume, volume of neuron nuclei and neuron surface area.

Medial PFC plays a key role in controlling the hypothalamic-pituitary-adrenal (HPA) axis and regulates the stress response of other structures [8]. Depression shows a good response to pharmacological treatments, and among the various drug agents, selective serotonin reuptake inhibitors (SSRIs) and tricyclic antidepressants (TCAs) are widely used in adult patients [25]. Sertraline is an antidepressant which is used to treat major depression in adult patients. Its antioxidant and neuroprotective actions have also been reported in neurodegenerative diseases [43]. Curcumin is the principal curcuminoid of the popular Indian spice turmeric. It has been used to manage stress and depression related disorders in China [35] and is known to have anti-inflammatory, antioxidant, anti-carcinogenic, anti-microbial, and neuroprotective effects [3,16]. The previous studies showed that antidepressant like action of curcumin, its use in major depression, these including, inhibitor of monoamine oxidase (MAO) enzyme, regulations the level of various neurotransmitters, promotes hippocampal [17]. In another study, curcumin was shown to protect the dopamine-producing cells of the substantial nigra area of the brain in a rat model of Parkinson's disease [17].

The present study aimed to evaluate and compare the effects of a natural and a synthetic substance, i.e., curcumin and sertraline, on stress in an animal model. Design-based stereological methods were used to estimate the total dendritic length per neuron, density and morphology of the spines, mean volume of the neuron and nucleus and mean surface area of the neuron in the mPFC of rats. Mean volume was estimated using the nucleator method. Estimation of the neuron surface area received less attention and here the surfactor method was used for the estimation. In the method of length estimation presented here, there is no need for the time-consuming method of dendrite tracing using instruments such as the camera lucida. In addition, in the tracing method, some dendrites that are anterior or posterior to the dendrite might not be identifiable by the researchers.

Material and methods

Animals

In this study, 42 adult male Sprague-Dawley rats (240 to 280 g) were obtained from the Laboratory Animal Center of Shiraz University of Medical Sciences, Shiraz, Iran. The Ethics Committee of the University approved the animal experiment (Approval No. 91-6124). The male rats were randomly assigned to experimental and control groups. Each group included 6 rats that were housed under standard conditions, room temperature (22-24°C), and a 12 : 12 h light-dark schedule and had free access to water and food. The animals were divided into seven groups: (I) stress + water group daily receiving stress and distilled water, (II) stress + olive oil group daily receiving stress and olive oil, (III) curcumin group receiving curcumin (100 mg/kg/day) [23,24], (IV) sertraline group receiving sertraline (10 mg/kg/day) [43], (V) stress + curcumin group daily receiving stress and curcumin (100 mg/kg/day) [23,24], (VI) stress + sertraline group daily receiving stress and sertraline (10 mg/kg/day) [43], and (VII) the control group. All the animals received 1 ml of the medications by gavage.

Stress model

The animals were submitted to a chronic variable stress (CVS) regime over a 56-day period or remained in their home cages without stress manipulation [40]. The CVS is described in Table I.

Table I. Protocol for induction of chronic variable stress (CVS) in 56 days for the rat model

Day	Stressor applied
1	Cold restraint (1.5 h)
2	Inclination of home cages (4 h)
3	Flashing light (2 h)
4	Restraint (2 h)
5	Isolation
6	Isolation
7	Isolation
8	Damp bedding (2 h)
9	Inclination of home cages (6 h)
10	No stressor applied
11	Flashing light (2 h)
12	Water deprivation (24 h)
13	Restraint (3 h)
14	Damp bedding (3 h)
15	Inclination of home cages (4 h)
16	Cold restraint (2 h)
17	Flashing light (3 h)
18	Restraint (2.5 h)
19	Damp bedding (3 h)
20	Isolation
21	Isolation
22	Isolation
23	Cold restraint (1.5 h)
24	Water deprivation (24 h)
25	Inclination of home cages (4 h)
26	Restraint (3 h)
27	Flashing light (3 h)
28	Restraint (1 h)
29	Damp bedding (2 h)
30	No stressor applied
31	Water deprivation (24 h)
32	Inclination of home cages (6 h)
33	Flashing light (2 h)
34	Cold restraint (2 h)
35	Isolation
36	Isolation
37	Isolation
38	Flashing light (3 h)
39	Damp bedding (2 h)
40	Restraint (3 h)
41	Cold restraint (1.5 h)
42	Inclination of home cages (4 h)
43	Flashing light (2 h)
44	Restraint (2 h)
45	Isolation
46	Isolation
47	Isolation
48	Damp bedding (2 h)
49	Inclination of home cages (6 h)
50	No stressor applied
51	Flashing light (2 h)
52	Water deprivation (24 h)
53	Restraint (3 h)
54	Damp bedding (3 h)
55	Inclination of home cages (4 h)
56	Cold restraint (2 h)

Tissue preparation

The rats were deeply anesthetized and quickly decapitated. Then, the brain was exposed by an incision along the midline of the skull. A small amount of fixative was poured on the exposed brain immediately. Afterwards, the brains were removed and the left medial prefrontal cortex was dissected out 4.70-2.70 mm ventral and 2.20-1.40 mm dorsal to the Bregma [26].

Estimation of total length of dendrite per neuron

Length estimation should be done on vertical uniform random sections [1,9-11,15]. Briefly, 9-10 cylinders were punched out using a trocar with 1 mm diameter perpendicular to the pial surface of the mPFC cortex (Fig. 1). All the cylinders of each animal were randomly rotated along their vertical axes and embedded in one paraffin block. Then, 100 µm thickness slabs were obtained using a microtome. The brain samples were transferred into freshly prepared chromatin solution containing 3% potassium dichromate and 4% or 5% paraformaldehyde in either distilled water (i.e., not buffered) or PBS solutions with pH of 5.8, 7.4, or 7.6. The chromatin solutions also contained both 2% glutaraldehyde and 2% chloral hydrate. All the chromatin solutions were daily changed with freshly prepared solutions. After being kept in chromatin for 48 hours, the brains

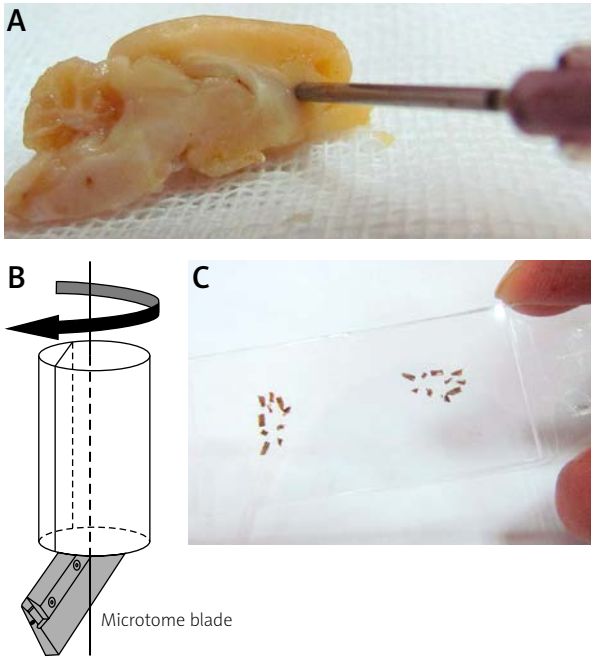

Fig. 1. Vertical uniform random sectioning. **A)** The vertical cylinders were punched out from the mPFC cortex vertical to its pial surface. **B-C)** The cylinder was randomly rotated along its vertical axis. The cylinders were sectioned using a microtome and mounted on a slide.

were washed several times with a 2% silver nitrate solution in distilled water before being incubated in silver nitrate for another 48 hours for heavy metal precipitation to occur. During the whole staining process, the brains were covered with aluminum foil to avoid light exposure [7]. Mean dendritic length per neuron was calculated using the following formula [11]:

$$\bar{l}_N = \frac{\textit{Total dendritic length in the population}}{\textit{Total number of neurons in the population}}$$

To estimate the length, a vertical section was considered. A cycloid grid and a counting frame were superimposed on the live images of the mPFC parallel to the vertical axis of the cylinder. Using a microscope (Nikon E-200) equipped with an objective lens (100×, numerical aperture of 1.4) connected to a computer, a fixed slab height of T (here 100 µm) was scanned inside the section thickness (Fig. 2). To estimate the dendrite length per neuron, two quantities were measured: i) the number (Q^-) of cell bodies of the neurons using the optical disector method, and ii) the total number of intersections (I) between the dendrite axes and the

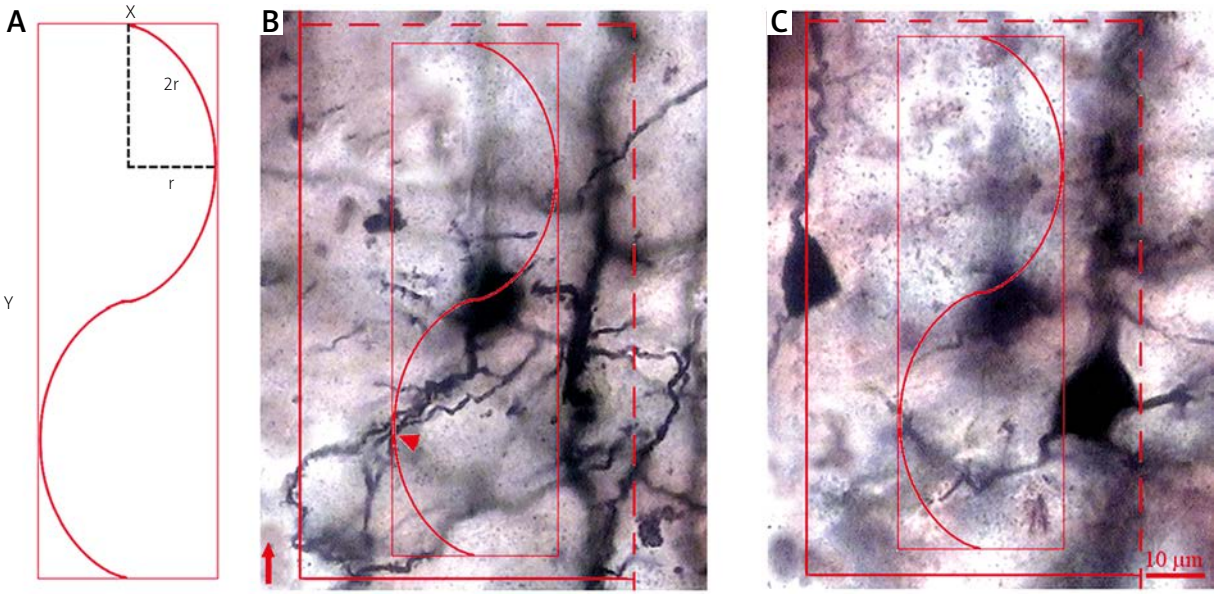

Fig. 2. Estimation of dendrite length. **A)** Four cycloids were located at a rectangle. The length of each cycloid was equal to twice the length of its minor axis (*r*). The area associated with the cycloids was calculated by multiplying X by Y and dividing by the length of the four cycloids to achieve the area per length. **B-C)** When the sections were scanned, the number of cell bodies of the neurons was counted using the optical disector method and unbiased counting frame. The total number of intersections between the dendrite axes and the cycloid was counted (arrow head). The cycloid was positioned parallel to the vertical axis (arrow).

oriented cycloid (Fig. 2) [1,9-11,15]. The following formula was used:

$$\bar{I}_N = 2.\frac{a}{l}.\frac{1}{asf}.M^{-1}.\frac{\sum I}{\sum Q^-}$$

Where "al" is the test area per cycloid test length, "asf" is the area associated with the cycloid grid divided by the area of the counting frame, and "M" is the final magnification at ×4000.

Estimation of density and morphology of dendritic spines

To estimate the density and morphology of spines, the above-mentioned dendrites were considered. Dendritic spines were identified as small protrusion that extended less than 3 µm from the parent dendrite. Dendritic protrusion was classified as spines when they exhibited a characteristic enlargement at the tip, including stubby form or mushroom-type spines. The spines without enlargement were defined as thin filopodia-like protrusions [4]. Spines were counted only if they appeared continuous with the parent dendrite. Density and morphology of spines were quantified and expressed as the number of spines per neuron [4].

Estimation of mean volume of neuron and nucleus

The volume was estimated using the nucleator method. The mPFC was cut into isotropic uniform random pieces using the orientator method [9,10]. They were embedded in a paraffin block, sectioned (25 µm thickness) and stained with cresyl violet. The neurons were sampled using an optical disector [9,10]. For each sampled nucleolus, two horizontal directions (intercept, ln) were considered from the central point within the nucleolus to the cell or nucleus borders (Fig. 3). From a series of these measurements (120-200 intercepts in each group), the mean nucleus and cell volume in the number weighted distribution was estimated using [9, 10]:

$$V_N = \frac{4\pi}{3} \times \overline{l_n^3}$$

Estimation of mean surface area of neuron

The mean surface area of the neurons was estimated using the surfactor method. As mentioned earlier, to estimate the mean cell volume, the isotropic intercept emanating from the nucleus to the border of the particle was measured on the sampled cells using the disector principle (ln) (Fig. 3). The acute angle β ($0 < \beta \leq \pi/2$) between the intercept length and the tangent to the boundary of the cell at the point of the intersection was also measured. Finally, the surface area was measured using the following formula:

$$S_v = 4\pi \times \overline{l_n^2} \times c(\beta),\ c\beta = 1 + \left(\frac{\pi}{2} - \beta\right) \times \cot\beta$$

For the sake of simplicity, the angles were classified by the transparent protractor overlaid on the images. The protractor was a half circle which was divided into twelve 15° classes (Fig. 3) [13].

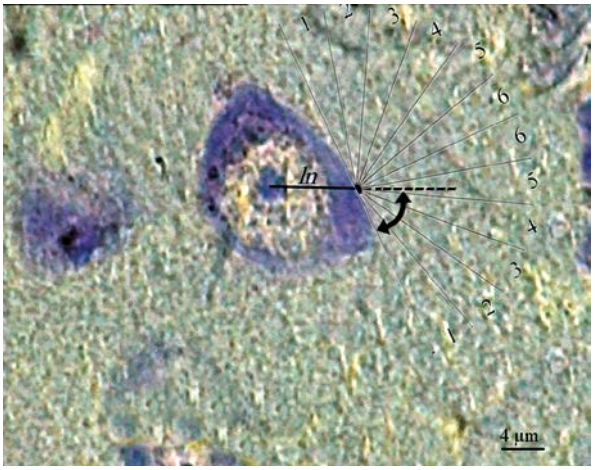

Fig. 3. Nucleator and surfactor methods. A cell is sampled using an optical disector. For each sampled nucleolus, right and left horizontal directions are considered from the central point within the nucleolus (only right is presented here). The distance (intercept, ln) in both directions from the point to the boundary of the nucleus and the neuron borders is recorded and used for volume estimation. For surface area estimation, the isotropic intercept emanating from the nucleolus to the border of the particle is measured on the sampled cells (ln). The acute angle "β" (curved arrow) between the intercept length and the tangent to the boundary of the cell at the point of the intersection is shown. The angle is classified by the protractor, which was divided into twelve 15° classes (here 5).

Statistical analysis

The data were analyzed using the Kruskal-Wallis test and the Mann-Whitney *U*-test. $P \leq 0.05$ was considered as statistically significant.

Results

Total length of dendrite per neuron

The results showed that dendritic length of the mPFC was reduced by 15% in the stress + olive oil in comparison with the stress + curcumin groups ($p < 0.004$). Further analysis revealed a significant decrease of 16% in the stress + distilled water in comparison with the stress + sertraline groups ($p < 0.004$) (Fig. 4).

Density and morphology of spines

The analysis of dendritic spine densities in the mPFC showed that the stress reduced the spine densities. The results showed that total spine density was reduced by 50% on average in the stress (+ olive oil or + distilled water) groups in comparison with the control group ($p < 0.01$) (Fig. 5). Analysis of spine morphology showed that density of the thin spines per neuron was reduced by 60% on average in stress (+ olive oil or + distilled water) rats in comparison to the control rats ($p < 0.01$) (Fig. 5). The density of the mushroom spines was reduced by 40% on average in stress (+ olive oil or + distilled water) rats in comparison to the control rats ($p < 0.01$) (Fig. 5). The stubby spines of the mPFC remained unchanged (Fig. 5). The data revealed that treatment of the stressed rats with curcumin and sertraline prevents spine loss.

Volume and surface area of neurons

Mean volume of the neuron and nuclei in the mPFC was decreased by 14% on average in the stress (+ distilled water or + olive oil) rats in comparison to the control rats ($p < 0.01$) (Fig. 6). Mean surface area of the neuron was decreased by 10% on average in the stress (+ distilled water or + olive oil) rats in comparison to the control rats ($p < 0.01$) (Fig. 6).

The data revealed that treatment of the stressed rats with curcumin or sertraline prevents reduction of the volume and surface area of the neurons.

Discussion

The present study investigated the morphological changes of the dendrites and neurons in mPFC as a result of chronic variable stress using stereological methods. The results showed that chronic stress changes the morphology of dendrites and neurons in the mPFC. Moreover, this adverse stress effect was shown to be prevented by treatment with curcumin and sertraline.

Stress-induced remodeling in the mPFC has been suggested to have distinct functional consequences [18]. Therefore, evaluation of the dendritic morphology is a valuable parameter. The reduction in the dendritic length per neuron, density and morphology of spine is in accordance with the studies conducted by Cook and Wellman [5], Izquierdo *et al*. [12], and Shansky *et al*. [38,39] showing stress to induce significant changes in the morphology of the pyramidal neurons and decrease in length of dendrites or retraction of

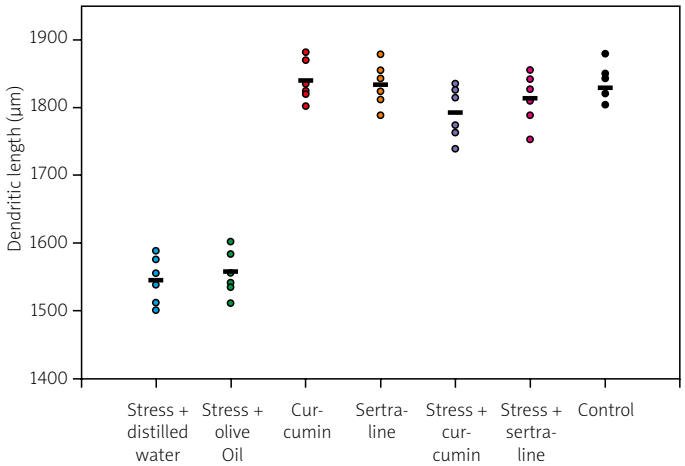

Fig. 4. Length of dendrites. Dot plot showing the total length of the dendrites per neuron in different groups including control, distilled water, olive oil, curcumin, sertraline with or without stress treatment.

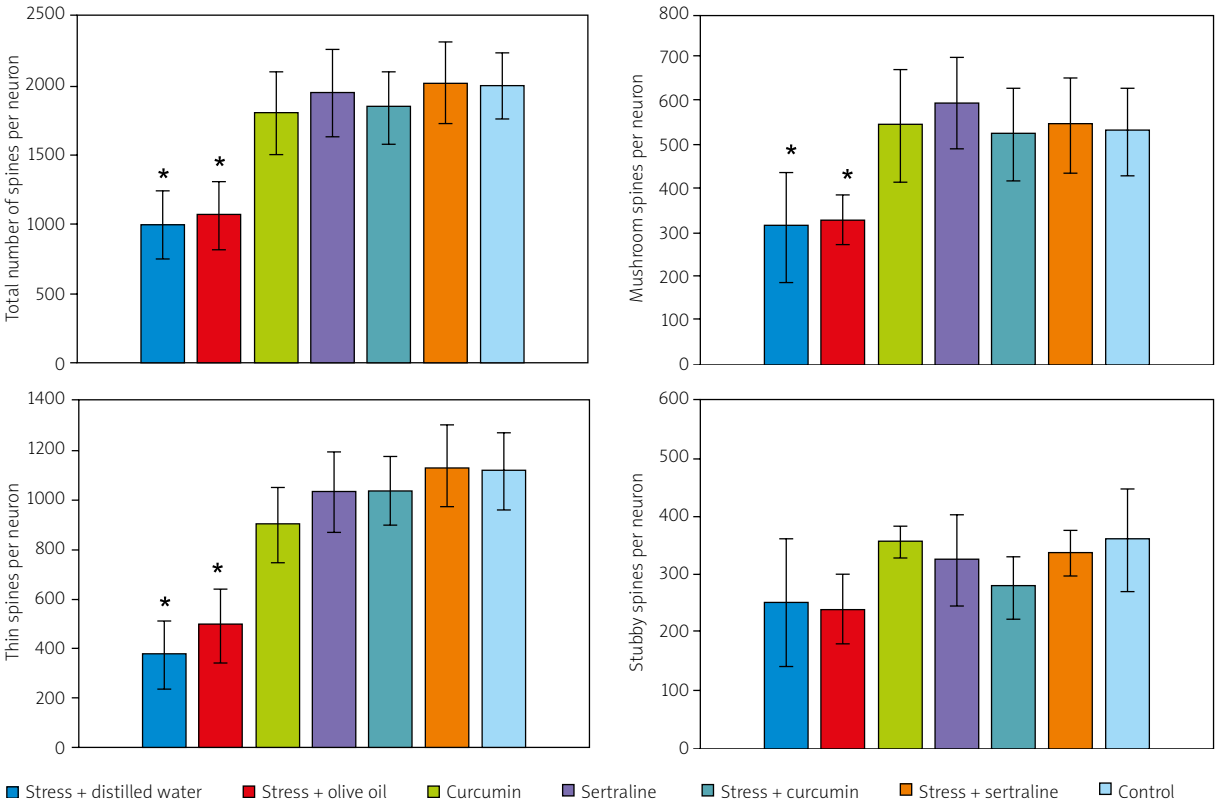

Fig. 5. Density of spines. The total density and the density of different spine types (thin, mushroom and stubby) per neuron of the mPFC in the different groups are shown. The significant difference between stress (+ olive oil and + distilled water) with the other groups is indicated. *$p < 0.01$.

the apical dendritic arbor in the pyramidal cells in the PFC. These changes in the dendritic length, density and morphology of the spine have been shown to be accompanied by impairments in the cognitive functions selectively mediated by the mPFC [18].

In general, the length estimation method mostly relies on tracing images of the dendrites. However, the technique presented here is a design-based stereological method and does not require tracing, which is a time-consuming procedure. In addition, tracing might be vulnerable to mistake when the branches cannot be traced on the obscure sides of the dendrites.

Our study revealed that chronic exposure to stress reduced the spine density in the mPFC and also reduced the thin and mushroom spines in mPFC, whereas stubby spines in the mPFC remained unchanged. However, it is hypothesized that thin and mushroom spines represent learning spines and memory spines, respectively. It is the result of their constant changing in response to neuronal activity (e.g., chronic stress) [36]. This is in accordance with our previous study showing that stress impairs learning and memory [23].

The present study also indicated that chronic exposure to stress reduced the volume of neurons, neuron nuclei and surface area of neurons in the mPFC. Furthermore, clinical studies showed that structural brain modifications in depressed patients are similar to those found in animal models of chronic variable stress (such as decreased neuronal soma size and neuronal density) in the mPFC. The findings of this study are thus in line with previous reports of reduced neuronal soma size in the prefrontal cortex. Reduced neuronal soma size is also described in major depressive disorder [29,32]. The surface area of the neuron is important in their functions and synaptic activities. However, this parameter has received less attention in histopathological research.

The chronic stress-induced factors that lead to these changes are not fully understood. Nevertheless, previous studies have shown that repeat-

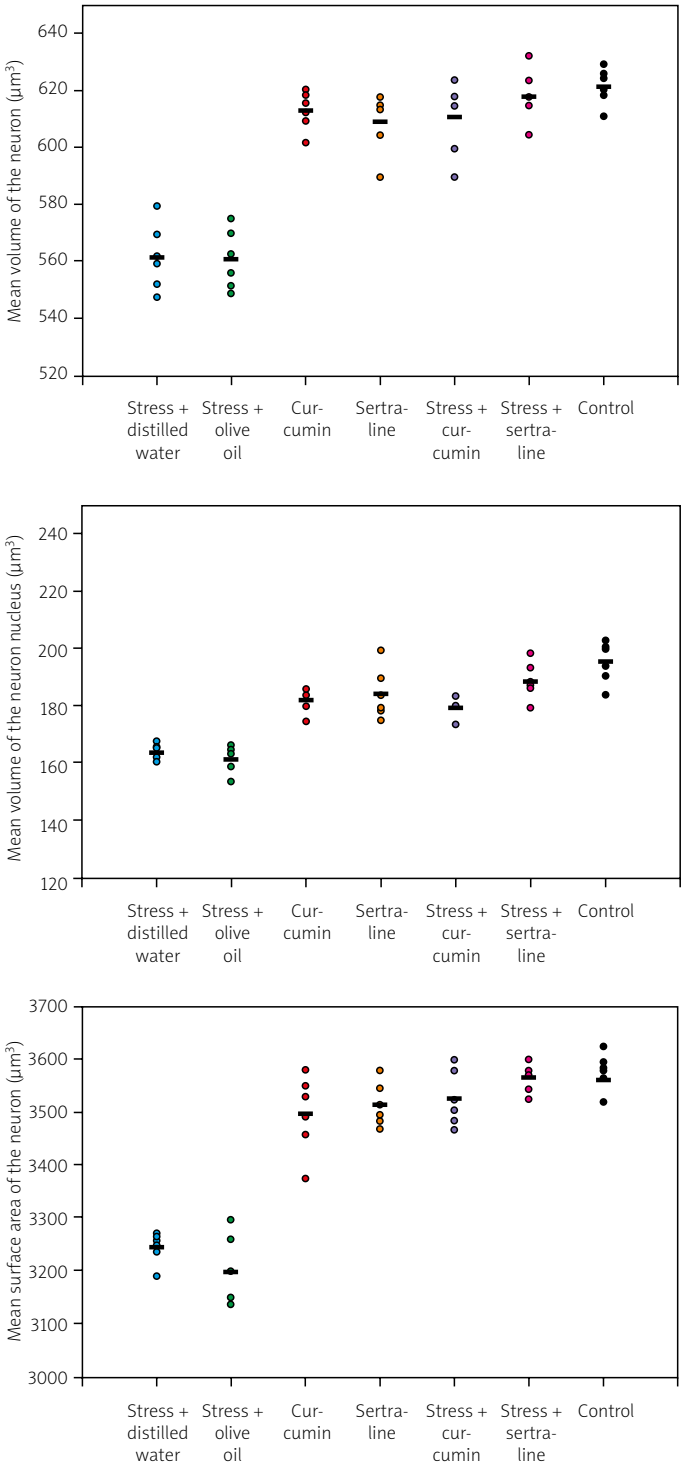

Fig. 6. Volume and surface area. Dot plot showing mean volume of the neuron, mean volume of the neuron nuclei and mean surface area of the neuron of the mPFC in different groups.

ed stress reduced dopamine [22,27], noradrenalin [14], and serotonin in the mPFC [20]. Experimental findings also emphasize that serotonin changes spine density and dendrite length in the mPFC by acting on 5-HT receptors [21]. The mPFC seems to be severely sensitive and reacts faster to stressful events [41]. Glucocorticoid receptors are present in the mPFC of rats. Also, catecholamines and glucocorticoids are the key mediators of the stress response and release upon the nervous system [8,34]. The medial prefrontal cortex plays a key role in controlling the hypothalamic-pituitary-adrenal axis and regulates the stress response of other structures [8]. The present study also demonstrated that sertraline and curcumin had protective effects on the morphological changes of dendrites and neurons of the mPFC destroyed by stress. Selective serotonin reuptake inhibitors are the most widely prescribed antidepressants today and exert their antidepressant-like effects by inhibiting the neuronal reuptake of serotonin and increasing the synaptic concentrations of serotonin. Sertraline treatment also reduced acetylcholinesterase enzyme levels in all regions of the brain [43]. Previous studies showed that fluoxetine (a selective serotonin reuptake inhibitor) could cause an increase in the total dendritic length in CA1 but not in the dentate gyrus [25]. Our finding is also in accordance with these reports. The effect of curcumin was also evaluated and compared with sertraline in the present investigation. This compound showed the same protective effects as sertraline on dendrite length after stress induction. Although the mechanism of the antidepressant effect of curcumin is not completely understood [16], previous studies have reported that antidepressant effects may be obtained by several mechanisms, such as inhibition of serotonin uptake [6,33]. In addition, curcumin is an antidepressant which is well proven in inhibiting the monoamine oxidase enzyme and modulating the release of serotonin and dopamine [16]. However, evidence has shown that curcumin administration also increased hippocampal neurogenesis in chronically stressed rats by modulation of the hypothalamic-pituitary-adrenal axis and regulation of 5-HT1A receptors as well as the brain-derived neurotrophic factor in the hippocampus [42]. This idea is supported by the finding that antidepressants can promote neurogenesis [42]. As it appears, different factors might be effective in curcumin's mechanism of action. However, to our knowledge, no studies have been conducted on the effects of curcumin on the dendritic and neuron morphology after stress. In conclusion, the present findings demonstrate that curcumin and sertraline could protect against the adverse effects of stress on dendritic length, density, morphology of the spine, volume of neurons, volume of neuron nuclei and surface area of neurons of the mPFC.

Acknowledgements

The work was performed at the Histomorphometry and Stereology Research Centre, Shiraz University of Medical Sciences, Shiraz, Iran. This study is part of a thesis written by Mohammad-Amin Abdollahifar, PhD student of Anatomy. The work was financially supported by the Research Vice-Chancellor of Shiraz University of Medical Sciences (Grant No. 91-6124). The authors would like to thank RouzDarou Pharmaceutical Company for their kind provision of sertraline. They are also grateful to the Research Improvement Center of Shiraz University of Medical Sciences and Ms. A. Keivanshekouh for improving the use of English in the manuscript.

Disclosure

Authors report no conflict of interest.

References

1. Baddeley AJ, Gundersen HJ, Cruz-Orive LM. Estimation of surface area from vertical sections. J Microsc 1986; 142: 259-276.
2. Boda B, Alberi S, Nikonenko I, Node-Langlois R, Jourdain P, Moosmayer M, Parisi-Jourdain L, Muller D. The mental etardation protein PAK3 contributes to synapse formation and plasticity in hippocampus. J Neurosci 2004; 24: 10816-10825.
3. Brouet I, Ohshima H. Curcumin, an anti-tumour promoter and anti-inflammatory agent, inhibits induction of nitric oxide synthase in activated macrophages. Biochem Biophys Res Commun 1995; 206: 533-540.
4. Chapleau CA, Carlo ME, Larimore JL, Pozzo-Miller L. The actions of BDNF on dendritic spine density and morphology in organotypic slice cultures depend on the presence of serum in culture media. J Neurosci Methods 2008; 169: 182-190.
5. Cook SC, Wellman CL. Chronic stress alters dendritic morphology in rat medial prefrontal cortex. J Neurobiol 2004; 60: 236-248.
6. Cryan JF, Leonard BE. 5-HT1A and beyond: the role of serotonin and its receptors in depression and the antidepressant response. Hum Psychopharmacol 2000; 15: 113-135.
7. de Ruiter JP, Uylings HB. Morphometric and dendritic analysis of fascia dentata granule cells in human aging and senile dementia. Brain Res 1987; 402: 217-229.

8. Diorio D, Viau V, Meaney MJ. The role of the medial prefrontal cortex (cingulate gyrus) in the regulation of hypothalamic-pituitary-adrenal responses to stress. J Neurosci 1993; 13: 3839-3847.
9. Gundersen HJ, Bagger P, Bendtsen TF, Evans SM, Korbo L, Marcussen N, Møller A, Nielsen K, Nyengaard JR, Pakkenberg B, et al. The new stereological tools: disector, fractionator, nucleator and point sampled intercepts and their use in pathological research and diagnosis. APMIS 1988; 96: 857-881.
10. Gundersen HJ, Bendtsen TF, Korbo L, Marcussen N, Møller A, Nielsen K, Nyengaard JR, Pakkenberg B, Sørensen FB, Vesterby A, et al. Some new, simple and efficient stereological methods and their use in pathological research and diagnosis. APMIS 1988; 96: 379-394.
11. Howard CV, Cruz-Orive LM, Yaegashi H. Estimating neuron dendritic length in 3D from total vertical projections and from vertical slices. Acta Neurol Scand Suppl 1992; 137: 14-19.
12. Izquierdo A, Wellman CL, Holmes A. Brief uncontrollable stress causes dendritic retraction in infralimbic cortex and resistance to fear extinction in mice. J Neurosci 2006; 26: 5733-5738.
13. Karlsson LM, Cruz-Orive LM. Estimation of mean particle size from single sections. J Micros 1997; 186: 121-132.
14. Kitayama I, Kayahara T, Nakano K, Murase S, Otani M, Nomura J. Long-term stress degenerates, but imipramine regenerates, noradrenergic axons in the rat cerebral cortex. Biol Psychiatry 1997; 42: 687-696.
15. Kristiansen SL, Nyengaard JR. Digital stereology in neuropathology. APMIS 2012; 120: 327-340.
16. Kulkarni SK, Bhutani MK, Bishnoi M. Antidepressant activity of curcumin: involvement of serotonin and dopamine system. Psychopharmacology (Berl) 2008; 201: 435-442.
17. Kulkarni S, Dhir A, Akula KK. Potentials of curcumin as an antidepressant. ScientificWorldJournal 2009; 9: 1233-1241.
18. Liston C, Miller MM, Goldwater DS, Radley JJ, Rocher AB, Hof PR, Morrison JH, McEwen BS. Stress-induced alterations in prefrontal cortical dendritic morphology predict selective impairments in perceptual attentional set-shifting. J Neurosci 2006; 26: 7870-7874.
19. Lorenzetti V, Allen NB, Fornito A, Yücel M. Structural brain abnormalities in major depressive disorder: a selective review of recent MRI studies. J Affect Disord 2009; 117: 1-17.
20. Mangiavacchi S, Masi F, Scheggi S, Leggio B, De Montis MG, Gambarana C. Long-term behavioral and neurochemical effects of chronic stress exposure in rats. J Neurochem 2001; 79: 1113-1121.
21. Miner LA, Backstrom JR, Sanders-Bush E, Sesack SR. Ultrastructural localization of serotonin2A receptors in the middle layers of the rat prelimbic prefrontal cortex. Neuroscience 2003; 116: 107-117.
22. Mizoguchi K, Yuzurihara M, Ishige A, Sasaki H, Chui DH, Tabira T. Chronic stress induces impairment of spatial working memory because of prefrontal dopaminergic dysfunction. J Neurosci 2000; 20: 1568-1574.
23. Noorafshan A, Abdollahifar MA, Karbalay-Doust S, Asadi-Golshan R, Rashidiani-Rashidabadi A. Protective effects of curcumin and sertralineon the learning and memory impairment, anxiety, and anhedoniain chronic stressed rats. Exp Neurobiol 2013; 22: 96-106.
24. Noorafshan A, Asadi-Golshan R, Karbalay-Doust S, Abdollahifar MA, Rashidiani-Rashidabadi A. Curcumin, the main part of turmeric, prevents learning and memory changes induced by sodium metabisulfite, a preservative agent, in rats. Exp Neurobiol 2013; 22: 23-30.
25. Norrholm SD, Ouimet CC. Chronic fluoxetine administration to juvenile rats prevents age-associated dendritic spine proliferation in hippocampus. Brain Res 2000; 883: 205-215.
26. Paxinos G, Watson C. The rat brain in stereotaxic coordinates. Academic Press, San Diego 2007.
27. Pascucci T, Ventura R, Latagliata EC, Cabib S, Puglisi-Allegra S. The medial prefrontal cortex determines the accumbens dopamine response to stress through the opposing influences of norepinephrine and dopamine. Cereb Cortex 2007; 17: 2796-2804.
28. Perez-Cruz C, Simon M, Flügge G, Fuchs E, Czéh B. Diurnal rhythm and stress regulate dendritic architecture and spine density of pyramidal neurons in the rat infralimbic cortex. Behav Brain Res 2009; 205: 406-413.
29. Pierri JN, Volk CL, Auh S, Sampson A, Lewis DA. Decreased somal size of deep layer 3 pyramidal neurons in the prefrontal cortex of subjects with schizophrenia. Arch Gen Psychiatry 2001; 58: 466-473.
30. Radley JJ, Rocher AB, Miller M, Janssen WG, Liston C, Hof PR, McEwen BS, Morrison JH. Repeated stress induces dendritic spine loss in the rat medial prefrontal cortex. Cereb Cortex 2006; 16: 313-320.
31. Radley JJ, Sisti HM, Hao J, Rocher AB, McCall T, Hof PR, McEwen BS, Morrison JH. Chronic behavioral stress induces apical dendritic reorganization in pyramidal neurons of the medial prefrontal cortex. Neuroscience 2004; 125: 1-6.
32. Rajkowska G, Miguel-Hidalgo JJ, Wei J, Dilley G, Pittman SD, Meltzer HY, Overholser JC, Roth BL, Stockmeier CA. Morphometric evidence for neuronal and glial prefrontal cell pathology in major depression. Biol Psychiatry 1999; 45: 1085-1098.
33. Rush AJ, Trivedi MH, Wisniewski SR, Stewart JW, Nierenberg AA, Thase ME, Ritz L, Biggs MM, Warden D, Luther JF, Shores-Wilson K, Niederehe G, Fava M; STAR*D Study Team. Bupropion-SR, sertraline, or venlafaxine-XR after failure of SSRIs for depression. N Engl J Med 2006; 354: 1231-1242.
34. Sánchez MM, Young LJ, Plotsky PM, Insel TR. Distribution of corticosteroid receptors in the rhesus brain: relative absence of glucocorticoid receptors in the hippocampal formation. J Neurosci 2000; 20: 4657-4668.
35. Sanmukhani J, Anovadiya A, Tripathi CB. Evaluation of antidepressant like activity of curcumin and its combination with fluoxetine and imipramine: an acute and chronic study. Acta Pol Pharm 2011; 68: 769-775.
36. Segal I, Korkotian I, Murphy DD. Dendritic spine formation and pruning: common cellular mechanisms? Trends Neurosci 2000; 23: 53-57.
37. Selye H. The evolution of the stress concept. Am Sci 1973; 61: 692-699.
38. Shansky RM, Hamo C, Hof PR, McEwen BS, Morrison JH. Stress-induced dendritic remodeling in the prefrontal cortex is circuit specific. Cereb Cortex 2009; 19: 2479-2484.
39. Shansky RM, Morrison JH. Stress-induced dendritic remodeling in the medial prefrontal cortex: effects of circuit, hormones and rest. Brain Res 2009; 1293: 108-113.

40. Tagliari B, Noschang CG, Ferreira AG, Ferrari OA, Feksa LR, Wannmacher CM, Dalmaz C, Wyse AT. Chronic variable stress impairs energy metabolism in prefrontal cortex and hippocampus of rats: prevention by chronic antioxidant treatment. Metab Brain Dis 2010; 25: 169-176.
41. Vertes RP. Differential projections of the infralimbic and prelimbic cortex in the rat. Synapse 2004; 51: 32-58.
42. Xu Y, Ku B, Cui L, Li X, Barish PA, Foster TC, Ogle WO. Curcumin reverses impaired hippocampal neurogenesis and increases serotonin receptor 1A mRNA and brain-derived neurotrophic factor expression in chronically stressed rats. Brain Res 2007; 1162: 9-18.
43. Yildirim E, Erol K, Ulupinar E. Effects of sertraline on behavioral alterations caused by environmental enrichment and social isolation. Pharmacol Biochem Behav 2012; 101: 278-287.

Folia Neuropathologica

Atypical teratoid/rhabdoid tumor of the brain in an adult with 22q deletion but no absence of INI1 protein: a case report and review of the literature

Shumei Jin[1,2,3,4,*], Cuiyun Sun[1,2,3,*], Shizhu Yu[1,2,3], Qian Wang[1,2,3], Tongling An[1,2,3], Yanjun Wen[1,2,3]

[1]Department of Neuropathology, Tianjin Neurological Institute, Tianjin Medical University General Hospital, Tianjin, [2]Key Laboratory of Post-trauma Neuro-repair and Regeneration of Central Nervous System, Ministry of Education, Tianjin, [3]Tianjin Key Laboratory of Injuries, Variations and Regeneration of Nervous System, Tianjin, [4]Tianjin Huanhu Hospital, Tianjin, China

*Both authors contributed equally to this work.

Folia Neuropathol 2015; 53 (1): 80-85 DOI: 10.5114/fn.2015.49977

Abstract

We report a case of atypical teratoid/rhabdoid tumor (AT/RT) of the central nervous system (CNS) in an adult and its immunological phenotype and chromosomal DNA imbalance characteristics, as detected by comparative genomic hybridization (CGH). The immunohistochemical characteristics showed that atypical rhabdoid cells were positive for epithelial membrane antigen, vimentin, desmin, and glial fibrillary acidic protein, but there was no absence of INI1 protein. The CGH results identified the imbalances of the case to be the loss of 1p, 5q, 12q, 15q, 19q and 22q and the gain of 9q. Our discovery raises the question whether INI1 is implicated in all cases and whether its deletion is necessary in the pathogenesis of AT/RT, and also whether additional genetic pathways might exist. These data will offer useful information for further research on AT/RTs.

Key words: *atypical teratoid/rhabdoid tumor, comparative genomic hybridization, loss of 22q, INI1 protein.*

Introduction

Atypical teratoid/rhabdoid tumors (AT/RTs) are highly malignant brain tumors predominantly occurring in young children [10], typically containing rhabdoid cells, often with primitive neuroectodermal cells and with divergent differentiation along epithelial, mesenchymal, neuronal or glial lines. The INI1 gene locus on chromosome 22q11.2 was also called hSNF5 or SMARCB1. It was thought that alterations of the *INI1* gene which resulted in the protein expression loss were a possible novel pathogenesis of AT/RT [7]. However, to date, no clinical, histological or molecular prognostic factors have been clearly demonstrated. In the 1990s, it was observed that AT/RT often demonstrates a loss of all or part of chromosome 22 [2,14]. But to our knowledge, AT/RTs have been reported in adults only in rare cases in the literature [11,13,15-17], and only a few cases of AT/RTs have been investigated by comparative genomic hybridization (CGH) [4,18]. Studies have shown that the wide absence of recurrent genomic alterations other than SMARCB1 aberrations was recently confirmed in whole exome sequencing [9]. A small subset of these tumors dis-

Communicating author:

Shizhu Yu, Department of Neuropathology, Tianjin Neurological Institute, Tianjin Medical University General Hospital, 154, Anshan Road, Heping District, Tianjin 300052, phone: 86-022-60817518, fax: 86-022-60817518, e-mail: tjyushizhu@yahoo.com

plays a loss of INI1 but has the atypical histopathological features of AT/RT [3]. The preservation and expression of the INI1 gene in a small population of AT/RTs therefore exists. We report here one case of AT/RT of the central nervous system (CNS) with loss of some of 22q but no absence of INI1 protein expression in adults, which is rare for this tumor, and these data offer useful evidence concerning its unique clinical, histological and molecular biological features.

Case report

A 38-year-old male patient complained of headache and vomiting for 12 days. Magnetic resonance imaging (MRI) showed an iso/hypointense mass on T2WI and isointense on T1WI with strong contrast enhancement in the occiput (Fig. 1). Surgical resection of the mass was performed. Radiotherapy was applied after the operation. Unfortunately, the patient died after three months following tumor recurrence.

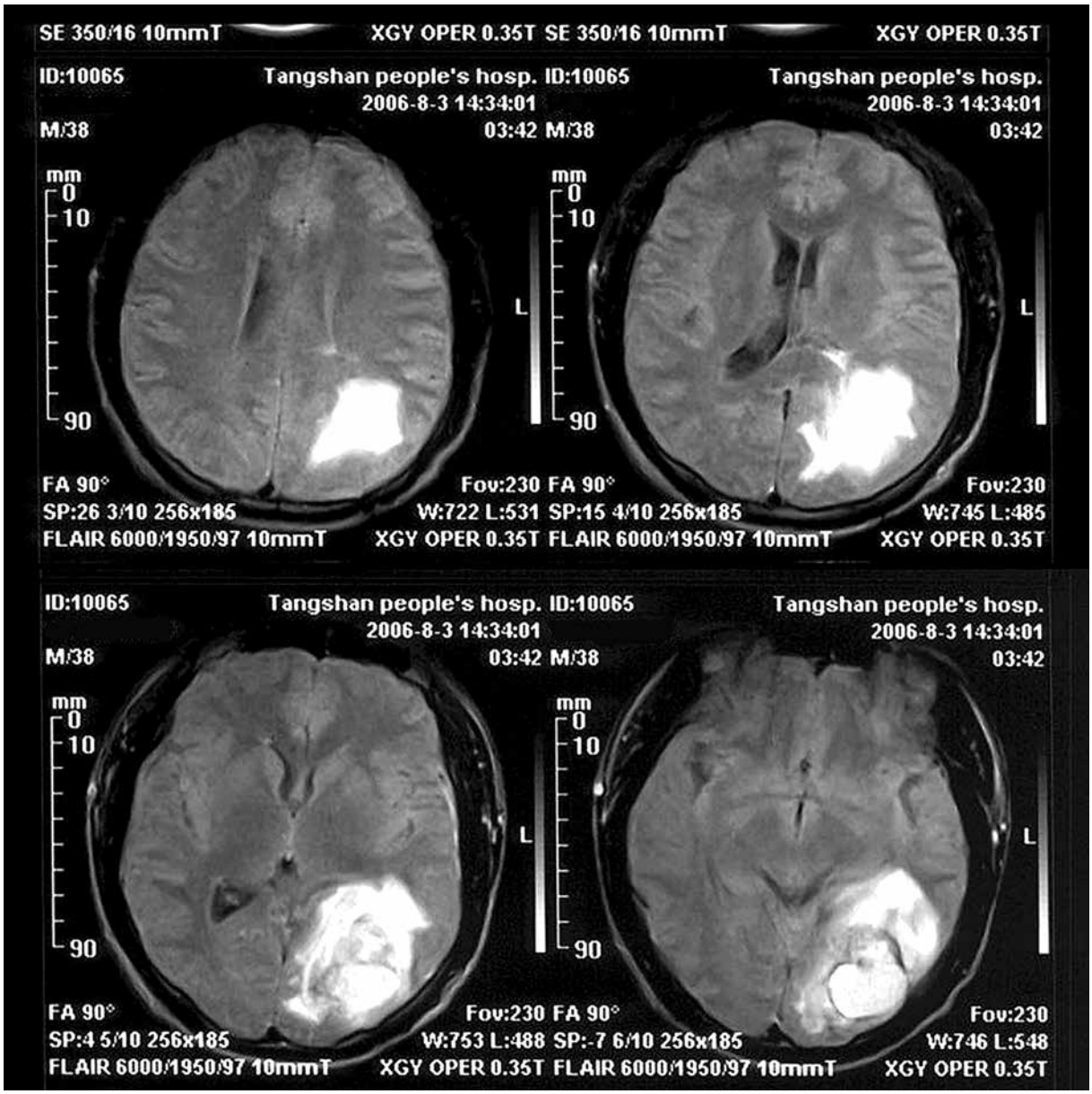

Fig. 1. Magnetic resonance (MR) images of one case of atypical teratoid/rhabdoid tumor. The fluid-attenuated inversion recovery (FLAIR) axial MR images show a temples-parietal-occipital borderline mass with a cystic component of hyperintensities and a solid contrast-enhanced component (A1-A4) and with peripheral edema.

Material and methods

INI1 antibody was obtained from DAKO (catalogue no. A-0150, Dako, Denmark), and other antibodies (include epithelial membrane antigen – EMA, vimentin – Vim, desmin – Des, glial fibrillary acidic protein – GFAP) for immunohistochemical (IHC) staining were purchased from Beijing Zhongshan Golden Bridge Biotechnology Co. Ltd. The reagents for CGH were from Invitrogen and Roche companies.

Tumor samples were observed by hematoxylin and eosin staining and immunohistochemical staining. Comparative genomic hybridization was performed according to the procedure described by Mohapatra *et al*. [12] to detect chromosomal DNA imbalances. The images then obtained for the analysis of the signals were analyzed using Leica CW4000 Karyo software.

Results

The hematoxylin and eosin (H&E) sections of the case showed that the histopathological features revealed rhabdoid cells which are characteristic features of an AT/RT. The immunohistochemical profile revealed that the rhabdoid cells characteristically showed positive for EMA, Vim, Des, and GFAP, but also no absence of INI1 protein. The MIB-1 proliferation index was 19.84% (Fig. 2). The results of the CGH analysis were obtained from high quality figures of CGH profiles. The common imbalances of this case were losses of 1p, 5q, 12q, 15q, 19q and 22q and the gain of 9q (Fig. 3).

Discussion

Atypical teratoid/rhabdoid tumors are rare, highly aggressive tumors of childhood, particularly under the age of 3 years. They are extremely rare in adults. The diagnosis is challenging, as there may be significant histological overlap with other embryonal tumors [1]. It usually occurs in very young children, although it has been reported in adults as well [11], but it rarely occurs in adults, and the true incidence of it is not yet known. Atypical teratoid/rhabdoid tumor is composed of rhabdoid cells entirely or in part with a combination of primitive neuroectodermal, mesenchymal and epithelial cells. The appearance of rhabdoid cells typically falls along a spectrum ranging from this rhabdoid phenotype to cells with less striking nuclear atypia and large amounts of pale eosinophilic cytoplasm. These rhabdoid cells

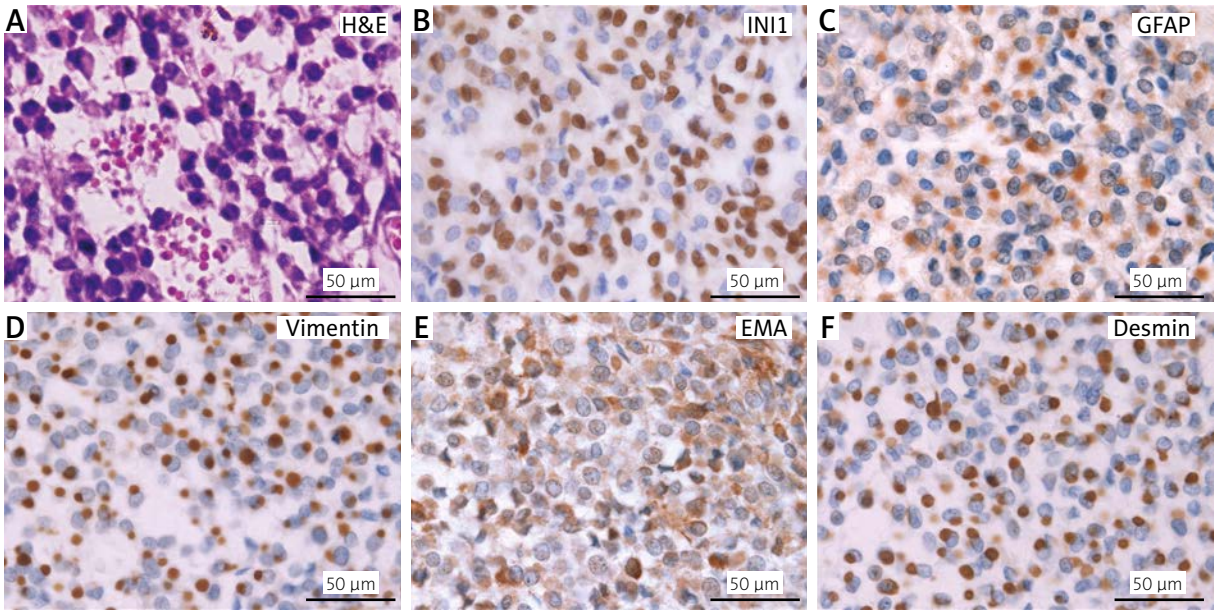

Fig. 2. Hematoxylin and eosin stain (H&E) and immunohistochemical features of the case. The H&E sections show the histopathological feature being composed of rhabdoid cells (**A**). The immunohistochemical analysis demonstrated atypical rhabdoid cells partially positive for INI1 (**B**), partially positive for glial fibrillary acidic protein (GFAP) (**C**), positive for vimentin (Vim) (**D**), partially positive for epithelial membrane antigen (EMA) (**E**) and positive for desmin (Des) (**F**).

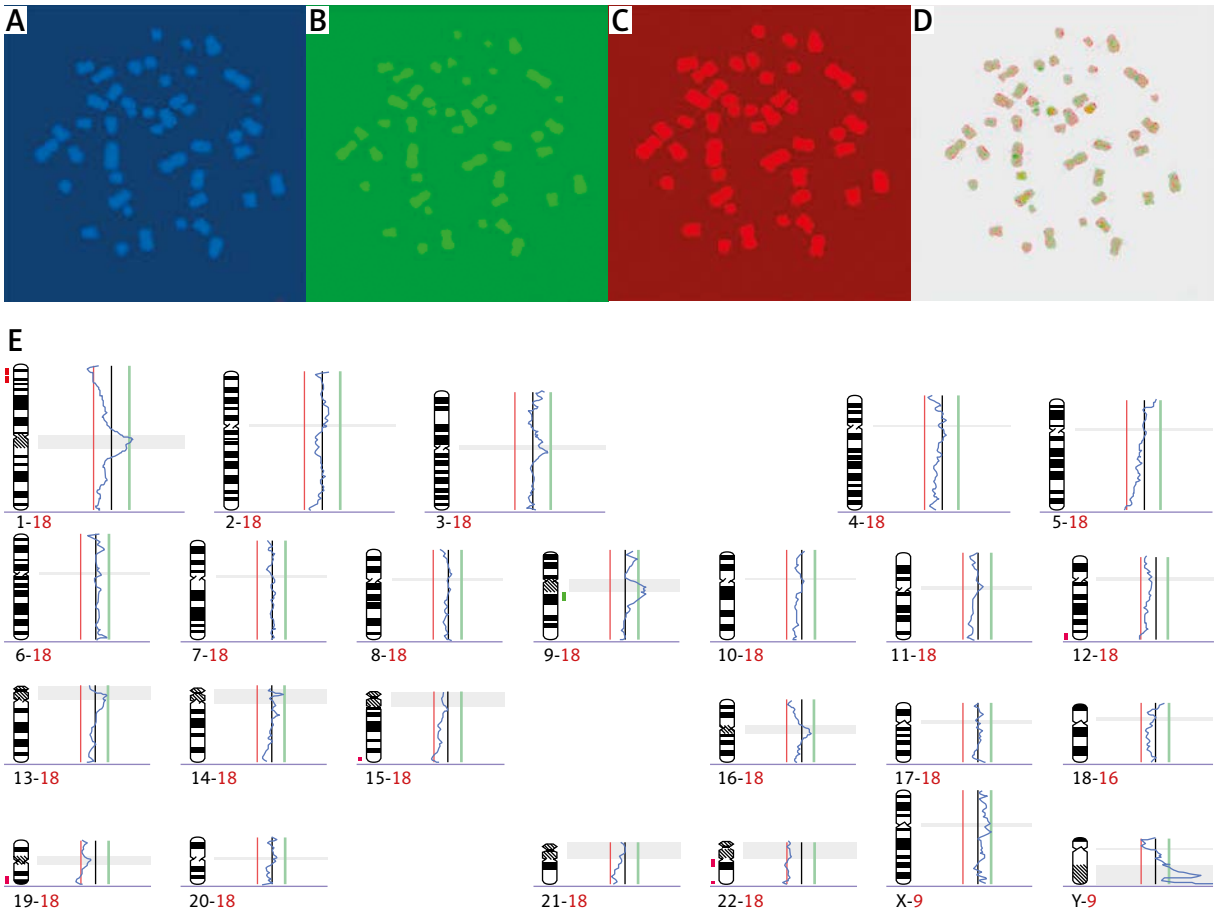

Fig. 3. Results of comparative genomic hybridization (CGH) analysis. The figure of above the blue represented chromosomes by DAPI (4',6-diamidino-2-phenylindole) staining (**A**). The green represented chromosomes by biotin-labeled tumor DNA generating green fluorescence (**B**). The red represented chromosomes digoxigenin-labeled normal reference DNA generating red fluorescence (**C**). Computer coincidence figure of A, B and C (**D**). The curve under represented the diagram auto-generated by the computer of the chromosomes gain or loss. Losses are indicated by the red line on the left of each chromosome scheme, whereas the green line on the right represents gains. The genomic DNA imbalances of both cases contain –1p, –5q, –12q, –15q, –19q, –22q and +9q.

may be arranged in nests or sheets and often have a jumbled appearance [10]. Rhabdoid tumors, in contrast, usually possess a distinctive genetic signature that accompanies the rhabdoid morphology, the INI1 mutation, or a deletion at the 22q11.2 locus. Multiple studies have also demonstrated that a loss of INI1 protein expression caused by homozygous deletions or truncating mutations of INI1 is associated with rhabdoid tumors.

In this case, light microscopy revealed a tumor composed of diffuse sheets of typical "rhabdoid" cells with eccentric nuclei, brightly eosinophilic cytoplasm and microvascular proliferation. The immunohistochemical features supported the reliability of our original diagnosis of AT/RT, but the INI-1 protein immunostaining was positive. This result was consistent with a recent published case report which illustrated an INI1+ AT/RT case in a 9-month-old boy from Los Angeles, and which showed retained INI1/SMARCB1 staining on immunohistochemical analysis [6]. The cellular origin of AT/RT is still unknown, but inactivating mutations of the hSNF5/INI1 gene located on chromosomal region 22q11.2 are regarded as a crucial step in their molecular pathogenesis [5]. The reports in the literature have demonstrated that AT/RT is often associated with characteristic genetic abnormalities, which include either monosomy 22 or deletion involving the hSNF5/INI1 gene located on

22q11.2, thus leading to the absence of INI1 protein [8]. However, inactivation of INI1 may not be specific for rhabdoid tumors. So far, only a few adult AT/RTs cases have been investigated by CGH, showing the expected loss of 22q, as well as additional losses on chromosomes 1p, 4p, 16p, 19p and 8p [4,18]. This case, as detected by CGH, indicated the losses of 1p, 5q, 12q, 15q, 19q and 22q and the gain of 9q. These divergent CGH results reflect the complicated pathogenesis of AT/RTs. Until now, most AT/RT studies have focused on DNA mutation or deletion. The posttranscriptional regulation of INI1 is still obscure. This case has 22q chromosomal deletion but no absence of INI1 protein. This similarly discrepant result was indicated by both CGH and IHC results. Nevertheless, CGH is a molecular cytogenetic method that is capable of detecting and mapping the relative DNA sequence copy number and identifying fragment gains or losses of DNA, and can thereby act as a screening method for chromosomal alterations. In the present case of AT/RT, the CGH result indicated deletion of part of 22q, but the INI1 gene protein was positive according to IHC, so we think that it was not the fragment of *INI1* gene location loss. This demonstrates that there is another gene related to the genesis of AT/RTs. Despite this assay being limited by the fact that there is not an adequate number of cases of AT/RTs, only occasionally occurring, we hypothesized that these results should be regarded as an exception of INI1 expression and genetic background. Whether or not INI1 proves to be implicated in all cases, our data suggest that apart from monosomy 22q, a better understanding of additional genetic pathways and the clinical and biological roles of these genes is greatly needed, and our data will offer useful information for further research in AT/RT. We speculate that the molecular biological features occurring in adults will differ from those occurring in children. It is therefore necessary to conduct further research on AT/RTs.

Acknowledgements

This research was supported by the State Key Development Program for Basic Research of China (973 Program, 2010CB529405), the National Natural Science Foundation of China (30770827), Tianjin Municipal Science and Technology Innovation System and Platform Construction Project (10SYSYJC28800), Tianjin Anti-cancer Special Major Science and Technology Project (12ZCDZSY17400), the Key Project of Tianjin Application Foundation and Frontier Technology Research (10JCZDJC19400), and the Key Project of Tianjin Higher Education Science and Technology Development Fund Project (2004ZD06, 20060202).

Disclosure

The authors report no conflict of interest.

References

1. Biegel JA, Fogelgren B, Zhou J-Y, James CD, Janss AJ, Allen JC, Zagzag D, Raffel C, Rorke LB. Mutations in the INI1 rhabdoid tumor suppressor gene in medulloblastomas and primitive neuroectodermal tumors of the central nervous system. Clin Cancer Res 2000; 6: 2759-2763.
2. Biegel JA, Rorke LB, Packer RJ, Emanuel BS. Monosomy 22 in rhabdoid or atypical teratoid tumors of the brain. J Neurosurg 1990; 73: 710-714.
3. Bourdeaut F, Freneaux P, Thuille B, Lellouch-Tubiana A, Nicolas A, Couturier J, Pierron G, Sainte-Rose C, Bergeron C, Bouvier R, Rialland X, Laurence V, Michon J, Sastre-Garau X, Delattre O. hSNF5/INI1-deficient tumours and rhabdoid tumours are convergent but not fully overlapping entities. J Pathol 2007; 211: 323-330.
4. Rickert CH, Paulus W. Chromosomal imbalances detected by comparative genomic hybridization in atypical teratoid/rhabdoid tumors. Childs Nerv Syst 2004; 20: 221-224.
5. Gessi M, Giangaspero F, Pietsch T. Atypical teratoid/rhabdoid tumors and choroid plexus tumors: when genetics "surprise" pathology. Brain Pathol 2003; 13: 409-414.
6. Hasselblatt M, Gesk S, Oyen F, Rossi S, Viscardi E, Giangaspero F, Giannini C, Judkins AR, Frühwald MC, Obser T, Schneppenheim R, Siebert R, Paulus W. Nonsense Mutation and Inactivation of SMARCA4 (BRG1) in an Atypical Teratoid/Rhabdoid Tumor Showing Retained SMARCB1 (INI1) Expression. Am J Surg Pathol 2011; 35: 933-935.
7. Jackson EM, Sievert AJ, Gai X, Hakonarson H, Judkins AR, Tooke L, Perin JC, Xie H, Shaikh TH, Biegel JA. Genomic analysis using high-density single nucleotide polymorphism-based oligonucleotide arrays and multiplex ligation-dependent probe amplification provides a comprehensive analysis of INI1/SMARCB1 in malignant rhabdoid tumors. Clin Cancer Res 2009; 15: 1923-1930.
8. Judkins AR, Mauger J, Ht A, Rorke LB, Bielgel JA. Immunohistochemical analysis of hSNF5/INI1in pediatric CNS neoplasms. Am J Surg Pathol 2004; 28: 644-650.
9. Lee RS, Stewart C, Carter SL, Ambrogio L, Cibulskis K, Sougnez C, Lawrence MS, Auclair D, Mora J, Golub TR, Biegel JA, Getz G, Roberts CW. A remarkably simple genome underlies highly malignant pediatric rhabdoid cancers. J Clin Invest 2012; 122: 2983-2988.
10. Louis DN, Ohgaki H, Wiestler OD, et al. World health organization classification of tumors. WHO classification of tumors of the central nervous system. 4th edn. IARC Press, Lyon 2007; 13-52.

11. Lutterbach J, Liegibel J, Koch D, Madlinger A, Frommhold H, Pagenstecher A. Atypical teratoid/rhabdoid tumors in adult patients: case report and review of the literature. J Neurooncol 2001; 52: 49-56.
12. Mohapatra G, Moore DH, Kim DH, Grewal L, Hyun WC, Waldman FM, Pinkel D, Feuerstein BG. Analysis of brain tumor cell lines confirm a simple model of relationship among fluorescence in situ hybridization, DNAindex, and comparative genomic hybridization. Genes Chromosomes Cancer 1997; 20: 311-319.
13. Pimentel J, Silva R, Pimentel T. Primary malignant rhabdoid tumors of the central nervous system: considerations about two cases of adulthood presentation. J Neurooncol 2003; 61: 121-126.
14. Rorke LB, Packer RJ, Biegel JA. Central nervous system atypical teratoid/rhabdoid tumors of infancy and childhood: definition of an entity. J Neurosurg 1996; 85: 56-65.
15. Samaras V, Stamatelli A, Samaras E, Arnaoutoglou C, Arnaoutoglou M, Stergiou I, Konstantopoulou P, Varsos V, Karameris A, Barbatis C. Atypical teratoid/rhabdoid tumor of the central nervous system in an 18-year-old patient. Clin Neuropathol 2009; 28: 1-10.
16. Shonka NA, Armstrong TS, Prabhu SS, Childress A, Choi S, Langford LA, Gilbert MR. Atypical teratoid/rhabdoid tumors in adults: a case report and treatment-focused review. J Clin Med Res 2011; 3: 85-92.
17. Takahashi K, Nishihara H, Katoh M, Yoshinaga T, Mahabir R, Kanno H, Kimura T, Tanino M, Ikeda J, Sawamura Y, Nagashima K, Tanaka S. A case of atypical teratoid/rhabdoid tumor in an adult, with long survival. Brain Tumor Pathol 2011; 28: 71-76.
18. Wharton SB, Wardle C, Ironside JW, Wallace WH, Royds JA, Hammond DW. Comparative genomic hybridization and pathological findings in atypical teratoid/rhabdoid tumor of the central nervous system. Neuropathol Appl Neurobiol 2003; 29: 254-261.

Instructions to Authors

This instruction is based upon *Uniform Requirements for Manuscripts Submitted to Biomedical Reviews* (the complete document appears in N Engl J Med 1997; 336, 309-315).

Aims and scope

Folia Neuropathologica is an official journal of the Mossakowski Medical Research Centre Polish Academy of Sciences and the Polish Association of Neuropathologists. The journal publishes original articles and reviews that deal with all aspects of clinical and experimental neuropathology and related fields of neuroscience research. The scope of journal includes surgical and experimental pathomorphology, ultrastructure, immunohistochemistry, biochemistry and molecular biology of the nervous tissue. Papers on surgical neuropathology and neuroimaging are also welcome. The reports in other fields relevant to the understanding of human neuropathology might be considered.

Ethical consideration

Papers describing animal experiments can be accepted for publication only if the experiment conforms to the legal requirements in Poland as well as with the European Communities Council Directive of November 24, 1986 or the National Institute of Health Guide (National Institute of Health Publications No. 80-23, Revised 1978) for the care and use of Laboratory Animals for experimental procedure. Authors must provide a full description of their anesthetics and surgical procedures. Papers describing experiments on human subjects must include a statement that experiments were performed with the understanding and consent of each subject, with the approval of the appropriate local ethics committee.

Submission of manuscripts

Articles should be written in English. **All new manuscripts should be submitted through the online submission at http://panel2.termedia.pl/fn**
For authors unable to submit their manuscript online, please contact with Prof. E. Matyja, Editor-in-Chief of *Folia Neuropathologica*, ematyja@imdik.pan.pl
The Editorial Board reserves the right to reject a paper without reviewers' opinion if the content or the form of the paper does not meet minimum acceptance criteria or if the subject of the paper is beyond the aims and scope of the journal.

Legal aspects

In sending the manuscript the author(s) confirm(s) that (s)he has (they have) not previously submitted it to another journal (except for abstracts of no more than 400 words) or published it elsewhere. The author(s) also agree(s), if and when the manuscript is accepted for publication, to automatic and free transfer of copyright to the Publisher allowing for the publication and distribution of the material submitted in all available forms and fields of exploitation. The author(s) accept(s) that the manuscript will not be published elsewhere in any language without the written consent of the copyright holder, i.e. the Publisher.
All manuscripts submitted should be accompanied by an authors' statement including signed confirmation of the above and confirming that this publication has been approved by all co-authors (if any), as well as by the responsible authorities at the institution where the work has been carried out. The authors' statement should be signed by ALL co-authors. Additionally, the author(s) confirm(s) that (s)he is (they are) familiar with and will observe the "Instruction to Authors" included in *Folia Neuropathologica* and also that all sources of financial support have been fully disclosed. Materials previously published should be accompanied by written consent for reprinting from the relevant Publishers. In the case of photographs of identifiable persons, their written consent should also be provided. Any potential conflict of interest will be dealt with by the local court specific to the Publisher. Legal relations between the Publisher and the author(s) are in accordance with Polish law and with international conventions binding on Poland.
Authors agree to waive their royalties.

Anonymous review

All manuscripts will be subject to a process of anonymous editorial review.

Preparation of manuscripts

Articles must be written in English, with British spelling used consistently throughout. Authors not entirely familiar with English are advised to correct the style by professional language editors or native English speakers.
- The length of original article should not exceed 20 printed pages including text, illustrations, tables, and references.
- Manuscripts should be typed using 12pts.font, double-spaced, and fully corrected. Allow a margin at least 2.5 cm at the top, bottom and left side of the page. Text should not be justified.

- The title page should contain: the author's full names, title of the paper, all authors' affiliations, full name and address of the communicating author (including e-mail address and fax number), running title (not exceed 40 characters including spaces).
- The abstract should not exceed 350 words. A list of 3–10 key words is recommended below the abstract.
- The manuscript body should be organized in a standard form with separate sections: Introduction, Material and Methods, Results, Discussion, and References. Review articles should be divided into sections and subsections as appropriate without numbering.
- Do not underline in the text. Avoid footnotes.
- All dimensions and measurements must be specified in the metric system.
- The source of any drug and special reagent should be identified.
- Particular attention needs to be paid to the selection of appropriate analysis of data and the results of statistical test should be incorporated in the results section.
- The nomenclature used should conform to the current edition of the Nomina Anatomica or Nomina Anatomica Veterinaria.
- Acknowledgements should be made in a separate sheet following Discussion and before References. These should contain a list of dedications, acknowledgements, and funding sources.
- Legends of figures and tables should be typed on separate pages.
- The editor reserves the right to make corrections.

Tables

- Tables numbered in Roman numerals require a brief but descriptive heading.
- The major divisions of the table should be indicated by horizontal rules.
- Explanatory matter should be included in footnotes, indicated in the body of the table in order of their appearance.
- Tables must not duplicate material in the text or in illustration.

Illustrations

All figures should be supplied electronically at resolution 300dpi in all standard formats (tiff, jpg, Adobe Photoshop, Corel Draw, and EPS). Name your figure files with "Fig" and the figure number, e.g., Fig1.tif

- The maximum figure size is 84 mm or 174 mm for use in a single or double column width, respectively.
- When possible, group several illustrations on one block for reproduction. Like all other figures, block should be prepared within a rectangular frame to fit within a single or double column width of 84 and 174 mm, respectively, and a maximum page height of 226 mm.
- Each figure should include scale magnification bar; do not use magnification factors in the figure legends.
- All figures, whether photographs, graphs or diagrams, should be numbered using Arabic numerals and cited in the text in consecutive numerical order
- **Immunohistochemical study requires color illustrations of very good quality. The papers with white and black immunohistochemistry will not be accepted.**
- **The expense of color illustrations must be borne by the authors.** The cost of color print for every successive 8 pages is 200 euro irrespective of the number of color pages, i.e., the price remains the same whether there is one or eight pages.

The Publisher makes out the bill to the communicating Author.

References

The list of references (written on a separate page) should include only those publications that are cited in the text. Avoid citation of academic books, manuals and atlases. References may be arranged alphabetically and numbered consecutively. References should be given in square brackets with no space between the comma and the consecutive number, e.g. [3,4,6-12].

References should be written as follows:

Journal papers: initials and names of all authors, full title of paper, journal abbreviation (according to Index Medicus), year of publication, volume (in Arabic numerals), first and last page (example below):

1. Valverde F. The organization of area 18 in the monkey. Anat Embryol 1978; 154: 305-334.
2. Uray NJ, Gona AG. Calbindin immunoreactivity in the auricular lobe and interauricular granular band of the cerebellum in bullfrogs. Brain Behav Evol 1999; 53: 10-19.

Book and monographs: initials and names of all authors, full title, edition, publisher, place, year (examples below):

1. Pollack RS. Tumor surgery of the head and neck. Karger, Basel 1975.
2. Amaral DG, Price JL, Pitkanen A, Carmichael ST. Anatomical organization of the primate amygdaloid complex. In: Aggleton JP (ed.). The amygdala. Wiley-Liss, New York 1992; pp. 1-66.

Reference to articles that are accepted for publication may be cited as „in press" or Epub.

Proofs

Corrections to the proofs should be restricted to printer's errors only; other alterations will be charged to the authors. In order to maintain rapid publication, proofs should be returned within 48 hours, preferably by e-mail, fax or courier mail. If the Publisher receives no response from the authors after 10 days, it will be assumed that there are no errors to correct and the article will be published.

Subscription information

The journal is published in one volume per year consisting of four numbers. The annual subscription price is 160 PLN for Institutions from Poland and 80 PLN for individual subscribers from Poland and 140 Euro for foreign Institutions and 70 Euro for foreign individual subscribers.
Payment should be made to:
Termedia sp. z o.o., ul. Kleeberga 8, 61-615 Poznań
BZ WBK III O/Poznań PL 61 1090 1359 0000 0000 3505 2645
SWIFT: WBKPPLPP

The publisher must be notified of a cancellation of a subscription not later than two months before the end of the calendar year. After that date the subscription is automatically prolonged for another year.
Publishing, Subscription and Advertising Office:
TERMEDIA Publishing House
ul. Kleeberga 2
61-615 Poznań, Poland
phone/fax +48 61 822 77 81
e-mail: termedia@termedia.pl
http://www.folianeuro.termedia.pl

Folia Neuropathologica

AUTHOR'S STATEMENT

Title of the article

.....

.....

.....

The author(s) hereby confirm(s) that:

☐ The above-mentioned work has not previously been published and that it has not been submitted to the Publishers of any other journal (with the exception of abstracts not exceeding 400 words).

☐ All co-authors named and the relevant authorities of the scientific institutions at which the work has been carried out are familiar with the contents of this work and have agreed to its publication.

☐ In sending the manuscript together with illustrations and tables agree(s) to automatic and free transfer of copyright to the Publisher allowing for the publication and distribution of the material submitted in all available forms and fields of exploitation, without limits of territory or language, provided that the material is accepted for publication. At the same time the author(s) accept(s) that the submitted work will not be published elsewhere and in whatever language without the earlier written permission of the copyright holder, i.e. the Publisher.

☐ (S)he (they) agree to waive his(her)(their) royalties (fees).

☐ (S)he (they) empower(s) the Publisher to make any necessary editorial changes to the submitted manuscript.

☐ All sources of funding of the work have been fully disclosed.

☐ The manuscript has been prepared in accordance with the Publisher's requirements.

☐ (S)he (they) is (are) familiar with the regulations governing the acceptance of works as published in *Folia Neuropathologica* and agree(s) to follow them.

☐ (S)he (they) agree to accept appropriate invoice from the Publisher in case colour illustrations are implemented.

Date *Signatures of **all authors***

The covering letter formula can be found at: www.folianeuro.termedia.pl
-The covering letter should be sent to Associate Editor:

Milena Laure-Kamionowska
-Editorial Office of Folia Neuropathologica
Mossakowski Medical Research Centre, Polish Academy of Sciences
Poland Medical Research Centre
ul. Pawinskiego 5
02-106 Warszawa, Poland

CONTENTS